Design, Synthesis, and Evaluation of Novel Lysophosphatidic Acid Receptor-Targeting Small Molecules as Therapeutic and Diagnostic Agents

A Thesis Submitted to the Faculty of Graduate Studies
Lakehead University, Thunder Bay, Ontario, Canada

By

Austin M. Hopkins

Submitted in partial fulfillment of requirements for the degree of Master of Science in Chemistry

Lakehead University
Thunder Bay, Ontario, Canada, 2023

Abstract

Breast cancer has the highest incidence rate of all cancers among Canadian women and accounts for nearly 14% of all cancer-related deaths in Canada. This type of cancer is often detected using medical imaging modalities such as mammography, breast ultrasound, and breast MRI, but each of these modalities can face harsh limitations for the detection of certain types of breast cancer. Positron emission tomography (PET) is another common imaging modality that is reported to have the highest sensitivity among all medical imaging modalities, but it is underused for breast cancer imaging due to the lack of a specific breast cancer-targeting PET radiopharmaceutical. Current breast cancer therapy methods also face limitations and are associated with negative effects. This leaves room for the development of a new PET radiopharmaceutical that is more specific for breast tumours, and for a new breast cancer chemotherapy agent. Lysophosphatidic acid receptor 1 (LPA_1) has been identified as having elevated expression in breast cancer, and activation of LPA_1 has been shown to increase cell migration and invasion. As such, the development of antagonists that target LPA_1 would have extensive clinical benefits.

This thesis focused on the design, synthesis, and biological evaluation of a library of highly potent and selective novel molecules targeting LPA_1 that are derived from the previously reported compound, RO6842262. A novel 3*H*-1,2,3-triazolo[4,5-*d*]pyrimidine scaffold was identified through scaffold hopping and molecular docking studies. Based on the chemical structure of this novel scaffold, a six-step synthetic scheme and a fluorine-18 radiolabeling scheme were proposed, and one final compound was able to be synthesized. This compound, (*R*)-1-(4'-(5-((1-(4-fluorophenyl)ethyl)amino)-3*H*-[1,2,3]triazolo[4,5-*d*]pyrimidin-3-yl)-[1,1'-biphenyl]-4-yl)cyclopropanecarboxylic acid, was synthesized using the (*R*)-1-(4-fluorophenyl)ethanamine building block, and the synthesis of other analogues is currently in progress. The cAMP assay was used to evaluate the biological activity of this compound and it was found that it is able to

inhibit LPA_1 signaling with relatively high potency. This novel compound had an IC_{50} value of 172.1 nM in this assay. Although it is less potent than RO6842262, the results of this study are promising. The synthesized final compound was also evaluated in a wound healing assay using the MDA-MB-231 cell line, where it was found to significantly inhibit LPA-induced cell migration in a time and dose-dependent manner. It is anticipated that future analogues will have increased potency, enabling their usage as breast cancer diagnostic and therapeutic tools.

Acknowledgements

I would like to express my deepest gratitude to my primary supervisor, Dr. Jinqiang Hou. Since I joined his group as a second-year undergraduate student in 2019, Dr. Hou has been a constant source of support, guidance, and encouragement. His kindness and willingness to guide me through the many challenges that I have faced have enabled me to perform at my best. I am truly grateful for his mentorship and the opportunities he has provided throughout my time in his lab.

I would also like to extend my appreciation to my committee members, Dr. Michael Campbell and Dr. Christine Gottardo. Their valuable feedback on my work and their kind allowance of me to use some of their lab equipment has been instrumental in shaping my research. As well, I am thankful for their time and effort in reviewing the first draft of my thesis. Additionally, thank you Dr. Gottardo and Dr. Rob Mawhinney for your efforts as program coordinators, and thank you Dr. Xiao-an Zhang from the University of Toronto for your efforts as the external examiner of this thesis.

My heartfelt thanks go to the members of my lab who have been with me on this academic journey. Dr. Dong Zhao, Dr. Taylor Hari, Wenjie Liu, Yang Mao, Qianqian Wang, Nolan Yurkiw, Jonas Olsen, Halen Kovacs, Arshdeep Kaur, Catherine Jiang, and Wendy Wang are all fantastic people and have provided a supportive and friendly environment, and I wish the best of luck to all of them going forwards. I am especially grateful to Dong for performing the biological assays for my final compound, Wenjie for the incredible support she has given me on a daily basis with my project, and to Yang for mentoring me during my undergraduate Honours thesis work.

I would like to thank the members of the Thunder Bay Regional Health Research Institute for their timely assistance whenever I encountered challenges or had questions. Dr. Guillem Dayer, Tanya Niederer, Shannon Maki, and Carmen Dore, your support has been invaluable, and I appreciate your willingness to help whenever needed.

Finally, I am deeply grateful to my family and friends who have stood by me throughout this journey. Their love, encouragement, and belief in me have been the driving force behind my success. I couldn’t have done this without their support.

To everyone mentioned above and to those who have supported me in ways I may have inadvertently omitted, thank you from the bottom of my heart. Your contributions have made this thesis possible, and I am forever grateful.

Table of Contents

Acknowledgements i

Table of Contents iii

List of Abbreviations vi

List of Tables viii

List of Figures ix

List of Schemes xi

Chapter 1: Background and Theory 1

1.1 – Overview of Cancer in Canada 1

1.1.1 – Historical and Current Diagnostic Breast Cancer Techniques 7

1.1.2 – Historical and Current Therapeutic Breast Cancer Techniques 14

1.2 – G Protein-Coupled Receptors 18

1.2.1 – Lysophosphatidic Acid Receptor Family 20

1.2.1.1 – Endothelial Differentiation Gene (EDG) Subfamily 22

1.2.1.2 – Non-Endothelial Differentiation Gene (Non-EDG) Subfamily 25

1.3 – Positron Emission Tomography 26

1.3.1 – PET Basics 27

1.3.2 – PET Radioisotopes 29

1.3.2.1 – Fluorine-18 30

1.3.3 – Use of PET for Cancer Detection 31

1.4 – Project Overview 32

Chapter 2: Ligand Design 33

2.1 – Targeting the LPA Receptors: Antagonists from the Past to Present 33

2.1.1 – LPA-Targeting Ligands in Clinical Trials 36

2.2 – Introduction to Scaffold Hopping 38

2.2.1 – Application of Scaffold Hopping to RO6842262 39
2.2.1.1 – Docking Studies Using AutoDock Vina 40
2.3 – Designing a Library of Novel Small Molecules 42
Chapter 3: Organic Synthesis and Structure Confirmation 45
3.1 – Proposal of a Rational Synthetic Scheme 45
3.2 – Experimental Methods and Data 46
3.2.1 – Synthesis of Compound 3 46
3.2.1.1 – Structure Confirmation for Compound 3 47
3.2.2 – Synthesis of Compound 4 48
3.2.2.1 – Structure Confirmation for Compound 4 49
3.2.3 – Synthesis of Compound 5 49
3.2.3.1 – Structure Confirmation for Compound 5 50
3.2.4 – Synthesis of Compounds 6a-c 50
3.2.4.1 – Structure Confirmation for Compounds 6a-c 52
3.2.5 – Synthesis of Compound 7a 53
3.2.5.1 – Structure Confirmation for Compound 7a 54
3.2.6 – Synthesis of Compound 8a 54
3.2.6.1 – Structure Confirmation for Compound 8a 55
Chapter 4: Biological Evaluation of Ligands 59
4.1 – cAMP Assay 59
4.2 – Wound Healing Assay 60
Chapter 5: Radiochemistry 63
5.1 – Common Fluorine-18 Radiolabeling Strategies 63
5.2 – Modification of Synthetic Scheme to Attain ^{18}F-Labelled Compounds 66
Chapter 6: Conclusion 69

References 71

List of Abbreviations

[^{18}F]-FDG	Fluorine-18 fluorodeoxyglucose
^{1}H	Hydrogen-1
^{13}C	Carbon-13
AC	Adenylyl cyclase
$CDCl_3$	Deuterated chloroform
CT	Computed tomography
DIPEA	*N,N*-Diisopropylethylamine
DMSO-d6	Hexadeuterodimethyl sulfoxide
EtOAc	Ethyl acetate
EtOH	Ethanol
FDG	Fluorodeoxyglucose
FLIPR	Fluorescent imaging plate reader
Gd	Gadolinium
GPCR	G protein-coupled receptor
HCl	Hydrochloric acid
HPLC	High-performance liquid chromatography
LiOH	Lithium hydroxide
LPA	Lysophosphatidic acid
LPA_x	Lysophosphatidic acid receptor ‘x’
m/z	Mass-to-charge ratio
MeOH	Methanol
MS	Mass spectrometry
MRI	Magnetic resonance imaging
MW	Molecular weight
Na_2CO_3	Sodium carbonate
Na_2SO_4	Sodium sulfate
NaOH	Sodium hydroxide
NMR	Nuclear magnetic resonance
$Pd(dppf)Cl_2$	[1,1'-Bis(diphenylphosphino)ferrocene]palladium(II) dichloride
PET	Positron emission tomography
PLC	Phospholipase C
S_N2	Bimolecular nucleophilic substitution
$SnCl_2$	Tin(II) chloride

SPIAd	Spiroadamantyl-1,3-dioxane-4,6-dione
THF	Tetrahydrofuran
TLC	Thin-layer chromatography
UV	Ultraviolet

List of Tables

Table 1 – Projected cases for most common cancers by sex among Canadians in 2021 **.....2**

Table 2 – Distribution of new cases for selected cancers among Canadians, 2013-2017 **.....3**

Table 3 – Distribution of projected cancer deaths for selected cancers by sex among Canadians in 2021**.....4**

Table 4 – Most common radionuclides used in PET imaging **.....30**

List of Figures

Figure 1 – Annual percent change in age-standardized mortality rates for selected cancers among Canadians, 1984-2019 ..... **5**

Figure 2 – Summary of LPA-mediated downstream signaling pathways **21**

Figure 3 – Sequence similarity matrix of the six identified LPA receptors **23**

Figure 4 – Chemical structures of selected lipid LPA_1 antagonists **34**

Figure 5 – Chemical structures of Ki16425 and derived LPA_1 antagonists **35**

Figure 6 – Chemical structures of ONO-7300243 and derived LPA_1 antagonists **36**

Figure 7 – Chemical structures of LPA_1 ligands in clinical trials **37**

Figure 8 – Discovery of the 3*H*-1,2,3-triazolo[4,5-*d*]pyrimidine core using scaffold hopping **39**

Figure 9 – Docking result of the novel scaffold in the orthosteric binding pocket of LPA_1 ..... **41**

Figure 10 – Superimposed docking results of RO6842262 and the novel scaffold **42**

Figure 11 – Proposed alcohol building blocks for the novel scaffold **43**

Figure 12 – Proposed amine building blocks for the novel scaffold **43**

Figure 13 – Proposed fluorine-containing amine building blocks for the novel scaffold **44**

Figure 14 – Proposed isosteric heterocycle building blocks for the novel scaffold **44**

Figure 15 – Mass spectrum for Compound **3** **48**

Figure 16 – ^{1}H NMR spectrum for Compound **4** **49**

Figure 17 – ^{1}H NMR spectrum for Compound **5** **50**

Figure 18 – ^{1}H NMR spectrum for Compound **6a** **52**

Figure 19 – ^{1}H NMR spectrum for Compound **6b** **52**

Figure 20 – ^{1}H NMR spectrum for Compound **6c** **53**

Figure 21 – ^{1}H NMR spectrum for Compound **7a** **54**

Figure 22 – ^{1}H NMR spectrum for Compound **8a** **55**

Figure 23 – ^{13}C NMR spectrum for Compound **8a** **56**

Figure 24 – Mass spectrum for Compound **8a** **56**

Figure 25 – HPLC chromatogram for compound **8a** using 254 nm channel **57**

Figure 26 – HPLC chromatogram for compound **8a** using 365 nm channel **58**

Figure 27 – cAMP assay results using Compound **8a** **59**

Figure 28 – Effects of LPA and **8a** on cell migration in wound healing assays using the MDA-MB-231 cell line **60**

Figure 29 – Quantification of the wound healing assay **61**

List of Schemes

Scheme 1 – Synthesis of novel 3*H*-1,2,3-triazolo[4,5-*d*]pyrimidine LPA_1 antagonists **.....45**

Scheme 2 – Alternate synthetic scheme for the synthesis of iodine-containing final compounds **.....66**

Scheme 3 – Proposed radiolabeling scheme to produce ^{18}F-labeled compounds**.....68**

Chapter 1: Background and Theory

1.1 – Overview of Cancer in Canada

Cancer poses a significant burden to Canadian society. According to Canadian Cancer Statistics 2021, it is estimated that 40% of all Canadians will develop cancer within their lifetime.[1] It is also estimated that 25% of all Canadians will die from cancer.[1] Taken together, it can be inferred that around 60% of Canadians that develop cancer will eventually succumb to this disease. Of course, the term 'cancer' does not refer to one condition in particular; this term broadly describes over 100 distinct diseases that are characterized by the uncontrolled growth of abnormal cells within the body. Different cancers can be broadly divided into four major categories based on their tissue origins and unique characteristics: carcinomas, sarcomas, melanomas, and blood cancers.[2] Carcinomas are the most common type of cancer and develop in epithelial tissue.[2] Examples of carcinomas include most cancers of the lungs, breasts, and liver.[2] Sarcomas are classified as cancers that originate from connective or supportive tissue, such as in bones, fat, or blood vessels, including osteosarcoma, liposarcoma, and angiosarcomas.[2] Melanomas are a category of cancers that start in melanocytes, which are cells that produce melanin, a class of chemical compounds that give skin its pigmentation.[2] Melanomas are typically cancers of the skin but can also develop in other regions of the body that contain melanocytes, including the eyes and the anus.[2] Finally, there are several subcategories of cancer that can all be described as blood cancers, including leukemias, lymphomas, and multiple myelomas.[2] Each of these encompass a range of distinct diseases; leukemias originate in the bone marrow and include acute lymphocytic leukemia, lymphomas originate in lymphocytes and include conditions such as non-Hodgkin lymphoma, and multiple myelomas are cancers that start in plasma cells, including smouldering (indolent) and active multiple myeloma.[2]

Table 1 (below) gives a representation of the 10 cancers with the highest predicted incidence rate among Canadians in 2021. It is evident that the majority of projected new cancer cases can

be classified as carcinomas, as lung and bronchus, breast, colorectal, prostate, and bladder cancers— the cancers with the five highest projected incidence rates among Canadians in 2021—commonly manifest as a form of carcinoma. In fact, a staggering sum of 118,900 new cases is attributed to the five highest ranking cancers alone, the majority of which can be classified as carcinomas, making up over half of all projected new cancer cases (229,200) among Canadians in 2021.[1] While it is acknowledged that sarcomas, melanomas, and blood cancers also play significant roles within the broad field of oncology, their distinctive characteristics, including different treatment methods, are beyond the scope of this investigation. As such, to streamline the research focus and delve deeper into the specific diagnostic and therapeutic aspects of cancer, the primary focus of this section from hereafter will be the most prevalent category of cancer, carcinomas, as highlighted above.

Table 1 – Projected cases for most common cancers by sex among Canadians in 2021[a]

		New cases (estimated)		
Type of cancer	**Classification[b]**	**Male**	**Female**	**Total**
Lung and bronchus	Carcinoma	14,800	14,800	29,600
Breast	Carcinoma	260	27,700	28,000
Colorectal	Carcinoma	13,700	11,100	24,800
Prostate	Carcinoma	24,000	—[c]	24,000
Bladder	Carcinoma	9,500	3,000	12,500
Non-Hodgkin lymphoma	Lymphoma	6,200	5,000	11,100
Melanoma	Melanoma	4,700	4,000	8,700
Uterus	Carcinoma	—	8,000	8,000
Kidney and renal pelvis	Carcinoma	5,200	2,600	7,800
Head and neck[d]	Carcinoma	5,400	2,000	7,400

[a]Data adapted from Canadian Cancer Statistics 2021.[1]

[b]Classification was given based on statistical prevalence of a particular class of cancer.

[c]Not applicable.

[d]The 'head and neck' cancer category includes oral, laryngeal, and nasal cavity sinus cancers.

Examining age-specific cancer incidences can also shed insight on current cancer trends among Canadians. **Table 2** displays the percent distribution of the five most prevalent types of cancer from **Table 1** partitioned between the four highest risk age groups as described by the Canadian Cancer Society. According to Canadian Cancer Statistics 2021, the age group of 50-69 accounted for 44.7% of all new cancer cases between 2013 and 2017, while the groups of 70-84 (34.4%), 30-49 (9.6%), and 85+ (9.3%) followed behind. The remaining age groups of 0-14 and 15-29 only collectively accounted for a total of 2.0% of all cancer cases in this time period, clearly demonstrating that these groups can be considered relatively low risk. It is for this reason that **Table 2** has omitted the ages of 0-29. Based on the available data, it can be observed that new breast cancer cases tend to occur more frequently for individuals belonging to working age groups, while new lung, colorectal, and bladder cancer cases progressively increase in frequency as age increases, peaking in the elderly age groups. Prostate cancer cases follow a similar trend, although recorded cases see a slight drop off after the age of 85. Furthermore, breast cancer cases lead the way for two of the highest risk age groups, including the single highest risk age group, the 50-69 group, while lung cancer and colorectal cancers are at the forefront of the 70-84 and 85+ age groups, respectively.

Table 2 – Distribution of new cases for selected cancers among Canadians, 2013-2017[a]

	Age group			
Type of cancer	**Percentage of cancer cases between ages of 30-49**	**Percentage of cancer cases between ages of 50-69**	**Percentage of cancer cases between ages of 70-84**	**Percentage of cancer cases ages 85+**
Lung and bronchus	3%	12%	**17%**	14%
Breast	**23%**	**14%**	9%	9%
Colorectal	9%	11%	13%	**15%**
Prostate	<3%	<3%	12%	7%
Bladder	<3%	4%	7%	7%

[a]Data adapted from Canadian Cancer Statistics 2021.[1]

In addition to considering new cancer cases among Canadians, it is of the utmost importance to consider deaths that have been caused by cancer. Perhaps the most direct way of doing this is to visualize the percent distribution of cancer deaths for the most prevalent cancers in Canada. In doing so, one can easily compare the proportion of deaths caused by one type of cancer to another. The five cancers that were selected for **Table 2** have been presented in **Table 3**, which shows the projected sex-based percent distribution for deaths attributed to these cancers among Canadians in 2021. Unsurprisingly, the three cancers with the highest prevalence, namely lung, breast, and colorectal cancers, rank among the highest in prevalence for cancer deaths as well. In 2021, lung cancer was projected to account for approximately 25% of all cancer deaths for both genders, while breast cancer had the next highest single-gender mortality percentage of 13.5% for females. Colorectal cancer made up approximately 11-12% for either gender, while prostate and bladder cancers rounded out the list with respective mortality percentages of 10.1% and 4.3% for males. For females, bladder cancer only was projected to account for 1.8% of female cancer deaths in 2021.

Table 3 – Distribution of projected cancer deaths for selected cancers by sex among Canadians in 2021[a]

	Percentage of Cancer Deaths (estimated)	
Type of cancer	**Male**	**Female**
Bladder	4.3%	1.8%
Breast	0.1%	13.5%
Colorectal	11.9%	10.8%
Lung and bronchus	**24.2%**	**25.8%**
Prostate	10.1%	—[b]

[a]Data adapted from Canadian Cancer Statistics 2021.[1]

[b]Not applicable.

Another useful approach for determining the prevalence of cancer-related deaths is by analyzing the recent mortality trends for cancer in Canada. **Figure 1** displays the annual percent

change in age-standardized mortality rates from 1984 to 2019 for bladder, breast, colorectal, lung and bronchus, and prostate cancers based on sex. From this figure, it can be seen that both colorectal and lung and bronchus cancers have seen a dramatic downwards shift in mortality rates over this time period for both genders. Curiously, bladder cancer has seen a sharp decrease in mortality rate for men but not for women. A recent review has attributed this mostly to the fact that although men have a threefold to fourfold higher risk of developing this particular cancer, women are more often diagnosed with more advanced, and hence, more deadly stages of the disease due to delays in seeking medical attention after observing haematuria.[3] Comparatively, while prostate and breast cancer mortality rates have been on the decline over the past 40 years, they have seen much milder reductions in mortality rate, declining by only approximately 1-1.5% each year.

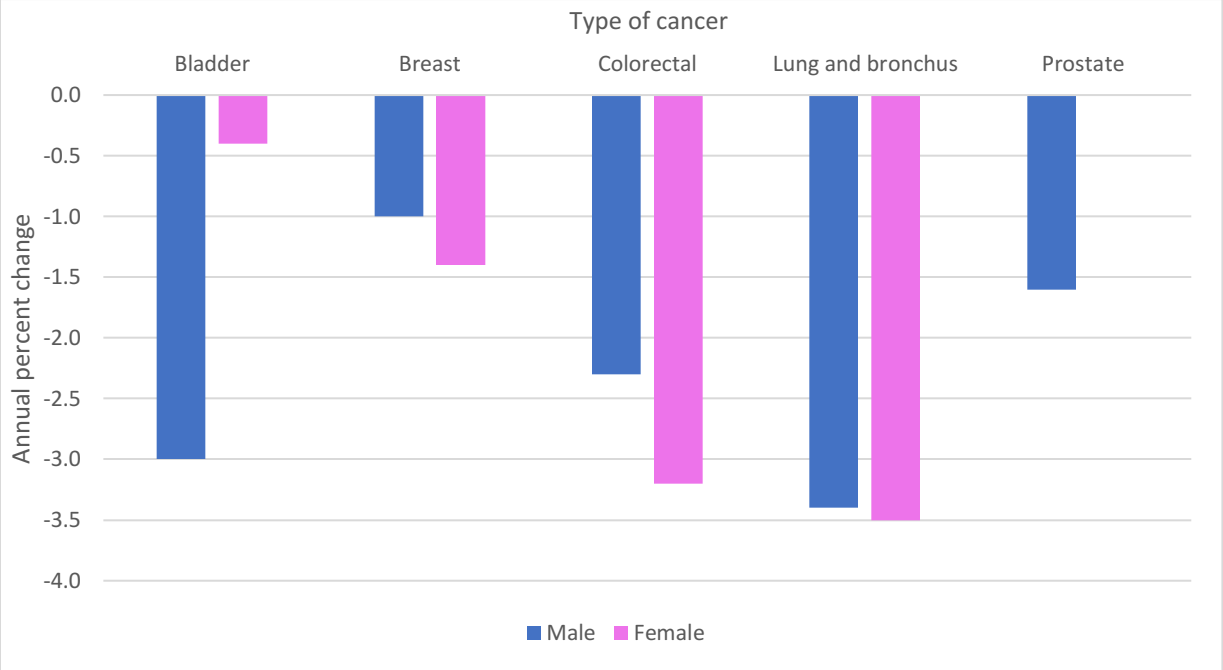

Figure 1 – Annual percent change in age-standardized mortality rates for selected cancers among Canadians, 1984-2019

[a]Data adapted from Canadian Cancer Statistics 2021.[1]

Based on the data that has been presented thus far, lung cancer and breast cancer stand out as the most prominent figures. Lung cancer was projected to have the highest incidence of new cases among all cancers in 2021 with 29,600 cases, accounted for the highest percentage of new cases among the age group of 70-84 from 2013-2017, and was projected to account for approximately 25% of all cancer-related deaths in Canada in 2021. Conversely, breast cancer followed closely behind in the number of projected new cases with 28,000, accounted for the highest percentage of new cases between the age groups of 30-49 and 50-69 from 2013-2017, and was projected to account for 13.5% of all cancer deaths among females in 2021. However, these two cancers have had markedly different changes in mortality rates over the past 40 years. Whereas lung cancer mortality rates have seen an annual percent change of around -3% each year within this time period, breast cancer mortality rates have only had an annual percent change of under -1.5% each year. The Canadian Cancer Society believes that these trends in lung cancer mortality rate are largely due to a decrease in the prevalence of tobacco smoking over time. Recent research estimates that over 70% of lung cancer cases in Canada are caused by the smoking of tobacco products.[4] This carries a strong significance as it is believed that people who smoke tobacco are around 25 times more likely to die from lung cancer than non-smokers due to the presence of harmful carcinogens in tobacco smoke.[5] It should follow, then, that as Canadians nationwide have steadily reduced their smoking of tobacco in recent years, lung cancer mortality rates have progressively dropped, as supported by **Figure 1**; even in the short period between 2015 and 2021, the number of Canadian smokers dropped from 5,344,100 in 2015 to 3,830,200 in 2021.[6] Major contributors for this include regulatory and legislative efforts from the Government of Canada regarding cigarette package labeling, such as the requiring of product packaging to be a plain brown colour and bearing appropriate health and safety warnings, as well as the launching of far-reaching anti-smoking campaigns.[7] As the public perception of smoking continues to drop, the incidence and mortality rate of lung cancer should continue to drop, with the Government of Canada aiming for less than 5% of tobacco use nationwide by 2035 to reduce the disease burden

of tobacco smoking.[7] Therefore, it seems that the best measure to prevent lung cancer deaths may ultimately lie outside of the clinic and, instead, in continuing to improve public awareness of the dangers of smoking. However, for breast cancer, similar preventative measures are not quite so apparent. Although incidence of breast cancer has been linked to controllable factors such as alcohol use and physical inactivity, these factors are not as critically central to the development of breast cancer as tobacco smoking is to lung cancer.[8] For breast cancer, it is believed that the best option to continue to lower the incidence and mortality rates is to develop more effective early screening and treatment methods.[9] Although existing tools for breast cancer diagnostics and therapeutics have proven to be fairly successful to this point, there is a clear need for improvement in both of these sectors as demonstrated by the data discussed earlier in this section. As such, it is the goal of this thesis to develop a new tool that can be used to further advance the area of breast cancer oncology in both the diagnostic and therapeutic concentrations. The following sections will discuss both the past and present diagnostic and therapeutic tools that have been used for the detection and treatment of breast cancer.

1.1.1 – Historical and Current Diagnostic Breast Cancer Techniques

Methods used for the detection and diagnosis of breast cancer have undergone a significant evolution throughout history. Indeed, breast cancer has been a constant throughout recorded history, being first mentioned in the Edwin Smith Papyrus, the earliest known treatise describing diseases, dating to the 16th century BCE during the New Kingdom period in ancient Egypt.[10] In this text are the first written accounts of breast cancer, wherein it is described that if a breast is cool to the touch and has bulges, and this sensation has spread across the breast, then the ailment is incurable.[11] Breast cancer is also mentioned in Classical antiquity by renowned scholars such as Hippocrates and Pliny the Elder. In one text from approximately the 5th century BCE, Hippocrates reported that tumours may be the result of an overabundance of black bile within the

body, while Pliny the Elder, in the 1st century AD, proposed that breast cancer is the result of childbirth.[12]

Over the next millennium, different theories regarding the origin of breast cancer were postulated and often attributed to various religious beliefs.[11] Throughout this time, breast cancer was typically diagnosed through the swelling of the breasts, with pain, numbness, and ulcerations occurring in more severe cases.[12] During the Age of Enlightenment, new theories regarding the origin of breast cancer began to appear. As interest in the natural sciences grew and scientific studies became more rigorous, many of these beliefs were more grounded in reality than the divine beliefs of the earlier millennium, such as Claude Deshais Gendron's proposal of breast cancer forming due to the mixing of lymph vessels with nerve and glandular tissue in the early 1700s.[13] Not long after Gendron's proposal was the first autopsy with intent to link a patient's illness to pathological findings after their death performed by Italian anatomist Giovanni Morgagni, paving the way for modern oncological studies.[14]

As medical technologies advanced through the late Modern period, detection of breast cancer become more sophisticated. The invention of the modern microscope in the 19th century allowed for the analysis of diseased human tissue in a way that was previously impossible, giving researchers insight on the inner workings of the body on a microscopic scale. Then, in 1913, the first X-ray of the breasts was performed by a German surgeon named Albert Salomon, who was studying the applications of radiology with mastectomy specimens. Since the 1960s, X-rays of the breasts, called 'mammograms', have played a central role in the diagnosis of breast cancer.[15]

In the modern age, there are several diagnostic techniques that are used for the detection and diagnosis of breast cancer. The most frequently used method today is mammography, which takes the form of X-ray images of the breasts.[16] Other commonly used techniques for the diagnosis of breast cancer include biopsies as well as other medical imaging modalities such as breast ultrasound and breast MRI.[16] Each of these will be discussed briefly, focusing on their

inherent advantages and disadvantages. It should be noted that other diagnostic techniques than the aforementioned do exist, but for the purposes of simplification, only the most prominent techniques will be discussed.

As mentioned earlier, mammography, or X-ray imaging of the breasts, is the most common method of detecting breast cancer used today. Mammography is performed using a machine that is specifically designed for mammographic imaging, wherein the patient's breasts are compressed by two plates that aid in spreading the breast tissue apart, which helps raise the image quality and reduce the radiation dose required.[17] Typical imaging times are fairly quick, with the mammogram itself usually lasting between 10-15 minutes. Its relatively low cost and infrastructural abundance make it one of the most practical ways of testing for breast cancer. In saying this, it is important to recognize that mammography can be divided into two subtypes: screening mammography and diagnostic mammography.[17] While it is certainly the most accessible technique used for breast cancer screening, it may not always be the best option when it comes to clinical diagnosis.

Screening mammography is by far the most common screening method in the developed world. Although modern therapeutic techniques have come a long way, the early detection of breast cancer is still the most effective method for reducing breast cancer mortalities.[18] Randomized control studies have shown that the attendance of regular mammographic screening can reduce breast cancer mortalities by around 30%, clearly demonstrating the impact of this tool.[18] The Canadian Cancer Society recommends women from ages 50-74 to schedule a screening mammogram biennially and recommends women from 40-49 and 75+ to consult their doctor about the benefits and limitations of having a mammogram.[19] Screening mammograms typically use involve a lower X-rays dosage than diagnostic mammograms, minimizing the risk associated with the imaging modality, but still posing a theoretical risk. If an abnormality in the breast is discovered, such as a lump in the breast, then diagnostic mammography may be used following the results of the screening.[17] Diagnostic mammography uses a higher radiation dose

than screening mammography, although the overall dosage is still relatively low. The procedure for diagnostic mammography usually takes longer than screening mammography as different angles may be used in order to ensure that sufficient information is obtained to make an informed diagnosis, but the overall methods are the same as in screening mammography.[17]

The main limitation of mammography is its ineffectiveness when used for patients with dense breast tissue.[18] In patients whose breasts are composed of mainly fatty tissue, the sensitivity of mammography is extremely high, with one digital mammography study reporting a sensitivity of 85% and specificity of 90% for women under the age of 50 with non-dense breasts and a sensitivity of 66% and specificity of 93% for women above the age of 50 with non-dense breasts.[20] However, for patients whose breasts are primarily composed of dense tissue, the sensitivity can reportedly drop to as low as 50%.[21] Dense breast tissue poses problems for radiologists as dense tissue appears light on the mammographic image, which is the same colour as many abnormalities, including tumours. This can lead to overdiagnosis, where a patient's condition is correctly assessed but subsequent clinical action does more harm than it would have if left undetected (due to unnecessary treatment or side effects from treatment), false positives, where a healthy patient is diagnosed as being diseased, or false negatives, where a diseased patient is believed to be healthy.[9,17] Comparatively, fatty breast tissue appears dark on the resulting image, making it much easier to find calcifications or other abnormalities and give an accurate diagnosis. In the case where results of a diagnostic mammogram are inconclusive, a secondary method may be used to try to determine if the perceived abnormality is truly due to cancer, which usually will take the form of a biopsy or another imaging modality.[17] Other disadvantages to mammography include patient anxiety, patient discomfort or pain to due breast compression, and the inherent dose of radiation required for this imaging modality that, though unlikely, may actually increase the risk of breast cancer.[22,23]

Breast ultrasound is another commonly used modality for the diagnosis of breast cancer. This modality is not typically used as a standalone method for diagnosing breast cancer but can prove

to be quite useful as a supplemental tool.[18] Breast ultrasound is performed by sending a cascade of acoustic waves through the tissue that are eventually reflected back by the interfaces between different types of tissue, and an ultrasound image can be constructed by a computer based on the reflectional data that is obtained. This procedure is most commonly conducted by the ultrasound operator using a rod-like device called a transducer that is pressed into and moved across the skin, earning the name of 'handheld' or 'manual' ultrasound.[24]

Breast ultrasound offers several advantages in the detection and evaluation of breast cancer. Notably, its effectiveness is not limited by breast tissue density, as studies have shown that the sensitivity of ultrasound is relatively consistent across different tissue densities.[25] Moreover, in certain cases, breast ultrasound may be used as the primary diagnostic tool for evaluating a patient's breast condition. For pregnant patients or those who should otherwise avoid exposure to X-rays, breast ultrasound will often be used as a valuable screening alternative to screening mammography.[26] Additionally, for younger women, who are typically considered low-risk individuals and tend to have denser breasts, breast ultrasound screening can be used to limit the amount of lifetime radiation exposure a patient receives while still yielding high-quality results.[24,27] Ultrasound has also been shown to be more accurate in the detection of small breast tumours. In a retrospective study performed with previously diagnosed breast cancer patients, breast ultrasound had a sensitivity of 83.7% while mammography only had a sensitivity of 65.2% for breast tumours <1.0cm in diameter.[25] Another benefit of ultrasound is that similarly to mammography, it is reasonably inexpensive and is widely available.[24] However, although the use of ultrasonic waves (compared to radiation-based imaging modalities) to generate an image does not pose any risk to humans, there are other disadvantages associated with breast ultrasound. One notable limitation of breast ultrasound is that the operator greatly influences the effectiveness of the test. Since in many cases, the majority of a particular manual breast ultrasound examination is not officially recorded as the operator may only target specific areas of concern, overlooked abnormalities in the breast may be missed entirely; since these results may not be documented,

later in-depth review of the results of a manual breast ultrasound can prove impossible.[24] This means that only highly experience breast ultrasound specialists should conduct these tests, but in many countries, it is often physicians that conduct them, resulting in lower reproducibility and poorer results.[24] In recent years, automated breast ultrasound has seen an increase in availability and should help reduce the operator dependence of breast ultrasound, but is underused since the technique is relatively new.[24] As well, ultrasound techniques also only have a limited penetration depth, meaning that for obese women, accurate results may not be obtained depending on the degree of obesity.[24] There are also concerns regarding the increased false positive rate of breast ultrasound compared to mammography. In a study performed on Chinese women, the specificity of breast ultrasound was only 43.5% while the specificity of mammography was 62.6%, raising concerns about breast ultrasound leading to a higher rate of unnecessary biopsies and increasing patient anxiety.[28] Nonetheless, breast ultrasound remains a capable tool in many cases.

Breast MRI is a lesser used yet still useful imaging modality for the diagnosis of breast cancer. Similar to ultrasound, it is often employed as a tool to supplement mammography rather than as the primary tool to diagnose breast cancer.[29] Magnetic resonance imaging involves the use of a strong magnetic field in combination with radio waves that are transmitted through the body that take advantage of the body's natural magnetic properties. Nuclei within the body, in most cases hydrogen nuclei, are aligned by the magnetic field, and then a radiofrequency pulse is used to disturb the alignment of these nuclei.[30] As the nuclei realign with the magnetic field, the nuclei release signals that are detected by a receiver coil. A computer reconstructs the received signals and builds an anatomical image in which different tissues can be distinguished based on the inherent magnetic properties of the tissues.[30] To enhance the detail and clarity of the resulting image, during the procedure, a chemical contrast agent, usually gadolinium-based, may be intravenously administered that improves the contrast between tissues.[31] The procedure is typically performed using a large circular machine with a central ring-shaped gap in which the

patient lies for approximately 30 minutes to one hour as the scan occurs. This procedure is generally how breast MRI scans are performed.

Breast MRI comes with several advantages. MRI does not involve the use of ionizing radiation, making it safer to use than mammography. Additionally, it is considered as having the highest sensitivity among common breast cancer imaging modalities and is also generally viewed as the best screening imaging modality for high-risk women.[32] In a 2015 study among patients with a familial history of breast cancer or had BRCA1 or BRCA2 mutations, which increase the risk of breast cancer development, breast MRI alone was able to detect 45% of all cancers found in the study and detected a total of 36 out of 40, giving it a sensitivity of 90%.[33] In the same study, two cases of cancer were detected by mammography alone, and no cancers were detected by ultrasound alone; reported sensitivities for both mammography and ultrasound in this study were 37.5%.[33] The sensitivity data obtained from this study closely agreed with the data from a similar study conducted in 2005.[34] However, MRI also has several disadvantages. Firstly, it is more costly than many other diagnostic methods, and MRI scan times are frequently longer than other medical imaging modalities.[32] This means that breast MRI is not suitable for widespread breast cancer screening. The ubiquitous use of gadolinium-based contrast agents also poses a risk. In recent years, there has been increasing concern that although these contrast agents are typically safe, improper clearance of the agents can lead to adverse toxic effects through the release of unchelated Gd^{3+} ions that can interact with various biological systems within the body.[31] Another strike against breast MRI is that it has limited use for patients with metal implants. The electromagnetic field that is applied for MRI can cause a variety of undesirable effects in tandem with metal within the body, such as causing the metal to forcibly shift or heat up, potentially causing damage to surrounding tissue, or causing an active device such as a pacemaker to malfunction.[35] Image quality may also undergo severe degradation due to magnetic inhomogeneities caused by the metal in question, limiting the usefulness of a particular image.[36]

Biopsies are currently the only techniques that can definitively be used to diagnose a patient with breast cancer with near 100% certainty.[29] A biopsy is a procedure that is performed by removing diseased or otherwise abnormal tissue from a patient to be used in future pathological evaluations, which may include hormone receptor status testing, human epidermal growth factor receptor 2 status testing, or tumour marker tests, among others.[29] There are many types of biopsy that may be used for breast cancer diagnosis. These include fine needle aspiration biopsies, where a thin needle and syringe are used to take tissue from a recognized lump within the breast, core biopsies, which removes tissue using a needle or probe that remains structurally intact, and vacuum-assisted biopsies, which allow for a large volume of tissue to be extracted with a single insertion.[37] Ultrasound or MRI may be used to guide a biopsy, allowing the doctor to have higher precision for retrieving tissue from the area of concern, especially if it is located deep within the breast.[37] Additionally, excisional biopsies, which involve the surgical removal the entirety of section of suspicious tissue, may be used, although the usage of this type of biopsy has waned in recent years due to its heightened cost and invasiveness.[38] Indeed, invasiveness is one of the main disadvantages of biopsies even in 2023. Although advancements made in terms of reducing the invasiveness of biopsies, biopsies by their very nature will always be considered invasive and they should only be used whenever truly required. Other disadvantages of breast biopsies include patient pain and anxiety, physical trauma associated with repeated insertions, and the requirement of having specialized laboratory equipment to perform certain biopsies and pathological tests.[38]

1.1.2 – Historical and Current Therapeutic Breast Cancer Techniques

Much like for breast cancer diagnostics, breast cancer therapeutics have significantly evolved through the ages. Early documented records, such as the Edwin Smith Papyrus, stated that there is no cure for breast cancer, but by Classical antiquity, evidence points towards a range of therapeutic techniques having been used with varying levels of efficacy.[11] Selected techniques

include those recorded by Roman Republic historian Cato the Elder, who described the use of a cabbage poultice as a universal remedy for tumours, and the use of caustic agents if breast cancer was suspected, as described by the Greek philosopher Celsus.[12] Surgical techniques were also in use around this time, with Celsus and Leonides of Alexandria, both from the 2nd century, having detailed incision and cauterization methods in their respective works.[12]

However, much like the diagnostic techniques described in the preceding section, throughout the medieval era and especially in the Christian world, treatments were often left to healers and religious miracles, with surgical techniques being viewed as acts of barbarism.[11] During this time, surgery was still conducted, albeit mainly in regions with less influence from the Christian Church and with greater frequency towards the end of this period; Albucasis (10th century), Henri de Mondeville (13th century), and Guy de Chauliac (14th century) are notable surgical practitioners from this era.[11]

As the Western world entered the Renaissance and Enlightenment eras, surgery grew immensely in popularity as rationalism and secularism took root. In 16th century Belgium, Andreas Vesalius, considered the founder of modern anatomy, published several influential books on human anatomy and was one of the first physicians to perform human dissections for the purpose of scientific study.[11] Scottish surgeon John Hunter, during 18th century England, was an early practitioner of using an observational and inductive surgical approach.[11]

By the 19th and 20th centuries, surgery was by far and away the predominant treatment method for breast cancer. This was aided by recent advancements in hygienic standards, such as disinfection, sterilization, and the use of sterile gloves when administering surgical treatment.[11] In fact, it was not until the late 1800s that an alternative treatment avenue entered the scientific sphere of knowledge. In a paper published in 1889, German surgeon Albert Schinzinger proposed that the removal of a woman's ovaries, called an oophorectomy, may be able to treat breast cancer.[39] This theory was put to the test six years later, where George Thomas Beatson, a

Glasgow-based surgeon, removed the ovaries of a patient with an advanced form of breast cancer; she went on to live for close to four years afterwards.[40] This marked the origin of hormone therapy for the treatment of breast cancer.

Other novel breast cancer treatment methods emerged around the time of Beatson's successful application of an oophorectomy. In January 1896, American medical student Emil Grubbé purportedly used X-rays for the treatment of a carcinoma of the left breast; this was likely the very first application of therapeutic X-rays in the world.[41] Early in the 20th century, chemotherapy was also introduced. German chemist Paul Ehrlich documented the screening of series of chemicals against animal disease models, including his use of a rabbit model of syphilis in 1908, which lead to the development of arsenic-based drugs such as arsphenamine.[42] Chemotherapy was also investigated by the American government during World War II. Although chemical gas agents were not used during this war, experience from World War I and a sulfur mustard spill in Italy during World War II had shown that these chemical agents were able to deplete lymph nodes and bone marrow in those affected, leading to further studies.[43] A few decades later, in the mid-1970s, Italian oncologist Gianni Bonadonna conducted the first adjuvant chemotherapy study for breast cancer.[43] Patients would first receive primary treatment in the form of surgery, and then would undergo chemotherapy to try to prevent the cancer from relapsing. The results of this trial were promising and led to many future adjuvant breast cancer studies.[43] Also in the 1970s, a modified radical mastectomy method was developed by American surgeon John Madden that would allow for the full removal of a breast tumour while preserving the pectoral muscles; earlier mastectomy methods had been developed over the past century, but these methods had required the removal of these muscles, leaving patients disfigured.[44] Since the 1970s, other types of breast cancer treatment have also emerged, including immunotherapy and targeted therapy.[45,46]

Today, there are several techniques that are used for breast cancer therapeutics. In the modern world, cancer therapeutics are usually selected based on the specific subtype of cancer

that is determined, and also based on the stage and whether a cancer is or isn't metastatic.[47] For nonmetastatic forms of breast cancer (stages 0-III), it is desirable to fully remove the tumour from the breast and lymph nodes, as well as prevent the tumour from reoccurring.[47] For metastatic breast cancer (stage IV), the focus shifts more from trying to cure the cancer to trying to prolong the patient's life and to relieve the associated pain and suffering, known as palliative care, although some treatments that are used during nonmetastatic stages are also used for stage IV cancer.[47] Treatment types can also be divided into two groups: local treatment and systemic treatment. Local treatment is focused on removing the cancerous tumour itself without affecting the rest of the body; local treatment is usually accomplished by surgical removal of the tumour, although radiation therapy can also be used in some instances.[47] Systemic therapy is a more complex type of therapy that attempts to rid the entire body of the cancer through the use of drugs that travel throughout your body.[47] Typical systemic therapy methods include chemotherapy, endocrine therapy, and targeted therapy.

The therapeutic approaches for breast cancer encompass surgery, radiotherapy, endocrine therapy, and chemotherapy. In the early stages of breast cancer, the standard chemotherapy approach consists of anthracyclines and taxanes.[48,49] However, selecting the appropriate chemotherapy becomes a difficult task depending on factors such as patient age, cancer stage, and marker expression level. Chemotherapy is frequently utilized as an adjuvant systemic therapy method following surgery or other primary treatments to mitigate the risk of cancer recurrence and enhance long-term outlooks. A complete discussion on chemotherapy methods is beyond the scope of this thesis, but it is believed that the development of additional chemotherapeutic agents would be beneficial to expand the current clinical chemotherapy repertoire.

Building upon the groundwork laid out in earlier sections, it is imperative to delve into the fundamental underpinnings of cancer at the molecular level. While an overview of breast cancer has been addressed from both a diagnostic and therapeutic point of view, these have mostly been at a macroscopic level. From a molecular stance, cancer is defined by a complex interplay of

genetic mutations, epigenetic modifications, and aberrant signalling pathways that, together, drive malignancy and the uncontrolled growth of cells.[50] However, while these physiological interactions may be complex and manifest in countless ways, there are underlying components that can grant valuable insight into the specific nature of an individual disease. Precisely, all types of cancer have distinct chemical signatures that can be used as distinctive indicators for diagnostic and therapeutic purposes. These chemical signatures, typically referred to as 'biomarkers', exist in many different forms, including genes, proteins, and antibodies, among others. When the body is in a diseased condition, these molecules may have increased or decreased production, depending on the nature of the condition. Therefore, these molecular biomarkers can be used as targets for drug development both diagnostically, as methods that target them can glean valuable information about the disease condition, and therapeutically, as the pharmacological regulation of these molecules can lead to therapeutic benefit.

1.2 – G Protein-Coupled Receptors: An Overview

A receptor is a protein target of a substance that, when activated by the substance, enacts a biological response. Receptors encompass a wide swathe of protein types, including enzymes, enzyme-linked receptors, G protein-coupled receptors (GPCRs), intracellular receptors, and ligand-gated ion channels.[51] Among these receptor types, G protein-coupled receptors clearly stand out from a pharmacological standpoint. GPCRs are a large family of cell surface receptor proteins that are implicated in countless diseases, and of the many hundreds of drugs that have been approved by the United States Food and Drug Administration, approximately one-third of these drugs target one or more of these receptors.[52] Furthermore, this receptor family has been noted as the largest group of druggable receptors within the entire human genome.[53] GPCR-targeting ligands include a surprisingly diverse array of molecules including nucleotides, peptides, photons, other proteins, and small molecules such as hormones and lipids, among others.[53]

Structurally, all GPCRs are composed of seven transmembrane alpha-helices that that have alternating intracellular and extracellular loop regions.[54] The N-terminus of a GPCR is typically located on the extracellular surface, while the C-terminus is typically situated within the cell itself.[55] This structural arrangement allows GPCRs to interact with both the extracellular and intracellular sides of the cell membrane, enabling them to function as key modulators of cell signaling. GPCR signaling is usually mediated by agonist ligands that bind to a specific binding site and enact a conformational change on the protein, thereby 'activating' the GPCR. This conformational change results in the recruitment of intracellular signaling components, such as heterotrimeric G proteins, kinases, arrestins, and scaffolding proteins. After recruitment of these signal transducers, a variety of signaling pathways will be activated through them, resulting in a cascade of downstream signaling effects that are enhanced by the actions of second messengers and downstream effectors. However, although these characteristics may be shared among all GPCRs, there are important differences that make each receptor unique. These differences include binding site shape and size, amino acid sequence, and the various associated intracellular signal transducers as noted above.

Due to their inherent signaling and functional properties, researchers around the globe have long sought to exploit these receptors for clinical benefit. GPCRs are involved in the regulation of a wide variety of cellular and physiological responses, including, but not limited to, cell growth, cell proliferation, sensory perception, immune responses, neurotransmission, appetite, and metabolism, and have been closely linked to the progression of many diseases such as cancer, Alzheimer's disease, and depression, clearly demonstrating their great importance within the human body.[56–61] For example, in terms of cancer development, GPCRs are known to modulate important pro-cancer effects such as resistance to apoptosis, initiation of angiogenesis, and cell invasion and metastasis.[62] Alas, to this point, only a fraction of GPCRs have an approved drug that targets them. Of the approximately 360 exploitable nonolfactory receptors, 60-70% do not have an approved drug, and over 100 of these have unknown endogenous ligands.[63] These

receptors represent an auspicious platform for future drug development, and their exploitation will likely provide valuable and clinically relevant therapeutic and diagnostic tools.

1.2.1 – Lysophosphatidic Acid Receptor Family

A prime example of an unexploited GPCR subfamily is the lysophosphatidic acid receptor subfamily, which is often abbreviated as 'LPAR' or shortened to 'LPA receptors'. This is a relatively small subfamily of receptors that are widely distributed in the cell membranes of a diverse array of human tissues, of which all belong to group A13 of the Rhodopsin-like receptors according to the G (Glutamate), R (Rhodopsin), A (Adhesion), F (Frizzled), and S (Secretin) (GRAFS) classification system.[56,64] There are six currently identified members of the LPA receptor family; LPA_1, LPA_2, and LPA_3 are grouped together in the endothelial differentiation gene (EDG) family, while LPA_4, LPA_5, and LPA_6 are grouped together in the non-endothelial differentiation gene (non-EDG) family.[56] Each LPA receptor is mediated by an endogenous group of ligands called lysophosphatidic acids (LPA).[56] This group of bioactive phospholipid ligands is characterized by a phosphate head bound to a single long fatty acid chain which may or may not be saturated and has variable chain length. LPA is found in many forms within the human body, but its most abundant forms are 16:0 LPA, 18:2 LPA, and 18:1 LPA.[65]

When an LPA receptor binds its endogenous ligand, LPA, a variety of signaling cascades are initiated. Through the recruitment of heterotrimeric G proteins, molecules such as Rho, a family of small GTPases involved in a variety of intracellular processes, phospholipase C (PLC), a class of phospholipid-cleaving enzymes, and Ras, which is a family of small GTPases involved in cell signal transduction, are activated, enacting a wide suite of cellular processes and physiological effects.[56] The specific interactions between each LPA receptor and their associated G proteins are summarized in **Figure 2**. LPAR-mediated signaling by LPA has been linked to many diseases, with studies confirming that activation or inhibition of these receptors can cause either pro or anti-cancer, pain, fibrosis, infertility, and neurodevelopmental effects, among others, depending on the

LPA receptor that is being acted upon.[66] Due to the important biological effects that mediation of these receptors can have, the LPA receptors are an attractive subfamily of receptors for future drug development. However, since each receptor plays a unique role in human physiology, it is important to consider the role of each individual receptor rather than treating the LPA receptors as a single functioning unit. The functional roles of each LPA receptor will be discussed in the following sections, with a particular emphasis on their roles in cancer development, if applicable.

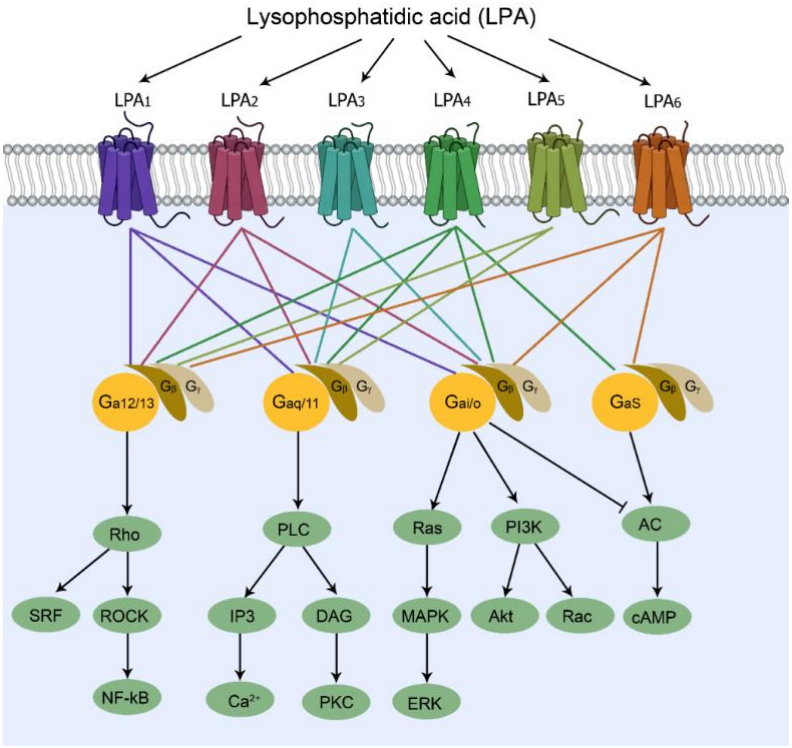

Figure 2 – Summary of LPA-mediated downstream signaling pathways[a]

[a]This figure has been directly resourced from "Liu, W., Hopkins, A. M. & Hou, J. The development of modulators for lysophosphatidic acid receptors: A comprehensive review. *Bioorganic Chemistry* **117**, 105386 (2021).

1.2.1.1 – Endothelial Differentiation Gene (EDG) Subfamily

LPA_1 was the first lysophosphatidic acid receptor to be discovered (1996), and as such, is perhaps unsurprisingly the most studied of the LPA receptors.[67,66] LPA_1 has a sequence similarity of 49-53% with the other EDG LPA receptors, but only shares ~18% sequence similarity with LPA_{4-6} (**Figure 3**). The LPA_1 receptor couples with $G_{i/o}$, $G_{q/11}$, and $G_{12/13}$ proteins, as shown by **Figure 2**.[66] LPA_1 signaling has been associated with many cellular activities, including cell proliferation, cell migration, cell invasion, and cell apoptosis.[56,68] This receptor has also been implicated in several cancers; LPA_1 expression levels have been found to have abnormal in many cell lines and tumours, including those for breast cancer, gastric cancer, liver cancer, lung cancer, and ovarian cancer.[69] The involvement of LPA_1 in ovarian cancer has been well documented; in a 2019 study, elevated expression of LPA_1 in ovarian serous cystadenocarcinoma was associated with markedly higher cell proliferation, invasion, and migration, as well as a worsened prognosis.[70] Enhanced intratumoral heterogeneity was also observed, and it was shown that these effects were due to activation of the PI3K/Akt pathway via the $G_{i/o}$ protein.[70] However, of particular interest to this thesis is the involvement of LPA_1 in breast cancer development. Studies have demonstrated that LPA_1 has an increased expression level in breast cancer cell lines compared to non-tumorigenic cell lines, and in several of these cell lines, the activation of LPA_1 was able to increase cell migration and invasion.[71–73] For example, the highly invasive breast cancer cell line MDA-MB-231 is a frequently used cell line to model mammary metastatic carcinoma *in vitro*. In a study performed by Li et al., the MDA-MB-231 cell line displayed an 86-fold increase in expression level compared to the MCF-10A cell line, which is widely used as a non-tumorigenic model for normal breast function.[74,75] As well, other common breast cancer cell lines, such as HS578T and MDA-MB-435, also display elevated expression levels of LPA_1 (6-16-fold increase).[74] In murine breast cancer models, inhibition of LPA_1 was shown to have anti-cancer effects. The silencing or pharmacological inhibition of LPA_1 has been demonstrated to greatly reduce tumor sizes and reduce breast cancer metastasis to the liver and the lungs, while the inverse was seen in murine

models with overexpression of LPA_1.[73,76,77] These results were largely supported by separate studies.[78,79] Due to the high amount of evidence, it is believed that the LPA_1 receptor has an important role in the progression of breast cancer, making it an appealing target for new pharmaceuticals. Its increased expression level in breast cancer may potentially allow for useful ligands that can target LPA_1 to exploit this for diagnostic imaging, while inhibition of LPA_1 may allow for novel breast cancer treatment methods by blocking its pro-cancer effects.

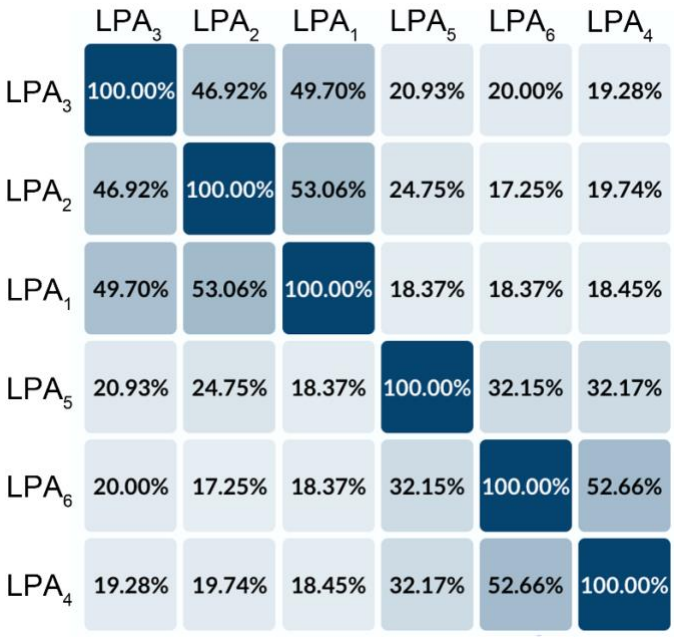

Figure 3 – Sequence similarity matrix of the six identified LPA receptors. Matrix was generated by UniProt Align tool using the following Accession Numbers: Q92633 (LPA_1); Q9HBW0 (LPA_2); Q9UBY5 (LPA_3); Q99677 (LPA_4); Q9H1C0 (LPA_5); and P43657 (LPA_6).

LPA_2 was discovered in 1998 using a gene sequence search.[80] This LPA receptor shares ~53% and ~46% of its amino acid sequence with LPA_1 and LPA_3, respectively, but only shares ~17-24% of its sequence with the LPA_{4-6} receptors (**Figure 3**). The activation of LPA_2 and its associated signaling pathways through the $G_{i/o}$, $G_{q/11}$, and $G_{12/13}$ proteins has been associated with cell survival, cell migration, anti-apoptosis, and the alteration of gene expression.[66,69] Furthermore, it has been reported that LPA_2 may play a role in the progression of breast, colon, endometrial, and

ovarian cancers, as well as melanoma; moreover, LPA_2 appears to be the most prominent LPA receptor involved in colon cancer.[66,81] Multiple reports have indicated that LPA_2 can enhance the proliferation of colon cancer cells through the activation of Kruppellike factor 5 and hypoxia-inducible factor 1α.[69,82] LPA_2 has also been shown to increase the resistance of tumor cells in the Caco-2 cell line to etoposide, a well-known chemotherapy drug, and the absence of LPA_2 was demonstrated to diminish tumour formation in murine models.[83,84] In terms of breast cancer development, LPA_2 has been reported to have increased expression level in surgically resected breast cancer tissue; increase breast cancer proliferation and migration; and present poor prognosis in the Chinese population among those with elevated expression levels.[69,85] However, it has also been shown that elevated levels of LPA are required to cause Rho-dependent cell migration via LPA_2 than LPA_1, suggesting that LPA_2 may contribute less to the progression of breast cancer than LPA_1.[86] Therefore, while modulation of LPA_2 might be worth pursuing for therapeutic purposes, it appears to represent a poorer target for breast cancer-specific pharmaceuticals compared to LPA_1.

LPA_3 was the third LPA receptor to be properly identified, with two research groups having reported the discovery of this receptor in 1999 through molecular cloning studies.[87,88] LPA_3 shares just under 50% of its amino acid sequence with both LPA_1 and LPA_2, and ~20% with each of the non-EDG receptors (**Figure 3**). This receptor couples with $G_{i/o}$ and $G_{q/11}$ to mediate LPA-induced adenylyl cyclase (AC) inhibition and activation, calcium mobilization, MAPK activation, and PLC activation, which results in physiological effects such as increased cellular motility and invasiveness.[66,69] LPA_3 is considered as one of the most prominent LPA receptors in several cancers, including in colon, liver, and lung cancers.[69] For example, in liver cancer, tumour cells with elevated expression of LPA_3 have been shown to have increased resistance to several chemotherapy drugs, and that it is likely a contributor to liver cancer proliferation and invasion.[89,90] LPA_3 has also been described as an essential contributor to cell viability and proliferation for melanoma.[91] However, LPA_3 appears to have a lesser role in breast cancer initiation and

progression. Although antagonism of the LPA_3 receptor has been shown to decrease cellular motility and invasion in triple-negative breast cancer, its expression level in several breast cancer cell lines is contested between different research groups.[92,76,93] As well, in FM3A mouse mammary cancer cells, LPA_3-expressing cells showed significantly lower expression of vascular endothelial growth factor-A and vascular endothelial growth factor-C than LPA_1-expressing cells, which are involved in tumour development, metastasis, and progression.[94] Due to the seemingly conflicting nature of LPA_3's involvement in breast cancer, this receptor is not currently regarded as having a high potential for breast cancer-specific pharmaceuticals. However, further inquiry may prove useful in ascertaining the specific role of LPA_3 in the development of breast cancer.

1.2.1.2 – Non-Endothelial Differentiation Gene (Non-EDG) Subfamily

The last three LPA receptors to be classified as such, LPA_{4-6} share 32-52% in amino acid sequence with each other, but only share ~17-25% in amino acid sequence with the three EDG receptors (**Figure 3**). LPA_4 was first discovered in 1997 as the orphan receptor P2Y9, but was later renamed to LPA_4 in 2003 after displaying specific binding for LPA in a calcium mobilization assay during what was considered a "de-orphaning project", becoming the first member of the non-EDG family of LPA receptors.[95–97] Prior to this, it was believed that endogenous LPA only enacted its biological functions through LPA_{1-3}. LPA_5 was similarly discovered and given a different name before subsequent reclassification as an LPA receptor. LPA_5 was discovered using a high-throughput database search and identified as GPR93 in 2001; interestingly, in this study, GPR93 was noted to have a high sequence similarity to P2Y5, which was the contemporary name for LPA_6 at that time.[98] GPR93 was later renamed as LPA_5 after a screening using reverse transfection and cell-based assays was performed in 2006.[99] Finally, LPA_6 was first discovered as 6H1 after isolation from a chicken T cell library in 1993, was later designated as P2Y5 in 1996 after it showed high sequence similarity with other P2Y receptors, and was again renamed in

2009 to LPA_6 after the receptor was shown to respond to LPA with activation of the $G_{12/13}$ Rho pathway.[100–102]

LPA_4 is known to couple to $G_{12/13}$, $G_{q/11}$, $G_{i/o}$, and G_s proteins, LPA_5 can couple to $G_{12/13}$ and $G_{q/11}$ proteins, and LPA_6 can couple to $G_{12/13}$, $G_{i/o}$, and G_s proteins. Through their associated signaling pathways, LPA_4 and LPA_5 are most notable for their ability to negatively regulate cell migration and invasion in mouse embryonic fibroblasts and sarcoma cells respectively, which is in direct contrast to the cellular effects of the three EDG receptors.[103,104] LPA_6 is most prominently known for being the first GPCR to be implicated as essential for the maintenance of human hair growth.[105] In terms of breast cancer research, LPA_6 has been reported as a potential tumor suppressor, and expression of LPA_6 was found to negatively correlate with cancer-promoting factors in a 2019 study.[106] Overall, however, relatively little is known about the relationship between the non-EDG receptors and disease conditions, much less their relationship with breast cancer. As the non-EDG LPA receptors are less studied than their EDG family counterparts due to their more recent identification as LPA receptors, it is impossible to give a definitive answer regarding their potential in breast cancer pharmacology. Further investigation is necessary to determine the potential of these receptors for breast cancer drug development.

1.3 – Positron Emission Tomography

Several medical imaging modalities have already been discussed earlier in this chapter, including X-ray, mammography, ultrasound, and MRI. However, one other important imaging modality that has yet to be discussed is positron emission tomography (PET). PET is a highly sensitive and non-invasive three-dimensional nuclear imaging modality that allows for the visualization and monitoring of physiological processes within the body. This type of imaging is called ‘functional imaging’; in contrast, X-ray, mammography, ultrasound, and MRI are typically used as ‘structural imaging’ modalities and are only able to show structural information within the body, although some methods have been developed to perform functional imaging with these

modalities in recent years. Functional imaging is often preferable due to its ability to determine metabolic activity and biochemical processes that are occurring in tissues and organs; whereas structural imaging allows for the visualization of abnormal tissue, functional imaging can allow for precise insight into the underlying physiological functions. This makes PET a valuable tool for the diagnosis of a variety of purposes, including the assessment of brain activity, the evaluation of cardiac performance, and the detection and characterization of tumours.

1.3.1 – PET Basics

Functional imaging with PET requires the administration of a pharmaceutical tagged with a radioactive isotope that has a known ability to bind to a specific target that is associated with the biological function of interest. An appropriately chosen biomarker should have a higher *in vivo* concentration when the body is undergoing the studied biological function, and the radiopharmaceutical should have high selectivity for this biomarker. After the radiopharmaceutical is administered to the patient, usually via intravenous injection, the radiopharmaceutical travels throughout the body and accumulates preferentially in regions where the biomarker is highly concentrated. While in the body, the radionuclide that is tagged onto the pharmaceutical undergoes beta-plus (β^+) decay, emitting a positively charged subatomic particle called a positron. The positron travels a short distance from the decay event before colliding with one of the many electrons within the body; this collision, known as annihilation, produces two 511 keV annihilation photons that travel in opposite directions and are detected by a ring of detectors that surround the patient. The detected photons are used to reconstruct an image that represents the distribution of the pharmaceutical within the body, which provides important information about physiological processes occurring in the patient's body. By analyzing the distribution of this radiopharmaceutical, researchers and clinicians can study and quantify the changes in function within the patient's body and can identify abnormal or diseased conditions.

Although PET is very useful imaging modality, it often cannot be used alone. PET is usually coupled with computed tomography (CT), which is a sophisticated X-ray imaging procedure that digitally combines a series of X-ray images taken from different angles to produce cross-sectional images of the body, giving detailed anatomical information with high image resolution. By combining the functional information of PET with the structural information of CT, this allows for the precise identification and localization of abnormalities within the body. While PET alone can be useful in certain cases, the combination of these two modalities certainly improves diagnostic accuracy. Other advantages of PET-CT include early disease detection, as many structural imaging modalities such as MRI struggle to detect the early stages of disease progression while PET can identify metabolic changes before structural changes become apparent; high sensitivity, as it is generally agreed upon that PET has the highest sensitivity of any imaging modality, meaning that diseased patients will have the highest chance of being correctly diagnosed; and a reduced need for multiple scans, as combining two complementary modalities into one scan reduces imaging time for the patient. Apart from PET/CT, PET/MRI has also seen use in recent years to obtain the anatomical background, although its use has been relatively limited.[107]

Although PET and PET/CT are highly effective, there are a few disadvantages. PET is one of the most expensive imaging modalities, and highly specialized machines are required for imaging. PET also has a relatively longer procedure and scan time. Combined, these make PET unfavourable for general screening purposes. PET and PET/CT also involve ionizing radiation, which always poses a risk for bodily harm, even if it is minimal. Standalone PET imaging also has lower spatial resolution than other common imaging modalities, but this can be mostly negated by coupling with CT.[108] These disadvantages notwithstanding, PET imaging represents an incredibly useful diagnostic imaging tool that is at the forefront of modern imaging techniques.

1.3.2 – PET Radioisotopes

There are several radioisotopes that are used for PET imaging. The chosen radioisotope varies depending on the application, with certain radioisotopes being more appropriate for the imaging of certain conditions while others are more applicable for other conditions. The most common radioisotopes that are currently in use are listed in **Table 4**; these are namely carbon-11 (^{11}C), nitrogen-13 (^{13}N), oxygen-15 (^{15}O), fluorine-18 (^{18}F), copper-64 (^{64}Cu), gallium-68 (^{68}Ga), rubidium-82 (^{82}Rb), and iodine-124 (^{124}I).[109]

Important factors when deciding which radionuclide to use for a particular PET imaging experiment include isotope half-life, emitted positron energy, biological target, and availability and ease of production. When using small molecules radiopharmaceuticals, a short half-life can be beneficial as these molecules usually will quickly distribute throughout the body and because a short half-life can allow for multiple imaging procedures in one day, if desired; however, if the half-life is too short, then it may be required to prepare the radiopharmaceutical on-site, which requires special facilities. A longer half-life means that images can be taken over a longer period of time with a single injection, which may be beneficial for some applications. Typically, long-lived radioisotopes are tagged onto pharmaceuticals such as peptides or proteins. Positron energy is also a large factor to consider. A higher positron energy means that a given positron will have higher penetrating power, meaning it will travel farther from the point of decay before annihilation. Therefore, a radionuclide that generates low-energy positrons is generally desirable, since the shorter the distance that the emitted positrons travel, the more accurate the resulting image will be. The biological target, or biomarker, also can be an important factor when selecting the radioisotope. If the target is located in the brain, for instance, metal radioisotopes may have a difficult time crossing the blood-brain barrier and reaching the target, as is the case for $^{64}CuCl_2$.[110] Lastly, the availability of a radionuclide and its ease of production also play an important role in selecting the most desirable radionuclide for a particular application. In order to use a radionuclide, it must first be generated; this requires specific production facilities such as cyclotrons and

radionuclide generators. If a radionuclide with a short half-life is desired, then it is crucial for the correct production facilities to be located nearby. Radionuclides with longer half-lives have the benefit of being able to be transported over longer distances, making them accessible even in locations without dedicated radionuclide production facilities. From a synthetic standpoint, radionuclides also should be easily incorporable into the pharmaceutical; radionuclides should be added to pharmaceuticals as late into the synthetic scheme as possible, and reactions should be fast and high yielding. Depending on the chemical structure of the unlabelled pharmaceutical, certain radionuclides may be preferable due to better chemical compatibility.[109]

Table 4 – Most common radionuclides used in PET imaging[109]

Radionuclide	Half-life	Positron energy (keV, max)
^{11}C	20.4 minutes	960
^{13}N	9.97 minutes	1190
^{15}O	2.05 minutes	1720
^{18}F	109.7 minutes	635
^{64}Cu	12.7 hours	653
^{68}Ga	67.7 minutes	1900
^{82}Rb	1.27 minutes	3150
^{124}I	4.18 days	2138

1.3.2.1 – Fluorine-18

^{18}F is possibly the most advantageous radionuclide for PET imaging. It can be easily produced in high quantities by a cyclotron and owing to its medium-length half-life of just under two hours, it can be generated and transported over a short distance to other healthcare facilities while also being cleared from the body relatively quickly. ^{18}F is attractive for this thesis, since a cyclotron

facility is available nearby. ^{18}F also has the lowest maximum positron energy out of all of the common PET radionuclides, meaning the images that are produced from the usage of ^{18}F-radiopharmaceuticals tend to have higher accuracy. Fluorine also has the benefit of acting as an isostere of common functional groups such as hydrogen and hydroxyl groups; the substitution of these groups with fluorine can, in many cases, improve the pharmaceutical's metabolic stability and target affinity.[111,112] Additionally, a diverse set of radiofluorination reactions have been developed for the addition of ^{18}F to pharmaceuticals, meaning that chemical incorporation of this radionuclide can be performed using a variety of methods.[113] Overall, it can be concluded that fluorine-18 is a highly useful radionuclide for PET imaging. The application of fluorine-18 PET imaging to the work of this thesis will be further explored in Chapter 5.

1.3.3 – Use of PET for Cancer Detection

PET oncology can be used for tumour detection, tumour staging, evaluation of treatment response, detection of recurrent cancer, and radiation treatment planning.[114] In this field, the most common radiopharmaceutical used is fluorodeoxyglucose F-18, or [^{18}F]FDG, being used for the PET imaging of over 90% of cancers.[115] This chemical compound is a glucose analogue with one hydroxyl group substituted for one ^{18}F atom, and it imitates the biological activities of glucose within the body. Nearly all cells metabolize glucose, and therefore [^{18}F]FDG, as their primary source of energy through a biochemical process called mitochondrial oxidative phosphorylation, which oxidizes glucose to adenosine triphosphate (ATP).[116] However, compared to healthy cells, tumour cells have an increased uptake of glucose due to the Warburg effect; this effect describes the preference of cancer cells to metabolize glucose through aerobic glycolysis rather than mitochondrial oxidative phosphorylation, and due to the relative inefficiency of aerobic glycolysis, tumor cells are required to consume an elevated level of glucose.[116] The increased uptake of glucose/[^{18}F]FDG can be exploited by using PET imaging; PET imaging can reveal areas with elevated uptake, which can be indicative of cancerous tissue. Unfortunately, cancerous tissue is

not the only type of abnormal tissue with increased uptake. For breast cancer imaging, false positives may be observed as a variety of benign conditions within the breast also have an increased uptake of [^{18}F]FDG, as is the case with certain acute and chronic infections and atypical ductal hyperplasia.[117] Likewise, false negatives may also occur. Less aggressive subtypes of breast cancer may be overlooked on PET/CT images as the degree of [^{18}F]FDG uptake may not be different enough to make a decisive diagnosis, especially for smaller tumours.[117] Therefore, a new radiopharmaceutical that displays a higher selectivity for breast cancer tumours would be invaluable for the evaluation and diagnosis of breast cancer.

1.4 – Project Overview

It is clear that there is a need for both new breast cancer diagnostic tools and breast cancer therapeutics tools. Existing tools may be useful in many cases but are limited due to a variety of factors. As such, the primary goals for the research presented in this thesis are to develop a novel breast cancer imaging agent that can be used in PET imaging, and to develop a ligand that displays antagonistic qualities for the LPA_1 receptor. This will be accomplished using a combination of computational drug design, organic synthesis, biological evaluation, and radiochemistry.

Chapter 2: Ligand Design

In order to achieve the two goals detailed in Section 1.4, it is necessary to select an appropriate target within the body. As highlighted in Chapter 1, LPA_1 from the EDG-family of LPA receptors represents an intriguing target for both breast cancer diagnostics and therapeutics. Its increased expression level in breast cancer tumours and many breast cancer cell lines indicates that targeting LPA_1 with a radiopharmaceutical may have diagnostic benefits with PET imaging, while its role in the progression of breast cancer means that antagonism of this receptor may have important therapeutic implications.

2.1 – Targeting the LPA_1 Receptor: Antagonists from the Past to Present

Initial studies into LPA_1 antagonist development were performed by making minor modifications to a previously identified LPA_1 agonist, *N*-acyl ethanolamide phosphoric acid, which shares high structural similarity to endogenous LPA (**Figure 4**). Derivative compounds of *N*-acyl ethanolamide phosphoric acid containing bulky groups such as aromatic rings demonstrated antagonistic tendencies after performing these structural substitutions; one compound in particular, VPC12249, which contained a bulky benzyl-4-oxybenzyl substituent, was found to have no agonistic activity whatsoever while displaying moderate selectivity for LPA_1.[118] Other lipid-based LPA_1 analogues have also been reported, such as derivatives of the naturally occurring LPA analogue, cyclic phosphatidic acid.[119]

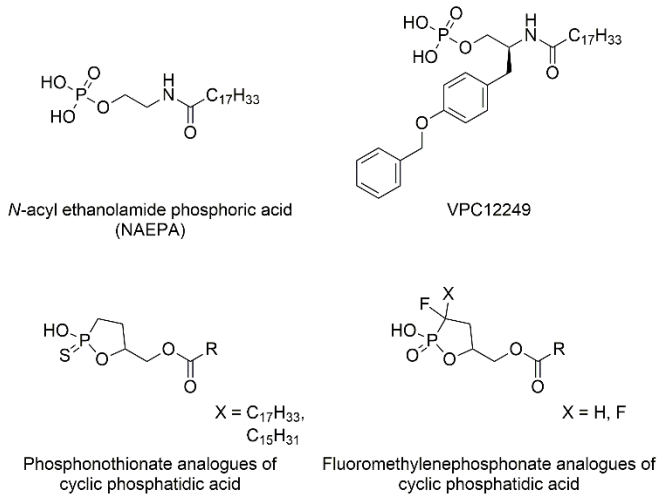

Figure 4 – Chemical structures of selected lipid LPA_1 antagonists

However, because lipid-based compounds often display poor bioavailability due to their innately high hydrophobicity, recent studies have shifted their focus from the synthesis of lipid-based LPA analogues to non-lipid small molecules that have increased hydrophilicity (**Figure 5**). One of the first non-lipid LPA_1 antagonists was discovered by the Kirin Brewery Co. Ltd. in 2003. This compound, called Ki16425, demonstrated good antagonism against both LPA_1 and LPA_3 in both a calcium flux assay and a GTP [$\gamma^{35}S$] assay.[120] After the discovery of this compound, several research groups synthesized derivatives of Ki16425, including a series of analogues developed by Amira Pharmaceutical. The most promising ligands from this study included AM966, AM095, and BMS-986020. These compounds showed high potency and selectivity for LPA_1, with half-maximal inhibitory concentrations (IC_{50}) in the low nanomolar range for LPA_1 and in the micromolar range for $LPA_{2\text{-}6}$. Major structural changes from Ki16425 to these newer ligands were the substitution of a sulfur atom for an additional phenyl group, the shortening of the long aliphatic chain, the oxidation of the ester group to a carboxylic acid, and in the case of BMS-986020, the addition of a cyclopropane group in the carboxylic acid alpha position.[121,122]

In 2012, a new analogue which utilized the beneficial structural changes demonstrated by Amira Pharmaceuticals was reported by a research group from Roche. This compound, called RO6842262, was structurally identical to BMS-986020 except the isoxazole core in BMS-986020

was replaced with a triazole core. This change enhanced the potency and selectivity for LPA_1 even further, with an LPA_1 IC_{50} value of 25 nM and an LPA_3 IC_{50} value of > 30,000 nM in a calcium flux assay; other LPA receptors were not tested. In human lung fibroblasts, RO6842262 demonstrated an ability to decrease LPA-induced cell proliferation and contraction.[123,124] The same research group from Roche reported a novel series of carboxylic acid 5-amino-4-cyanopyrazole analogues two years later that also acted as LPA_1 antagonists. Three compounds in this series had high potency and selectivity for LPA_1 in a FLIPR assay, although were slightly worse in both categories compared to RO6842262 (LPA_1 IC_{50} = 74-111 nM, LPA_3 IC_{50} > 30,000 nM).[125]

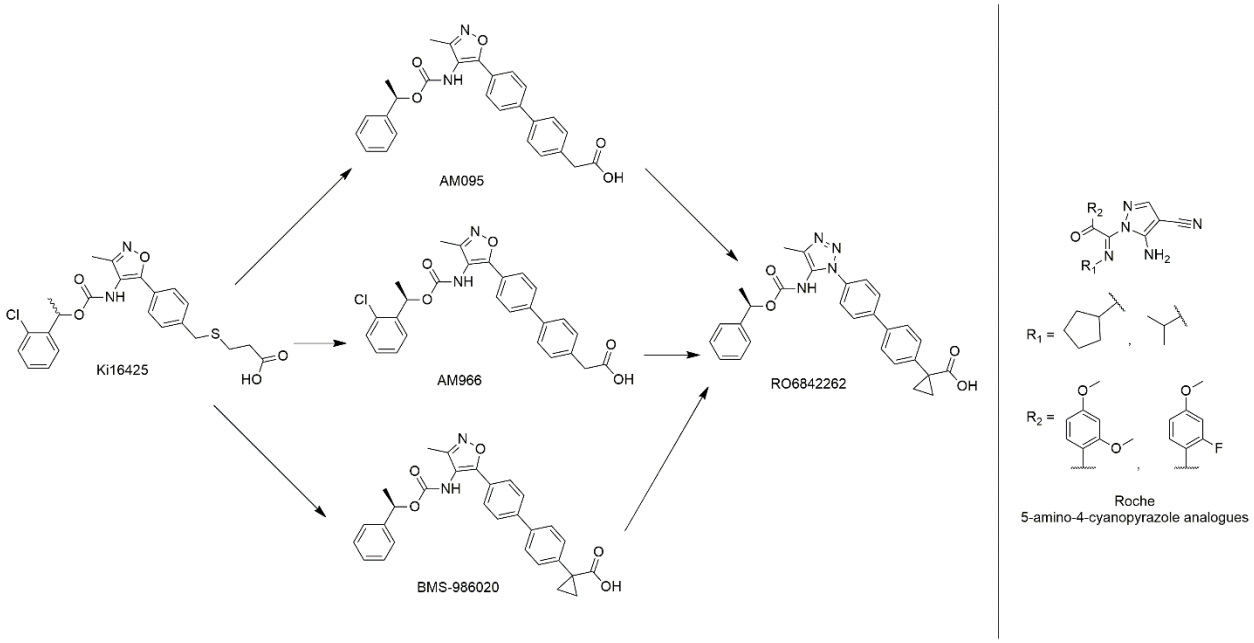

Figure 5 – Chemical structures of Ki16425 and derived LPA_1 antagonists

In 2016, researchers at Ono Pharmaceutical Co., Ltd. published their discovery of a novel compound with high potency and selectivity for LPA_1 that was optimized from a high-throughput screening (LPA_1 IC_{50} = 160 nM, LPA_2 IC_{50} = 8,600 nM, LPA_3 IC50 > 10,000 nM). This compound, ONO-7300243, demonstrated therapeutic abilities in both a rat intraurethral pressure model that was induced by LPA and in the lung cancer cell line, A549.[126,127] Further optimization led to the

development of ONO-0300302, which had an IC_{50} of 0.16 nM for LPA_1 in a calcium assay after a 24-hour incubation period. However, the selectivity of this compound was not explored.[128] Finally, Astellas Pharma Inc. reported the biological activity of their ONO-7300243 analogue, ASP6432, that contained a sulfamoyl thiazole moiety that is linked to the amide through a methylene bridge. This compound had an IC_{50} of 11 nM for human LPA_1 and IC_{50} values of > 10,000 nM, > 10,000 nM, 114 nM, and > 30,000 nM for the $LPA_{2\text{-}5}$ receptors, respectively, demonstrating high potency and selectivity for LPA_1, except for the relatively high activity shown towards the LPA_4 receptor.[129]

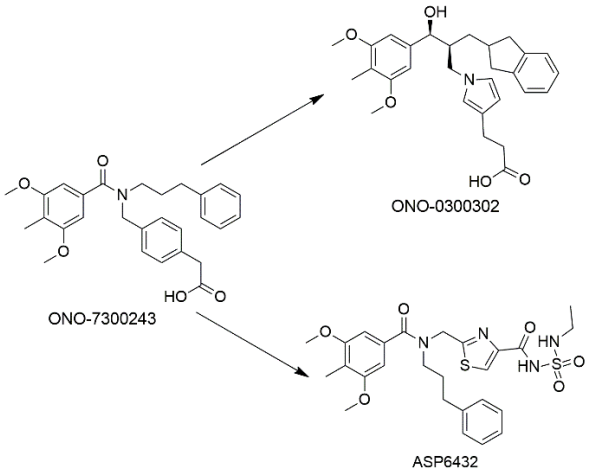

Figure 6 – Chemical structures of ONO-7300243 and derived LPA_1 antagonists

2.1.1 – LPA-Targeting Ligands in Clinical Trials

As of now, there are no drugs targeting LPARs that have been approved by the FDA. However, there are several LPA_1 antagonists that have entered clinical development.[130–133] SAR100842 is an LPA_1 inhibitor developed by Sanofi-Aventis with an IC_{50} of <0.1 μM.[134] This compound inhibited downstream $G_{\alpha i}$ and β-arrestin signaling without any effect on $G_{\alpha q}$ signaling *in vitro*, and therefore turned out to be a negative allosteric modulator of the LPA_1 receptor.[135] Currently, this compound is at phase II of clinical trials for the treatment of systemic sclerosis.[133] The therapeutic effect of SAR100842 was observed in patients with diffuse cutaneous systemic sclerosis after oral dosing, demonstrated by a decreased modified Rodnan skin thickness score and severity of pruritus.[136]

BMS-986020 (**Figure 5**) is an α-substituted AM095 analogue with a cyclopropane moiety.[137] Clinical trials showed that treatment with BMS-986020 in patients with idiopathic pulmonary fibrosis could ameliorate the decline in pulmonary function and improve the bio markers of fibrosis or inflammation compared with patients treated with a placebo.[131,138] In a mouse model of ischemia, administration of BMS-986020 improved brain functions and survival rate by attenuating microglial activation, lipid peroxidation, and cell apoptosis.[139]

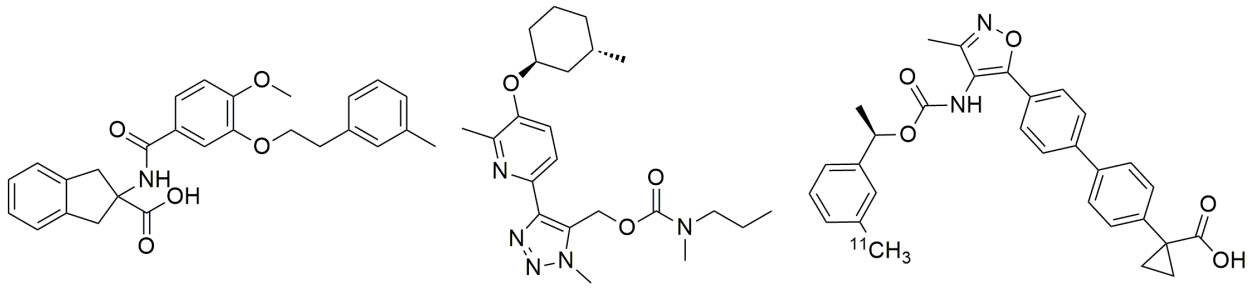

Figure 7 – Chemical structures of LPA_1 ligands in clinical trials

BMS986278 is a potent antagonist that blocks LPA_1-mediated G_i, G_q, G_{12}, and β-arrestin signaling pathways in primary human lung fibroblasts.[140,141] Phase I studies showed that it was generally well-tolerated and did not pose the same risk for hepatobiliary toxicity as BMS986020. It is currently in phase II trials for the treatment of lung fibrosis.[142] To date, there is only one PET radioligand reported that targets the LPA_1 receptor; currently, it is at phase I of clinical trials.[132] This compound, ^{11}C-BMT-136088, was imaged and evaluated with PET using rhesus monkeys *in vivo*. The pharmacokinetic parameters showed that ^{11}C-BMT-136088 is a promising tracer to detect potential upregulation of the LPA_1 receptor in lung fibrosis with PET.[143,144] It is anticipated that ^{11}C-BMT-136088 will also be beneficial for clinical evaluation of BMS-986020.

Although several small molecules targeting LPA_1 have made it to clinical trials for their evaluation in lung fibrosis and systemic sclerosis, to this point, there are no clinical trials involving the evaluation of small molecules targeting LPA_1 for breast cancer regulation. Furthermore, while a small number of molecules targeting other receptors have been identified with varying results,

these have largely been repurposed from targeting other diseases or cancer types.[145] As a result, these repurposed ligands are generally non-specific for breast cancer. As such, a novel ligand that can specifically target the LPA_1 receptor for breast cancer diagnostics or therapeutics would hold great significance.

2.2 – Introduction to Scaffold Hopping

Scaffold hopping is a strategy employed in medicinal chemistry that is used to explore alternative chemical frameworks while preserving or enhancing the desired biological activity of a well-characterized drug molecule. This approach is derived from the concept that structurally diverse molecular scaffolds can exhibit similar biological activities by replicating analogous molecular interactions using bioisosteric replacements.[146] The goal of scaffold hopping is to identify novel 'scaffolds', or core structural components, that can serve as a foundation for the development of new drug candidates with improved pharmacological properties.[147] This drug discovery method has been successfully applied in many drug discovery projects in the literature, such as in the discovery of the investigational drug motesanib by the ring opening scaffold hopping of the known vascular endothelial growth factor 2 and Flt-1 inhibitor, PTK787/ZK222584.[148,149] By employing scaffold hopping, the drug discovery process can be accelerated by providing alternative starting points based on proven chemical compounds, leading to the facile development of more effective and safer drug candidates that are more readily patentable.

2.2.1 – Application of Scaffold Hopping to RO6842262

In Section 2.1, the triazole-based Ki16425 derivative, RO6842262, was identified as a highly potent ligand targeting the LPA_1 receptor. RO6842262 also displayed a high degree of selectivity for LPA_1, with > 1,200-fold selectivity for LPA_1 over LPA_3. RO6842262 also displayed an ability to attenuate cell proliferation and contraction in an *in vitro* experiment using human lung fibroblasts. Based on the promising results shown by the optimization of Ki16425 and subsequent development of RO6842262, it is believed that further structural optimization could yield an even more potent and selective LPA_1 antagonist. Since the biological activity of RO6842262 has already been determined, it is proposed that the application of scaffold hopping to this ligand could hold the key to obtaining an optimized structure with a novel chemotype that displays enhanced pharmacological properties.

One common strategy used in scaffold hopping is closing a ring structure. When a ligand interacts with its protein target, it must overcome an entropic barrier in order for binding to occur due to a loss of ligand mobility. However, this can be mitigated by reducing the mobility of the ligand before it even enters the biological system via a ring closure. By performing a ring closure in the core structure of the designed ligand, this can lock a molecule into its bioactive conformation, decreasing the entropy penalty that it faces when interacting with its target.[147] Armed with this knowledge, a ring closure was imposed upon RO6842262, exchanging its triazole carbamate core for a 3*H*-1,2,3-triazolo[4,5-*d*]pyrimidine core (**Figure 8**).

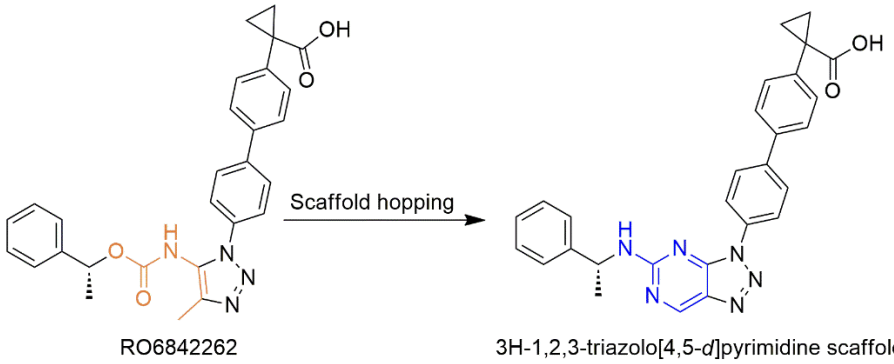

Figure 8 – Discovery of the 3*H*-1,2,3-triazolo[4,5-*d*]pyrimidine core using scaffold hopping

2.2.1.1 – Docking Studies Using AutoDock Vina

In order to compare the new scaffold to that of RO6842262, a molecular docking study was performed. Molecular docking is a computational drug design technique used to study the interactions between a ligand and its receptor. It is widely used in the early stages of drug discovery to predict how a potential drug molecule binds to its target protein and to estimate its binding affinity. To this end, AutoDock Vina was used. AutoDock Vina is a standard program used in molecular docking studies that employs a complex scoring function to evaluate ligand binding interactions. Various physical and chemical factors are taken into consideration, such as hydrogen bonding, hydrophobic interactions, and steric interactions.[150]

For this study, the crystal structure of LPA_1 (PDB ID:4z36) was used to perform molecular docking.[151] The three-dimensional structures of the proposed compounds were generated using DS Viewer 3.5 after importing from a two-dimensional chemical drawing program.[152] Molecular docking was performed for both RO6842262 and the novel scaffold using AutoDock Vina.[153] The dimensions of the grid box were set large enough to encompass the entire binding pocket of the LPA_1 structure. All other parameters were left as default.

Using AutoDock Vina, 13 different binding modes were predicted for RO6842262. Binding free energy ranged from -8.2 kcal/mol to -10.1 kcal/mol. For the 3*H*-1,2,3-triazolo[4,5-*d*]pyrimidine scaffold, 11 different binding modes were predicted. These binding modes ranged in binding free energy from -8.2 kcal/mol to -11.1 kcal/mol. For the top-ranked pose of RO6842262, several interactions were predicted, including pi-anion interactions between GLU293 and the phenyl ring adjacent to the carboxylic acid as well as between ASP129 and the triazole moiety, pi-alkyl interactions between MET198 and the phenyl ring that is directly bonded to the triazole moiety as well as between ALA300 and the phenyl ring that is linked to the scaffold via a secondary amine, and a pi-sigma interaction between ASP129 and the triazole core; each of these same interactions were also predicted between the novel scaffold and LPA_1. The top-ranked binding mode of the 3*H*-1,2,3-triazolo[4,5-*d*]pyrimidine scaffold is displayed in **Figure 9**. Overall, this molecule was found to have similar interactions with the orthosteric binding pocket (endogenous ligand binding

pocket) of LPA_1 as the top-ranked binding mode of RO6842262, with some distinctive differences. Hydrogen bonding was evident between Thr109, Lys294 and the carboxylic acid functional group, and many pi-anion and pi-alkyl interactions were conserved as previously mentioned. However, an additional hydrogen bonding interaction was predicted between Trp210 and the pyrimidine moiety for the new scaffold, whereas for the old scaffold, hydrogen bonding interactions involving the triazole core were not predicted. Additionally, another pi-pi stacking interaction was predicted between Trp271 and the phenyl group that is linked to the core of the molecule through an aminoethyl group that was not predicted for RO6842262. These may indicate a higher degree of stabilizing interactions between LPA_1 and the new scaffold than LPA_1 and RO6842262. This was supported by the predicted binding free energy of the novel scaffold having a value of -11.1 kcal/mol, while the top-ranked mode for RO6842262 only had a predicted binding free energy of -10.1 kcal/mol.

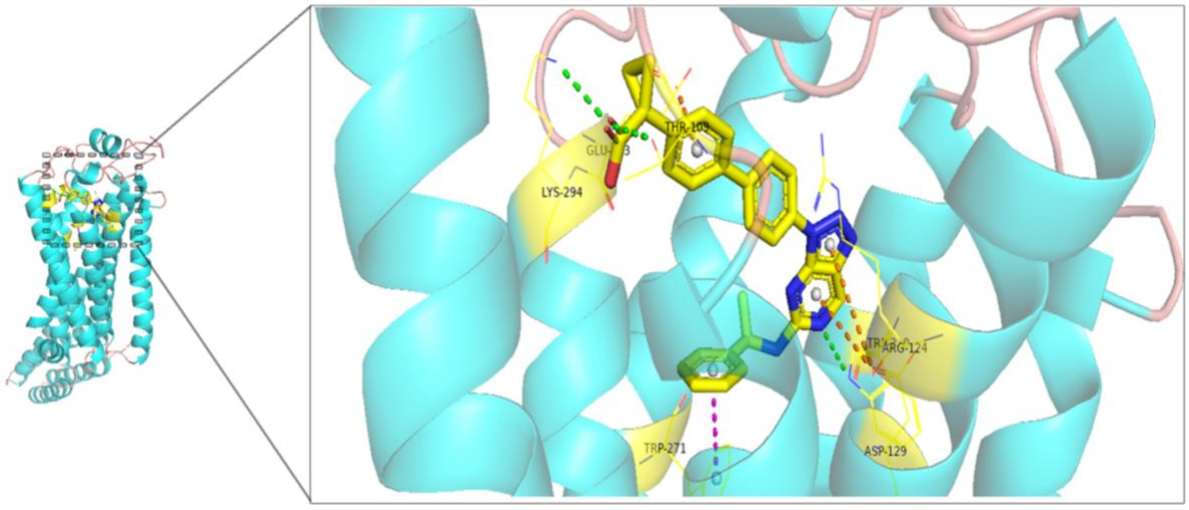

Figure 9 – Docking result of the novel scaffold in the orthosteric binding pocket of LPA_1 (left: overview of the ligand-bound LPA_1 complex; right: focused view of the ligand-receptor interactions for the 3*H*-1,2,3-triazolo[4,5-*d*]pyrimidine scaffold).

To complete this docking study, the top-ranked binding modes of RO6842262 and the novel scaffold were superimposed; this is displayed in **Figure 10**. These two molecules overlayed relatively favourably with only minor differences in molecular position. This indicates that the two scaffolds are likely to share a similar functional profile, which is a promising result for the novel scaffold.

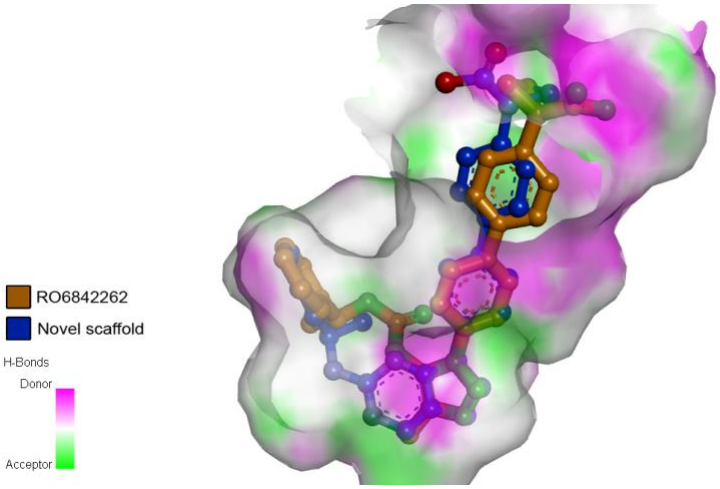

Figure 10 – Superimposed docking results of RO6842262 and the novel scaffold

2.3 – Designing a Library of Novel Small Molecules

With the novel scaffold decided, a series of analogues will be required in order to fully explore its competency. Of note, there appears to be a sizeable sub-pocket within the orthosteric binding pocket of LPA_1; modification of the interacting moieties may help attain a higher binding affinity and increase selectivity of these analogues for this receptor. This sub-pocket is located near the bottom-left of the LPA_1 orthosteric binding pocket, around the region where the docked ligands contain a phenylethanol substituent (RO6842262) or a phenylethanamine substituent (see **Figure 10**). Therefore, the design of analogues with minor structural modifications and substitutions in this region appears to present an auspicious opportunity, as these may allow for increased favourable interactions between the ligands and the receptor.

In order to fully explore the structure-activity relationship between the ligands and the receptor, a range of different building blocks are proposed (**Figures 11-14**). These building blocks are all nucleophilic in nature and can be added to the scaffold via nucleophilic aromatic substitution. The first substitutions proposed (**Figure 11**) are the two stereochemical forms of phenylethanol, and phenylmethanol.

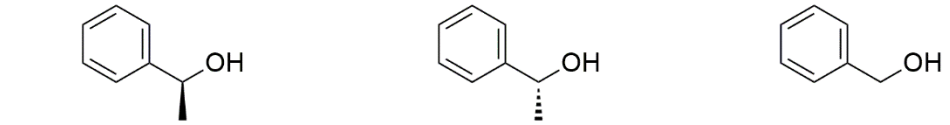

(*S*)-1-phenylethanol
1445-91-6

(*R*)-1-phenylethanol
1517-69-7

phenylmethanol
100-51-6

Figure 11 – Proposed alcohol building blocks for the novel scaffold

The (*R*)-1-phenylethanol building block is embedded in the structure of RO6842262, and so using this substituent for the novel scaffold would allow for a direct comparison between the two scaffolds. (*S*)-1-phenylethanol and phenylmethanol could also be used to determine the importance of the stereochemistry of this building block, and to determine the relative importance of this methyl group in general.

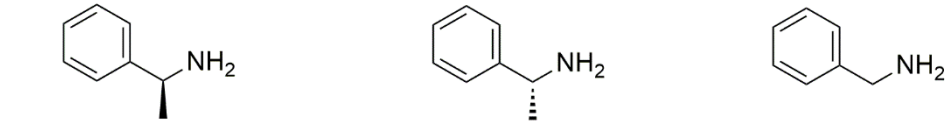

(*S*)-1-phenylethanamine
(2627-86-3)

(R)-1-phenylethanamine
(3886-69-9)

benzylamine
(100-46-9)

Figure 12 – Proposed amine building blocks for the novel scaffold

The second set of building blocks proposed (**Figure 12**) are the amine analogues of the compounds shown in **Figure 11**. Similar to the alcohol building blocks, the use of these three amine building blocks would be useful in determining the importance of stereochemistry and of the methyl group, in addition to determining the binding difference imposed by the substitution of the alcohol for an amine.

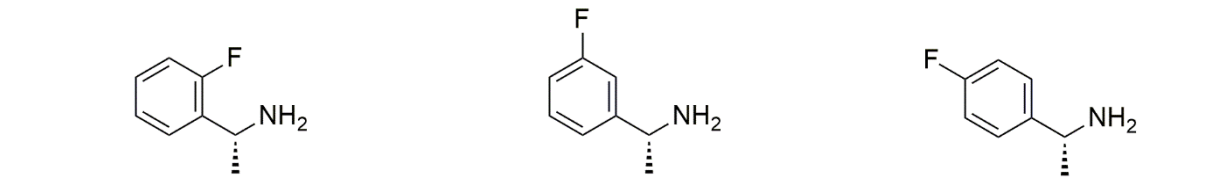

(*R*)-1-(2-fluorophenyl)ethanamine (185545-90-8)

(*R*)-1-(3-fluorophenyl)ethanamine (761390-58-3)

(*R*)-1-(4-fluorophenyl)ethanamine (374898-01-8)

Figure 13 – Proposed fluorine-containing amine building blocks for the novel scaffold

The third set of building blocks that are proposed (**Figure 13**) are fluorine-containing phenylethanamines. Substitutions at the ortho, meta, and para positions will allow for the determination of the optimal position for small substituents, as well as determining the optimal position for ^{18}F-labeling.

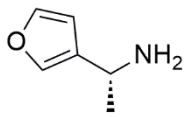

(*R*)-1-(furan-3-yl)ethanamine (2287239-47-6)

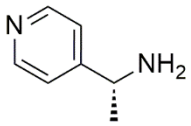

(*R*)-1-(pyridin-4-yl)ethanamine (1012067-91-2)

Figure 14 – Proposed isosteric heterocycle building blocks for the novel scaffold

The fourth set of building blocks (**Figure 14**) is centred around the use of isosteric heterocycles. The inclusion of heteroatoms may be able to exploit the hydrogen-bond donor residues located in the unexploited sub-pocket shown in **Figure 10**, thereby enhancing the interactions between ligand and receptor. Due to their ability to act as hydrogen bond receptors, oxygen and nitrogen are the most promising heteroatoms for these building blocks. Varying the size of the ring system, such as by using a five-membered ring instead of a six-membered ring, may also prove to be a worthwhile endeavour.

Chapter 3: Organic Synthesis and Structure Confirmation

3.1 – Proposal of a Rational Synthetic Scheme

With the ligand design components having been decided on, a rational synthetic scheme will need to be followed for the synthesis of these ligands. The synthesis of these analogues should be accomplished in as few reaction steps as possible and should be based on existing and well-known reactions and conditions. **Scheme 1** displays the synthetic scheme that was designed based on these principles. This is a six-step synthesis that uses common commercially available reagents and follows standard reaction procedures.

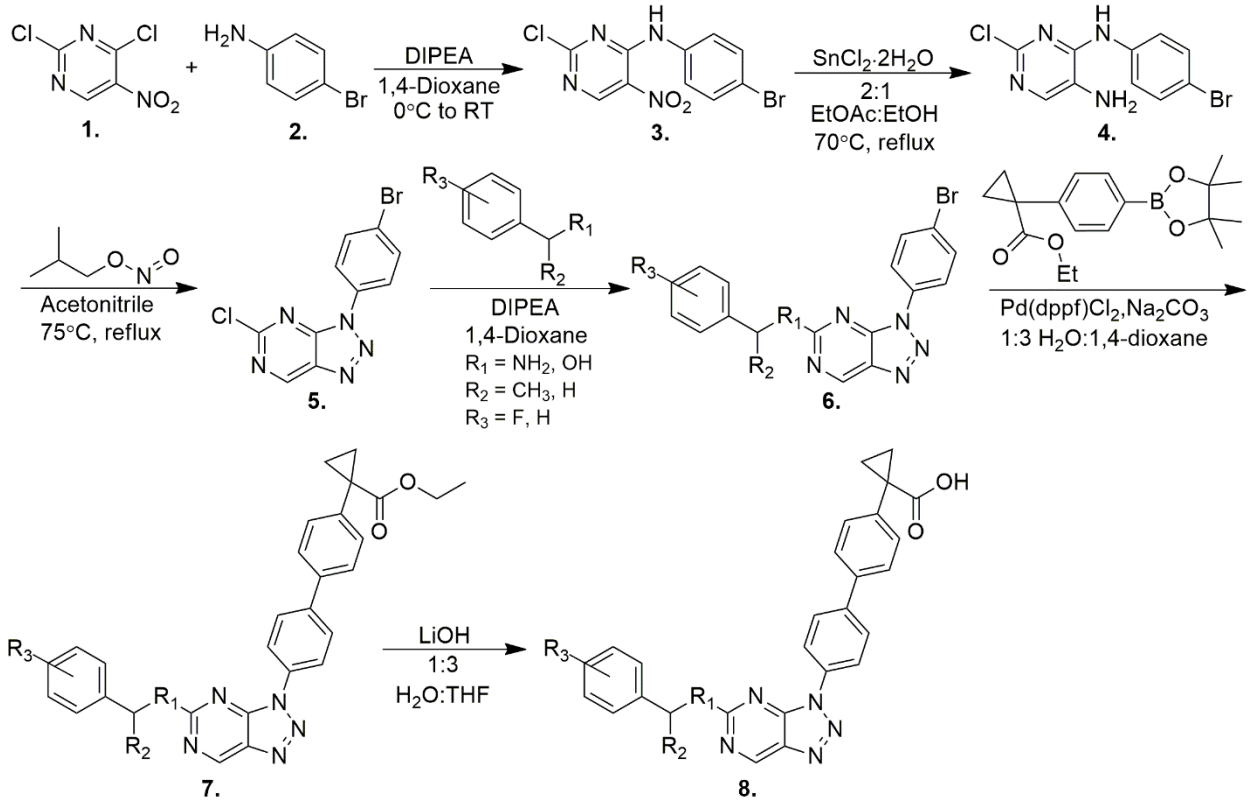

Scheme 1 – Synthesis of novel 3*H*-1,2,3-triazolo[4,5-*d*]pyrimidine LPA_1 antagonists

The first reaction is a nucleophilic aromatic substitution reaction in which the chlorine atom that is adjacent to the nitro group is replaced by 4-bromoaniline; a slight excess of the weak base, *N,N*-diisopropylethylamine (DIPEA), is used to neutralize the formed hydrochloric acid. This reaction is started at 0ºC and warmed up to room temperature to enhance the selectivity for the

indicated position.[154] In the second reaction, the nitro group contained in Compound **3** is reduced using $SnCl_2$•$2H_2O$ and ethanol (EtOH), which functions as both a solvent and a reagent. This technique has been reported to have high functional group tolerance, including in the presence of halogens.[155] The following reaction is a cyclization reaction, converting the primary and secondary amine from Compound **4** into a triazole ring using an alkyl nitrite at elevated temperature, forming a bicyclic system in Compound **5.**[156] The fourth reaction is another nucleophilic aromatic substitution; the remaining chlorine substituent on the pyrimidine is substituted by a selected nucleophilic building block, neutralizing the formed acid using DIPEA. Compound **6** then undergoes a Suzuki-Miyaura cross-coupling reaction under reflux using a bulky palladium catalyst in the presence of a base, coupling with an ester-containing boronic ester partner to produce Compound **7.**[157] In the final step, the ester group of the coupled intermediate is hydrolyzed using lithium hydroxide (LiOH) in a 1:3 ratio of water (H_2O) to tetrahydrofuran (THF), yielding the final carboxylic acid product **8** upon acid work-up.[158]

3.2 – Experimental Methods and Data

Section 3.2 will detail the experimental procedures that were performed as well as present the data that was collected to characterize each compound.

3.2.1 – Synthesis of Compound 3

*N-(4-bromophenyl)-2-chloro-5-nitropyrimidin-4-amine (**3**)*

A 0ºC solution of 4-bromoaniline (1893 mg, 11 mmol) in 1,4-dioxane (30 mL) was prepared using an ice bath. To this solution was slowly added 2,4-dichloro-5-nitropyrimidine (1940 mg, 10 mmol), shortly followed by the slow addition of *N,N*-diisopropylethylamine (1422 mg, 11 mmol) via syringe. The reaction mixture was allowed to warm to room temperature and then stirred for 1 hour. The reaction mixture was diluted with ethyl acetate and extracted with brine. The separated organic phase was dried over sodium sulfate, filtered, and evaporated. The residue was adsorbed to silica

and purified using flash silica gel column chromatography (EtOAc:Hexane = 1:10) to afford Compound **3** (2510 mg, yield: 76%). (APCI) m/z: [M + H]+ Calcd for $C_{10}H_7BrClN_4O_2^+$ 330.94; Found 331.5.

3.2.1.1 – Structure Confirmation for Compound 3

Structure was confirmed by mass spectrometry and following chemical reaction. Two regioisomers were produced due to the ability of the amine nucleophile to react at both the 2 and 4-chlorine positions. Some regioselectivity was conferred by adding the reagents at a decreased temperature, which was clearly visualized upon running thin-layer chromatography (TLC). The desired isomer was obtained in approximately a 3:1 ratio to the undesired isomer. Furthermore, both regioisomers were purified and were subsequently reduced, and then both were used in the cyclization reaction step. Since only the isomer with 4-bromoaniline substituted at the 4-position of the pyrimidine could undergo cyclization, the results of these parallel reactions confirmed that the more abundant isomer was the desired stereoisomer; the less abundant regioisomer substituted at the 2-position generated a variety of undesired products under cyclization conditions.

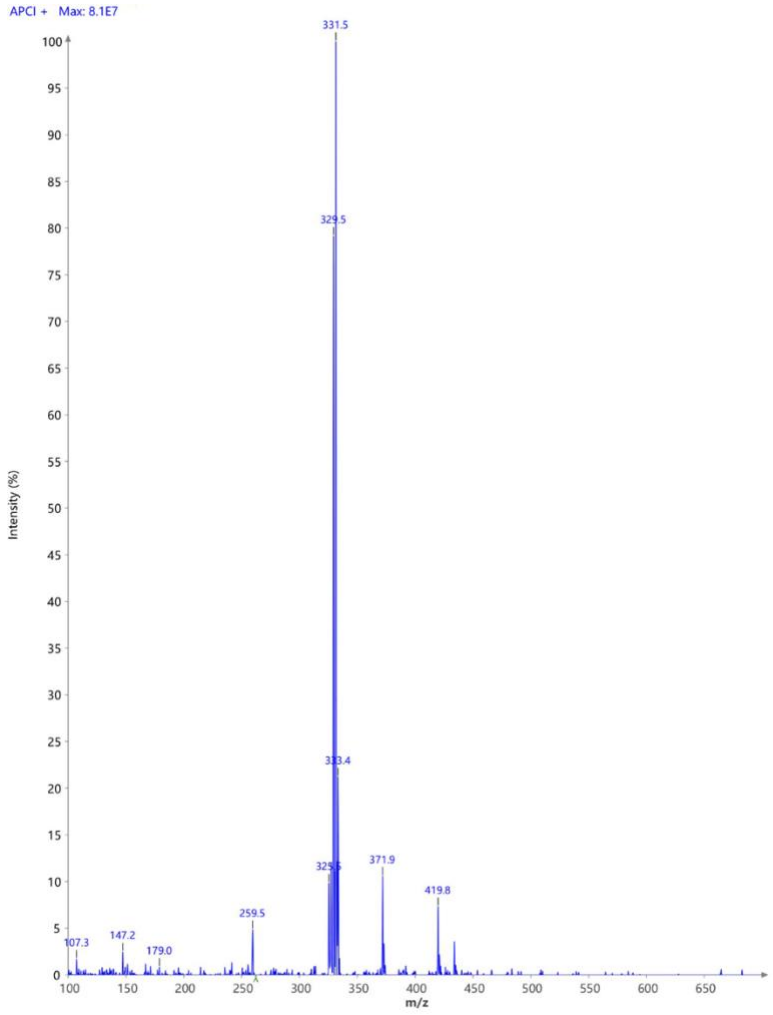

Figure 15 – Mass spectrum for Compound **3**

3.2.2 – Synthesis of Compound 4

*N^4-94-bromophenyl)-2-chloropyrimidine-4,5-diamine (**4**)*

Compound **3** (2510 mg, 7.61 mmol) was dissolved in a 1:2 mixture of EtOH:EtOAc (60 mL; EtOH = 342 mmol) and the reflux condenser was set up. $SnCl_2$•$2H_2O$ (5151 mg, 22.83 mmol) was weighed and slowly added to the stirring flask, and the reaction was heated to 70ºC. The reaction was stirred for 3 hours. After cooling to room temperature, a saturated solution of sodium carbonate was prepared and added to the reaction mixture. The basified solution was filtered through a pad of Celite, washed with EtOAc, dried over sodium sulfate, and evaporated. The residue was adsorbed to silica and purified using flash silica gel column chromatography (gradient;

1:10 EtOAc:Hexane to 1:1 EtOAc:Hexane) to afford Compound **4** (1640 mg, yield: 72%). ^{1}H NMR (500 MHz, $CDCl_3$) δ 7.89 (s, 1H), 7.55 (d, J = 9.0 Hz, 2H), 7.50 (d, J = 6.7 Hz, 2H), 7.09 (s, 1H), 3.10 (s, 2H). MS (APCI) m/z: [M + H]+ Calcd for $C_{10}H_9BrClN_4^+$ 300.97; Found 300.8.

3.2.2.1 – Structure Confirmation for Compound 4

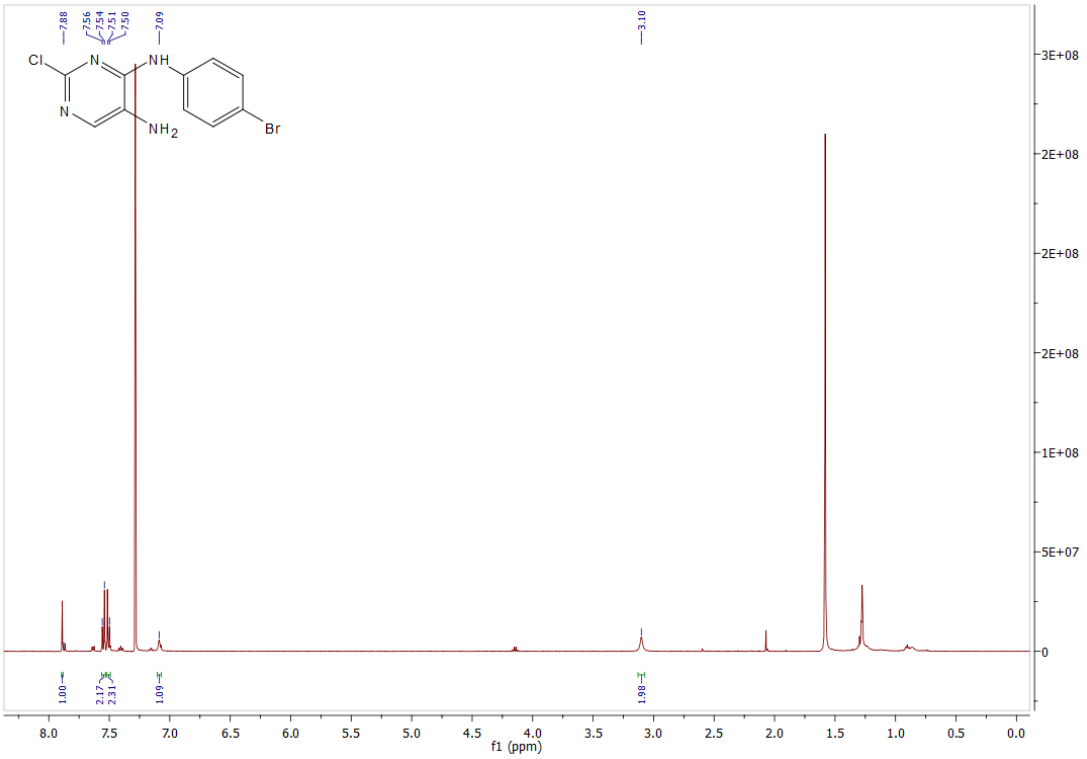

Figure 16 – ^{1}H NMR spectrum for Compound **4**

3.2.3 – Synthesis of Compound 5

*3-(4-bromophenyl)-5-chloro-3H-[1,2,3]triazolo[4,5-d]pyrimidine (**5**)*

To Compound **4** (1635 mg, 5.45 mmol) was added acetonitrile (25 mL), and a reflux condenser was set up. The solution was heated to 70ºC and isobutyl nitrite was slowly added via syringe. The reaction was allowed to continue for 16 hours and then slowly cooled to room temperature. EtOAc (50 mL) was added to the room temperature solution, after which it was further cooled to -20ºC. Orange-brown crystals formed and were collected by filtration and washed with cold EtOAc

and cold hexane. This recrystallization process was repeated a total of three times. The collected crystals were desiccated to give Compound **5** (1370 mg, yield: 80%). ^{1}H NMR (500 MHz, $CDCl_3$) δ 9.50 (s, 1H), 8.16 (d, J = 8.6 Hz, 2H), 7.78 (d, J = 8.7 Hz, 2H). MS (APCI) m/z: [M + H]+ Calcd for $C_{10}H_6BrClN_5^+$ 311.95; Found 311.9.

3.2.3.1 – Structure Confirmation for Compound 5

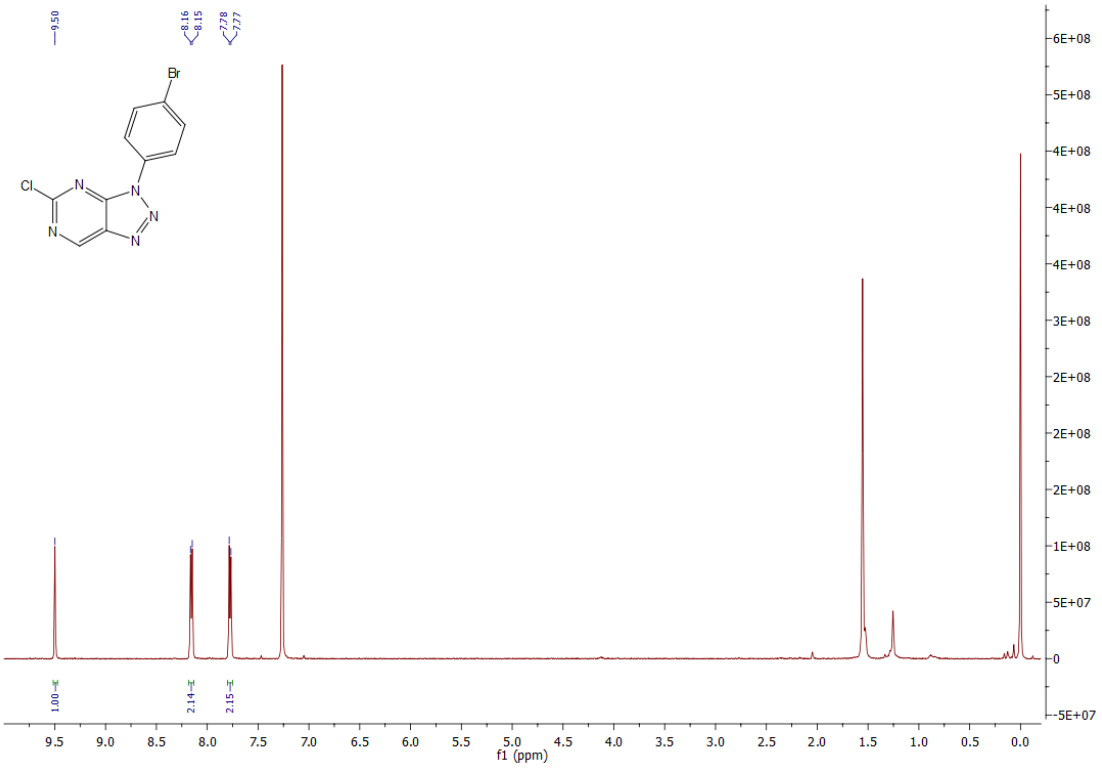

Figure 17 – ^{1}H NMR spectrum for Compound **5**

3.2.4 – Synthesis of Compounds 6a-c

*(R)-3-(4-bromophenyl)-N-(1-(4-fluorophenyl)ethyl)-3H-[1,2,3]triazolo[4,5-d]pyrimidin-5-amine (**6a**)*

Compound **5** (127 mg, 0.40 mmol) was dissolved in 1,4-dioxane (5 mL), and to this solution was added (*R*)-1-(4-fluorophenyl)ethanamine (55 mg, 0.40 mmol) and *N,N*-diisopropylethylamine (57 mg, 0.44 mmol) via syringe in short succession. The reaction was stirred for 16 hours and then

diluted with EtOAc (30 mL). A series of brine extractions were performed, and the separated organic layer was dried over sodium sulfate, washed with EtOAc, and filtered. The filtrate was concentrated and desiccated. The dried residue was adsorbed to silica and purified using flash silica gel column chromatography (1:7 EtOAc:Hexane) to afford Compound **6a** (50 mg, yield: 30%). ^{1}H NMR (500 MHz, $CDCl_3$) δ 9.09 (s, 1H), 7.97 (s, 2H), 7.64 (d, J = 8.5 Hz, 2H), 7.38 (dd, J = 8.6, 5.3 Hz, 2H), 7.05 (t, J = 8.6 Hz, 2H), 6.09 (s, 1H), 5.06 (s, 1H), 1.61 (d, J = 6.9 Hz, 3H). MS (ESI) m/z: [M + H]+ Calcd for $C_{18}H_{15}BrFN_6^+$ 413.05; Found 413.17.

Compound **6b** was prepared using the same procedures as **6a**, but (*R*)-1-phenylethanamine was used in place of (*R*)-1-(4-fluorophenyl)ethanamine. ^{1}H NMR (500 MHz, $CDCl_3$) δ 9.02 (s, 1H), 7.87 (d, J = 5.1 Hz, 2H), 7.55 (d, J = 8.0 Hz, 2H), 7.35 (d, J = 7.3 Hz, 2H), 7.31 (t, J = 7.5 Hz, 2H), 7.21 (d, J = 7.1 Hz, 1H), 6.01 (s, 1H), 4.98 (s, 1H), 1.56 (d, J = 6.9 Hz, 3H).

Compound **6c** was prepared using the same procedures as **6a**, but (*S*)-1-phenylethanamine was used in place of (*R*)-1-(4-fluorophenyl)ethanamine. ^{1}H NMR (500 MHz, $CDCl_3$) δ 9.10 (s, 1H), 7.96 (d, J = 6.3 Hz, 2H), 7.65 (d, J = 8.1 Hz, 2H), 7.44 (d, J = 7.3 Hz, 2H), 7.40 (t, J = 7.5 Hz, 2H), 7.31 (d, J = 7.2 Hz, 1H), 6.15 (s, 1H), 5.08 (s, 1H), 1.66 (d, J = 6.9 Hz, 3H).

3.2.4.1 – Structure Confirmation for Compounds 6a-c

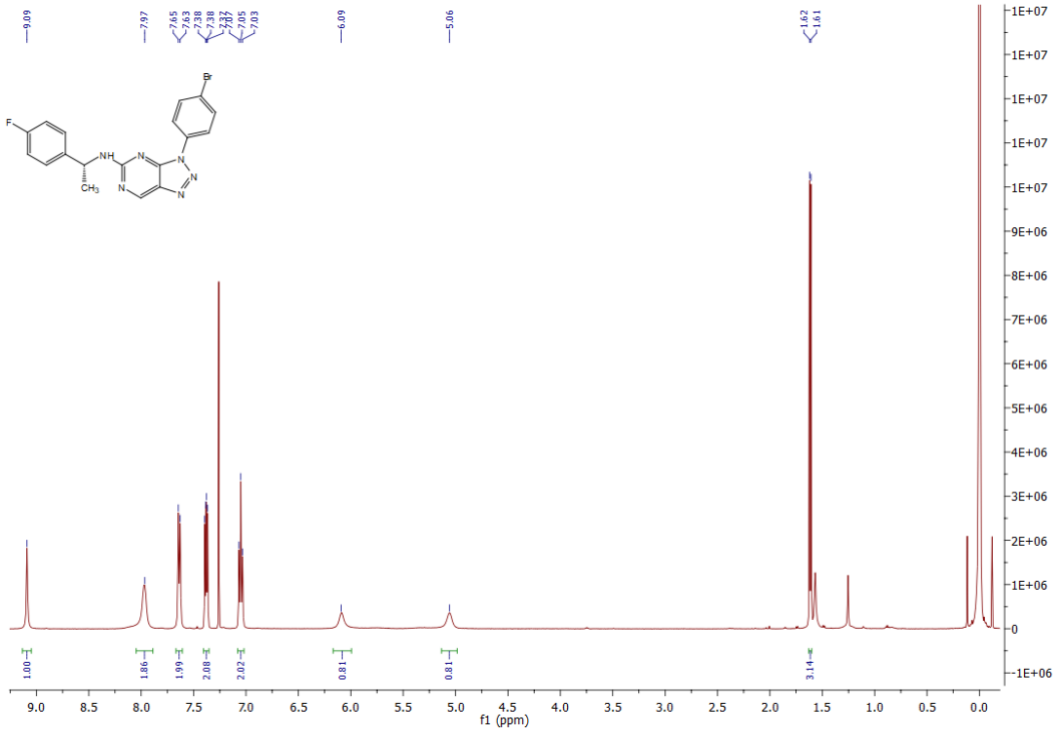

Figure 18 – ^{1}H NMR spectrum for Compound **6a**

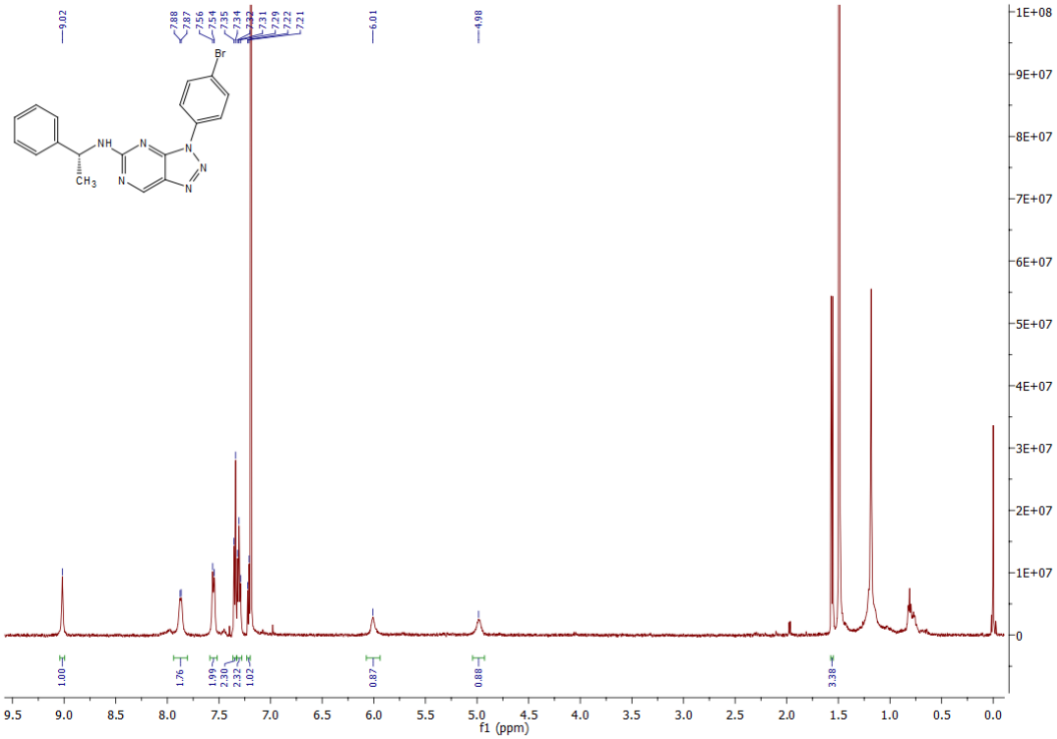

Figure 19 – ^{1}H NMR spectrum for Compound **6b**

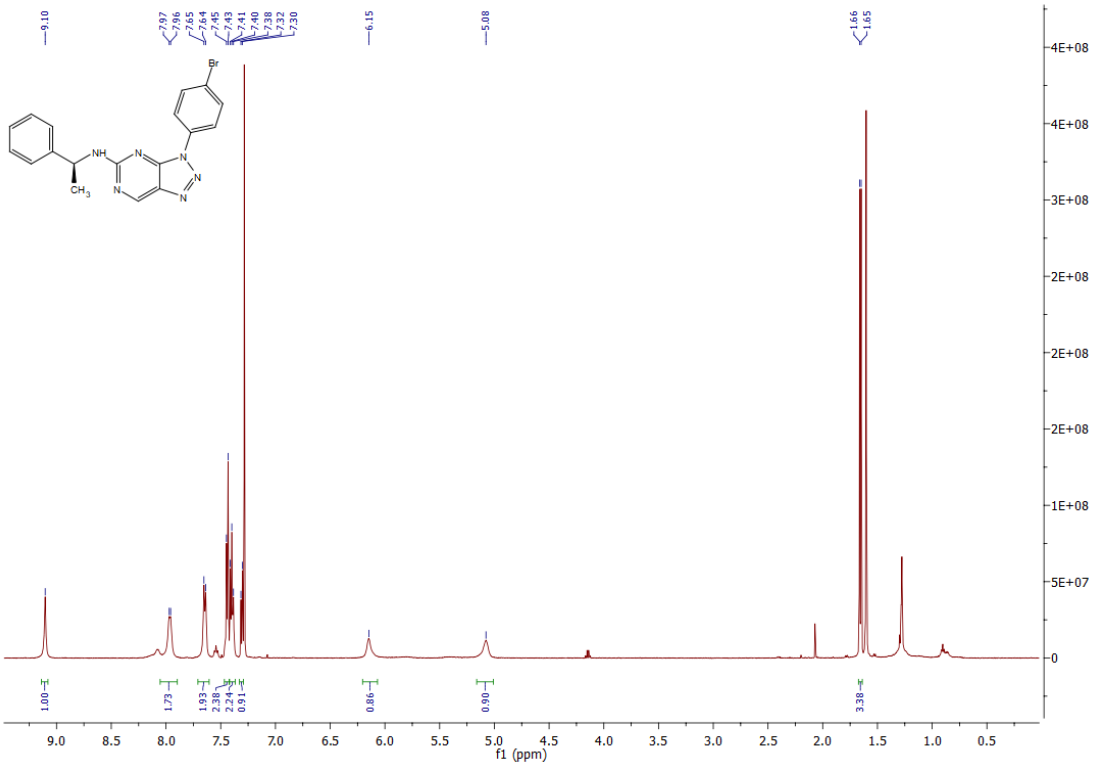

Figure 20 – ^{1}H NMR spectrum for Compound **6c**

3.2.5 – Synthesis of Compound 7a

*(R)-ethyl 1-(4'-(5-((1-(4-fluorophenyl)ethyl)amino)-3H-[1,2,3]triazolo[4,5-d]pyrimidin-3-yl)-[1,1'-biphenyl]-4-yl)cyclopropanecarboxylate (**7a**)*

Compound **6a** (101 mg, 0.24 mmol) was dissolved in 8 mL of a 1:3 mixture of H_2O:1,4-dioxane and the reflux condenser was prepared. The solution was heated to 80ºC, and Na_2CO_3 (54 mg, 0.515 mmol) was added to the solution. Ethyl 1-(4-(4,4,5,5-tetramethyl-1,3,2-dioxaborolan-2-yl)phenyl)cyclopropanecarboxylate (92 mg, 0.29 mmol) was added to the solution, quickly followed by the addition of $Pd(dppf)Cl_2$ (18 mg, 10 mol%). The solution was bubbled with argon and then stirred for 10 hours. The mixture was cooled and then filtered through diatomaceous earth and partitioned between EtOAc and brine. The organic phase was separated, dried over Na_2SO_4, filtered, and concentrated. The residue was dissolved in HPLC-grade acetonitrile and purified by HPLC (10 mL/min, 25% H_2O:75% Acetonitrile), affording pure Compound **7a** after

concentration of the HPLC fractions (17 mg, yield: 14%). ^{1}H NMR (500 MHz, $CDCl_3$) δ 9.11 (s, 1H), 8.13 (dd, J = 6.3, 3.2 Hz, 2H), 7.73 (d, J = 8.4 Hz, 2H), 7.60 (d, J = 8.2 Hz, 2H), 7.48 – 7.46 (m, 2H), 7.41 (dd, J = 8.3, 5.5 Hz, 2H), 7.05 (dd, J = 9.8, 7.5 Hz, 2H), 6.00 (s, 1H), 5.12 (s, 1H), 4.14 (q, J = 7.1 Hz, 2H), 1.66 (q, J = 4.0 Hz, 2H), 1.63 (d, J = 6.9 Hz, 3H), 1.26 – 1.23 (m, 4H), 1.21 (t, J = 7.1 Hz, 3H). MS (ESI) m/z: [M + H]+ Calcd for $C_{30}H_{28}FN_6O_2^+$ 523.23; Found 523.38.

3.2.5.1 – Structure Confirmation for Compound 7a

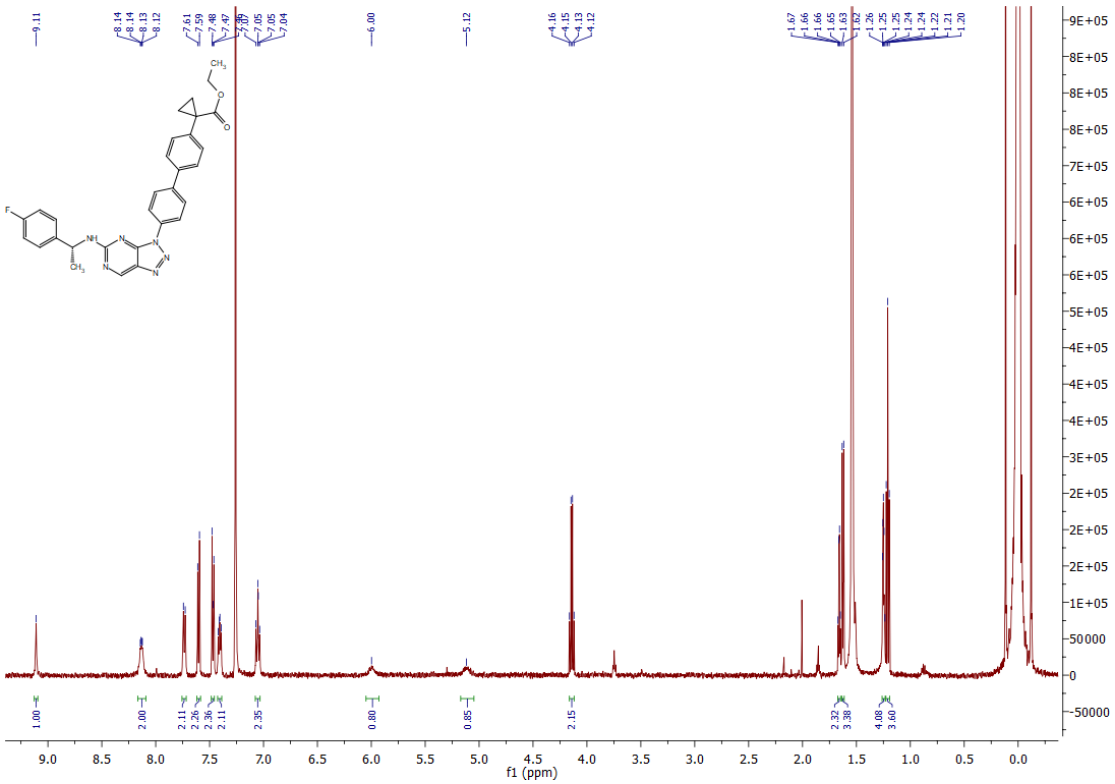

Figure 21 – ^{1}H NMR spectrum for Compound **7a**

3.2.6 – Synthesis of Compound 8a

*(R)-1-(4'-(5-((1-(4-fluorophenyl)ethyl)amino)-3H-[1,2,3]triazolo[4,5-d]pyrimidin-3-yl)-[1,1'-biphenyl]-4-yl)cyclopropanecarboxylic acid (**8a**)*

Compound **7a** (17 mg, 0.0325 mmol) was dissolved in 2 mL of a prepared 1:3 mixture of H_2O:THF. Lithium hydroxide pellets (17 mg, 0.709 mmol) were added to the solution, and the solution was

stirred for 1 week. The mixture was partitioned between EtOAc and brine, and the organic phase was separated, dried over Na_2SO_4, filtered, and concentrated. The residue was dissolved in a mixture of THF and HPLC-grade acetonitrile and purified by HPLC (10 mL/min, 40% H_2O:60% Acetonitrile), affording pure Compound **8a** after concentration of the HPLC fractions (10 mg, yield: 62%). ^{1}H NMR (500 MHz, DMSO) δ 9.22 (s, 1H), 8.76 (d, J = 5.9 Hz, 1H), 8.17 – 8.00 (m, 2H), 7.83 (d, J = 8.0 Hz, 2H), 7.60 (d, J = 6.9 Hz, 2H), 7.47 – 7.34 (m, 4H), 7.10 (dd, J = 24.7, 16.6 Hz, 2H), 5.03 – 4.94 (m, 1H), 1.43 (d, J = 6.2 Hz, 3H), 1.36 (s, 2H), 0.96 (s, 2H). ^{13}C NMR (126 MHz, DMSO) δ 162.43, 161.00, 160.51, 154.03, 150.07, 141.90, 139.96, 135.33, 131.49, 131.35, 128.48, 128.42, 128.00, 126.49, 120.86, 115.56, 115.39, 51.05, 29.72, 23.27, 15.39. MS (ESI) m/z: [M + H]+ Calcd for $C_{28}H_{24}FN_6O_2^+$ 495.19; Found 495.34.

3.2.6.1 – Structure Confirmation for Compound 8a

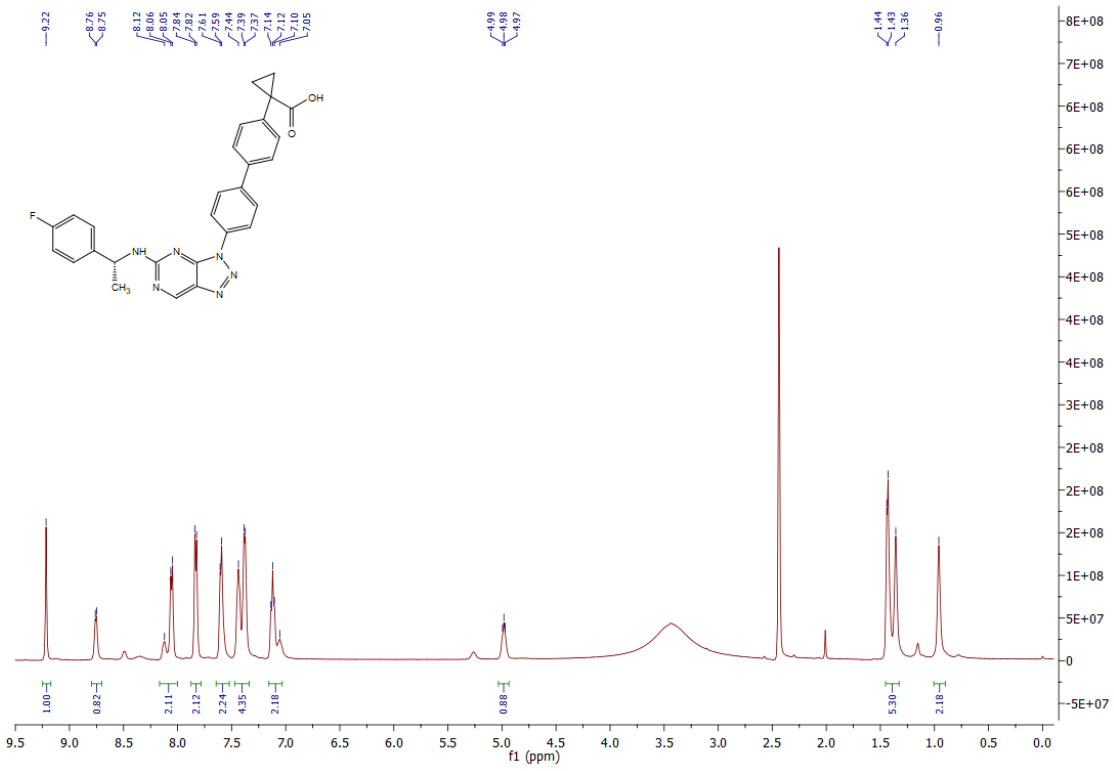

Figure 22 – ^{1}H NMR spectrum for Compound **8a**

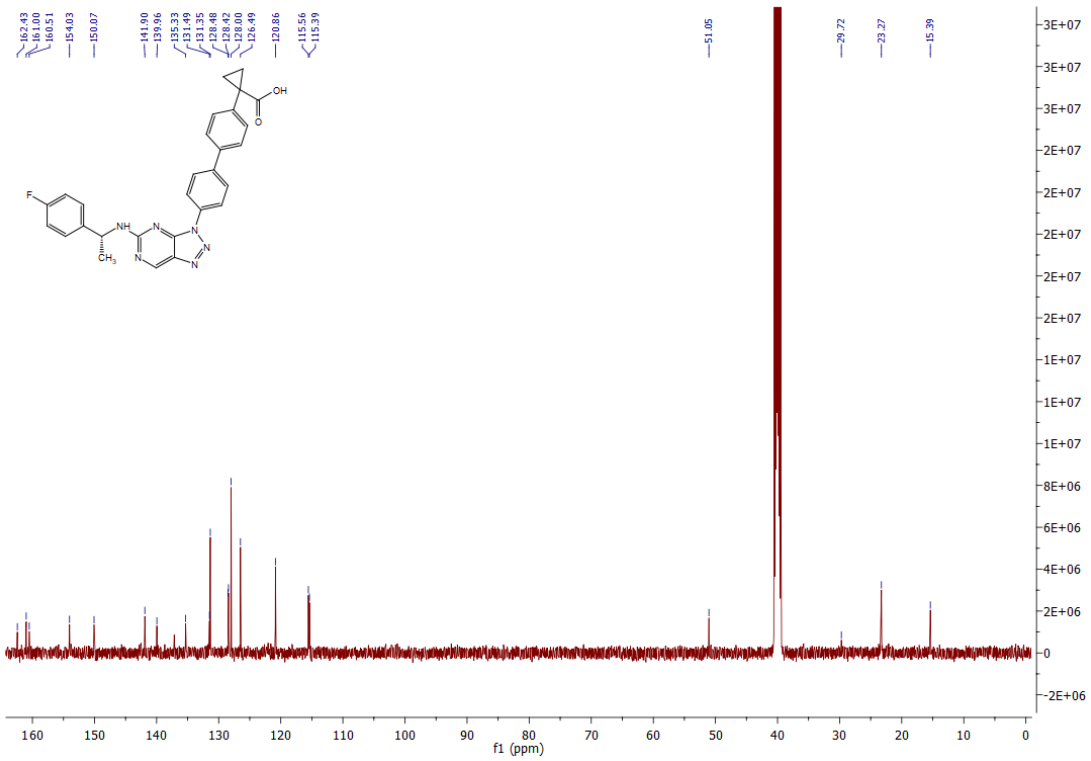

Figure 23 – ^{13}C NMR spectrum for Compound **8a**

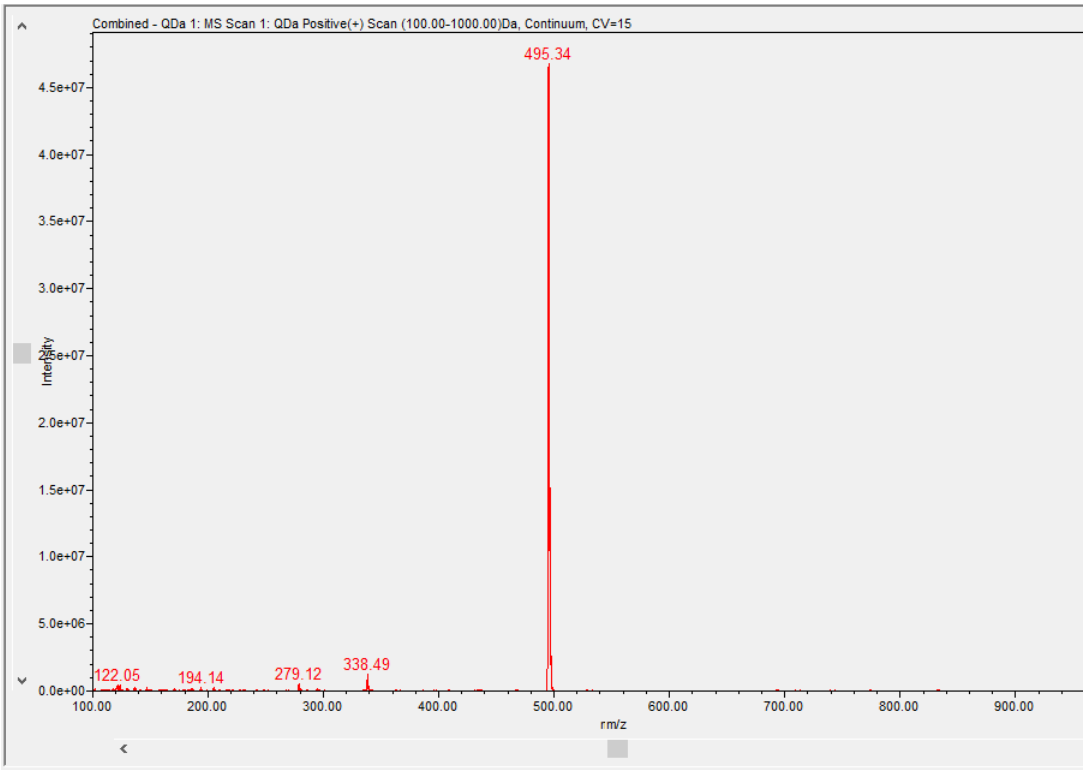

Figure 24 – Mass spectrum for Compound **8a**

Empower 3 SOFTWARE

Hou_group_report

SAMPLE INFORMATION

Sample Name:	2-AMH-143-5 pure	Acquired By:	JQ_Hou
Sample Type:	Unknown	Sample Set Name:	AMH
Vial:	1:E,2	Acq. Method Set:	Ana_AMH_3_20mins
Injection #:	1	Processing Method	PM_Yang
Injection Volume:	30.00 ul	Channel Name:	W2489 ChA
Run Time:	20.0 Minutes	Proc. Chnl. Descr.:	W2489 ChA 254nm
Date Acquired:	5/23/2023 4:40:01 PM EDT		
Date Processed:	5/23/2023 5:16:56 PM EDT		

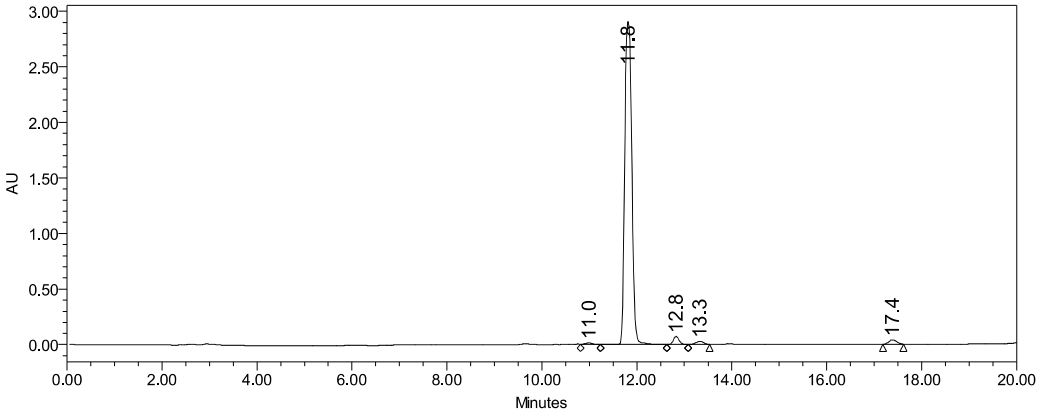

Channel: W2489 ChA; Processed Channel: W2489 ChA 254nm; Result Id: 39982; Processing Method: PM_Yang

Processed Channel Descr.: W2489 ChA 254nm

	Processed Channel Descr.	RT	Area	% Area	Height
1	W2489 ChA 254nm	10.995	160715	0.51	16090
2	W2489 ChA 254nm	11.816	29886760	95.06	2911568
3	W2489 ChA 254nm	12.829	604161	1.92	72325
4	W2489 ChA 254nm	13.332	303727	0.97	27275
5	W2489 ChA 254nm	17.388	485439	1.54	40974

Reported by User: JQ_Hou
Report Method: Hou_group_report
Report Method ID 2246
Page: 1 of 1

Project Name: Hou_group
Date Printed: 5/23/2023
5:17:32 PM America/Thunder_Bay

Figure 25 – HPLC chromatogram for compound **8a** using 254 nm channel

Empower 3 SOFTWARE

Hou_group_report

SAMPLE INFORMATION

Sample Name:	2-AMH-143-5 pure	Acquired By:	JQ_Hou
Sample Type:	Unknown	Sample Set Name:	AMH
Vial:	1:E,2	Acq. Method Set:	Ana_AMH_3_20mins
Injection #:	1	Processing Method	PM_Yang
Injection Volume:	30.00 ul	Channel Name:	W2489 ChB
Run Time:	20.0 Minutes	Proc. Chnl. Descr.:	W2489 ChB 365nm
Date Acquired:	5/23/2023 4:40:01 PM EDT		
Date Processed:	5/23/2023 5:21:27 PM EDT		

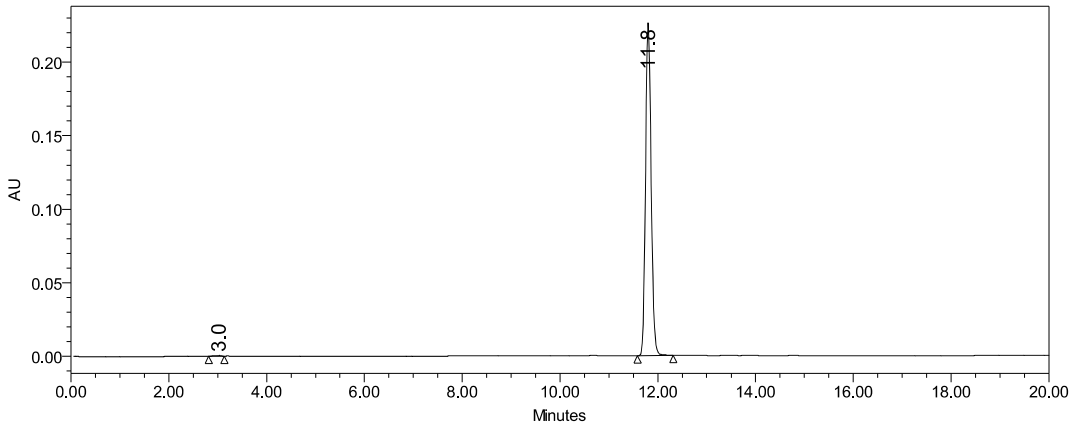

Channel: W2489 ChB; Processed Channel: W2489 ChB 365nm; Result Id: 39986; Processing Method: PM_Yang

Processed Channel Descr.: W2489 ChB 365nm

	Processed Channel Descr.	RT	Area	% Area	Height
1	W2489 ChB 365nm	3.030	4208	0.23	451
2	W2489 ChB 365nm	11.804	1801662	99.77	226293

Reported by User: JQ_Hou
Report Method: Hou_group_report
Report Method ID 2246
Page: 1 of 1

Project Name: Hou_group
Date Printed:
5/23/2023
5:21:47 PM America/Thunder_Bay

Figure 26 – HPLC chromatogram for Compound **8a** using 365 nm channel

Chapter 4: Biological Evaluation of Ligands

4.1 – cAMP Assay

As shown in **Figure 2**, LPA_1 activation leads to an inhibitory effect of cAMP production. Compound **8a** synthesized in this study was tested in an *in vitro* cAMP assay using the Chinese hamster ovary (CHO) cell line overexpressing the LPA_1 receptor. The common form of endogenous LPA, 18:1 LPA, was used to activate the LPA_1 receptors. LPA_1 antagonist activity is presented as IC_{50}, representing the concentration of **8a** required to reverse 50% of the inhibitory effect of 18:1 LPA on forskolin-mediated cAMP production. Intracellular cAMP levels were quantified by measuring the luminescence using the cAMP-Glo Assay kit and a microplate reader; binding of **8a** to LPA_1 leads to increased cAMP concentrations, which results in decreased luminescence. To generate the IC_{50} value of **8a**, the data were fit to a three-parameter logistic curve using GraphPad Prism. The results from this assay are summarized by the concentration-response curve showed below in **Figure 27**.

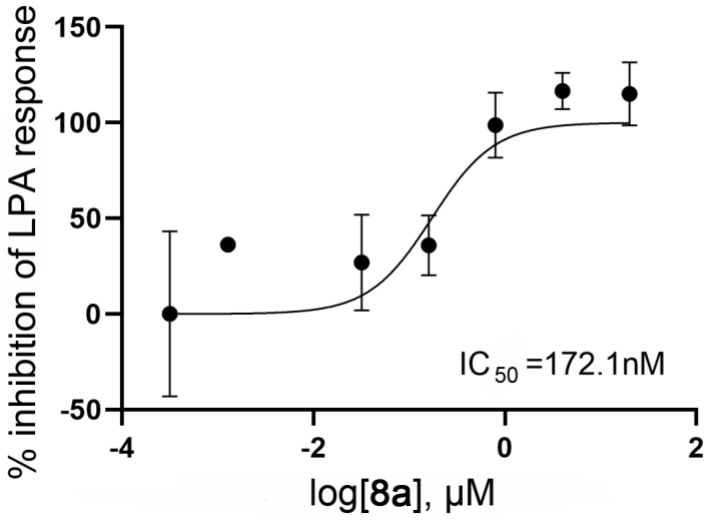

Figure 27 – cAMP assay results using Compound **8a**

Seven different concentrations of **8a** were used in this assay. Based on the data collected, it was determined that Compound **8a** has an IC_{50} value of 172.1 nM in the cAMP assay. While not

quite as potent as RO6842262, this result is still promising. This demonstrates that the novel scaffold not only functions as an LPA_1 antagonist, but it has a relatively high level of antagonistic activity. This an important and encouraging first step, as it paves the way for future analogues with different substituents that may have increased potency towards LPA_1.

4.2 – Wound Healing Assay

In addition to the cAMP assay, Compound **8a** was also tested in a wound healing assay. As discussed in Chapter 1, LPA_1 has been shown to have an increased expression level in many breast cancer cell lines compared to non-tumorigenic cell lines. In several of these cell lines, activation of LPA_1 leads to increased cell migration and invasion, showing the critical role of LPA_1 signaling in breast cancer progression, specifically in metastasis. A wound healing assay, also known as a scratch assay, is an assay that seeks to evaluate and quantify cell migration. Cells are plated in a 6-well plate and a wound is created by scratching the centre of the cell monolayer using a micropipette tip. After creation of the wound, cells are allowed to migrate over a certain period of time to 'close' the wound, and the migration rate can be quantified based on the results.

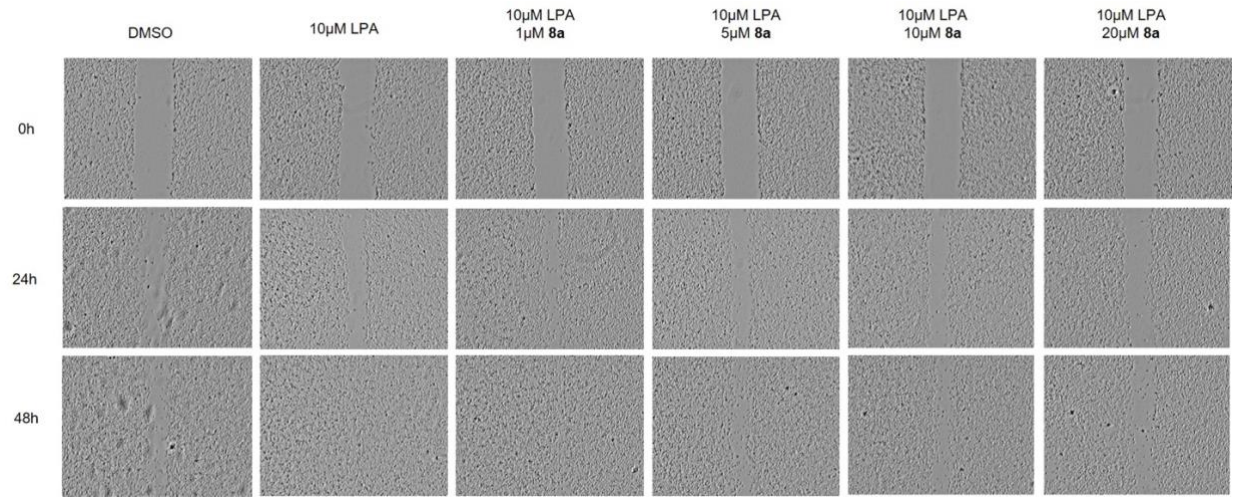

Figure 28 – Effects of LPA and **8a** on cell migration in wound healing assays using the MDA-MB-231 cell line

For the wound healing assay performed in this study, the MDA-MB-231 breast cancer cell line was seeded in a 6-well plate, and the wound was created after formation of the cell monolayer. In addition to a DMSO control group, five wells were stimulated with 10 μM LPA, and to four of these, Compound **8a** was added in four different concentrations (1 μM, 5 μM, 10 μM, and 20 μM). Microscope images of the wound were taken at the start of LPA stimulation, and again after 24 hours and 48 hours. Cell migration was quantified at both the 24-hour and 48-hour marks.

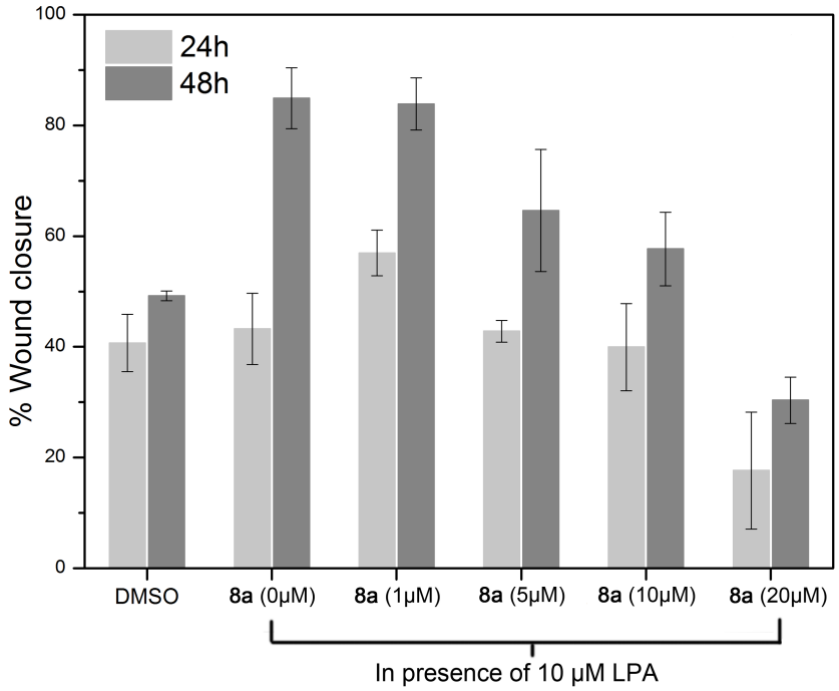

Figure 29 – Quantification of the wound healing assay

After the first 24 hours, the difference in cell migration was not readily apparent between groups with different treatment. Most groups achieved ~40% wound closure after this time, although the addition of 20 μM of Compound **8a** noticeably lowered the rate of wound closure. However, after the full incubation period of 48 hours, there was a noticeable downward trend in cell migration as the concentration of **8a** increased. Stimulation of cells with 10 μM LPA increased the percentage of wound closure from a baseline of 49% to 84%. The addition of only 1 μM **8a** only lowered the percentage of wound closure to 83%, but the addition of increasingly higher concentrations caused significantly decreased wound closure, with a maximum effect observed

using 20 μM **8a** (**Figure 29**), decreasing the percentage of wound closure from 84% to 30% after 48 hours. Therefore, it is clear that while LPA induces cell migration in the MDA-MB-231 breast cancer cell line, the addition of Compound **8a** can this inhibit LPA-induced cell migration in a dose and time-dependent manner, thereby demonstrating its therapeutic potential for the treatment of metastatic breast cancer.

In addition to the cAMP and wound healing assays, a calcium mobilization assay will be performed to further evaluate **8a** and any analogues that are synthesized in the future. The calcium mobilization assay will be used to test the synthesized ligands' ability to inhibit LPA_1 signaling through the $G_{q/11}$ protein. However, this assay has yet to have been performed as of now.

Chapter 5: Radiochemistry

As discussed in Chapter 1, PET imaging requires the usage of radioactive chemical isotopes. These isotopes must be tagged to drug compounds in a process known as 'radiolabeling'. There are many different methods that can be used to radiolabel a drug compound; each method has its own strategic advantages and disadvantages and can vastly differ based on both the desired radioisotope and the chemical structure of the drug compound. As ^{18}F has previously been identified as one of the most useful radioisotopes for PET imaging, Chapter 5 will explore several ^{18}F radiolabeling strategies that have reported in the recent literature, as well as propose an altered synthetic scheme for that will allow for the incorporation of this radioisotope into the chemical library that has been proposed in this thesis.

5.1 – Common Fluorine-18 Radiolabeling Strategies

Fluorine-18 radiolabeling of small molecules can be accomplished in a number of different ways. These can be broadly categorized under the reaction types of aliphatic nucleophilic fluorination, nucleophilic aromatic fluorination, electrophilic fluorination, and transition metal-mediated radiofluorination.[159]

Aliphatic nucleophilic fluorination is accomplished by the S_N2 substitution of a leaving group such as a halogen, tosylate, or triflate by ^{18}F. This is usually performed in basic conditions at moderate temperatures (RT to 100ºC) and requiring relatively short reaction times.[159] Additionally, phase transfer catalysts or tetrabutylammonium cations may be used to enhance the nucleophilicity and solubility of the fluorine anion. ^{18}F nucleophilic aromatic fluorination is performed in polar aprotic solvents and is characterized by the substitution of a leaving group such as a nitro group, halogen, or trimethylammonium salt, and typically requires the presence of electron-withdrawing groups in the ortho or para positions to activate the aromatic ring. Similar to aliphatic nucleophilic fluorination, the use of phase transfer catalysts or tetrabutylammonium cations is commonplace for these reactions. However, nucleophilic aromatic fluorination often is

conducted at higher temperatures (100-180ºC) than aliphatic nucleophilic fluorination, and comparatively, the application of this nucleophilic aromatic fluorination can be challenging due to the requirement of an electron-deficient ring. Electrophilic fluorination is another option for ^{18}F radiolabeling, although it is less preferred in radiopharmaceutical chemistry; production of ^{18}F for use in electrophilic reactions requires different production methods and involves the use of fluorine-19 as a carrier molecule, decreasing the specific activity, as well as requiring more complex purification methodology.[159,160] Regardless, electrophilic fluorination methods can still prove effective in certain scenarios. Electrophilic fluorination has been reported to work at a variety of reaction temperatures, and it can be highly useful when electron-rich arenes and alkanes are required to be labeled.[159] Lastly, transition metal-mediated radiofluorination is a recently discovered method that can be used to add ^{18}F to aromatic rings. Similar principles are used in these reactions as traditional transition metal mediated cross-coupling reactions, and it has been reported that transition metal-mediated radiofluorination has high functional group tolerance and may expand the amount of molecules that can radiolabeled with ^{18}F.[159] However, this is a relatively new field of research, and more research will need to be done in order to determine the scope of this type of fluorination method.

In recent years, a number of novel late-stage radiofluorination methods have been reported in an effort to maximize yield and increase the radiofluorination tolerance of different substrates. In 2016, a noteworthy radiolabeling method was reported by Rotstein et al. that sought to circumvent the limitations of standard nucleophilic and electrophilic fluorination.[161] This group reported the use of spirocyclic iodonium ylides as arene radiofluorination precursors for non-activated and sterically hindered molecules. This method was reported to have high functional group tolerance, high reactivity and regioselectivity, no metal of fluorine-19 required, and can be performed in a single radiochemical step.[161] This method firstly involves the synthesis of spiroadamantyl-1,3-dioxane-4,6-dione (SPIAd), which is an air and temperature-stable compound that can easily be purified in high yield. Reaction of SPIAd with an iodoarene in the presence of

an oxidizing agent in acidic media gives the corresponding iodonium ylide, upon which treatment of ^{18}F gives the radiolabeled compound with high radiochemical yield. This radiolabeling method has been demonstrated to work well with a variety of hindered and electron-rich substrates.[161]

In 2021, Chen et al. reported the discovery of a robust halide/^{18}F interconversion method using electron-rich halo(hetero) arenes. This group used acridinium photocatalysts for the photoredox-catalyzed radiofluorination of a diverse range of iodine, bromine, chlorine, and fluorine-containing organic compounds, including several pharmaceuticals.[162] Many of the tested compounds underwent halogen/^{18}F conversion site-selectively, while compounds with both bromine and chlorine substituents preferentially underwent conversion at the chlorine position. This method is advantageous as there is a lack of suitable direct radiofluorination methods for electron-rich aryl halides, of which an abundance of these compounds exists in the pharmaceutical industry. The reaction methods reported by Chen et al. are expected to allow for the easier transformation of fluorinated therapeutic pharmaceuticals into ^{18}F-labeled radiopharmaceutics than the standard methods that usually involve transition metal catalysis or the formation of a precursor molecule.[162]

Also in 2021, Zheng et al. yielded a radiofluorination method with high radiochemical yield and fast reaction time at mild temperatures using sulfur fluoride click chemistry.[163] This collaborative project between The Scripps Research Institute and ShanghaiTech University demonstrated the radiosynthesis of 25 different structurally diverse aryl fluorosulfates that have higher stability than previously reported aryl sulfonyl fluorides.[163] Furthermore, one of these synthesized hot compounds, an analogue of the anticancer drug olaparib, was successfully applied in a PET imaging experiment in a tumour-bearing mouse model. This represented the first PET image application using an S-^{18}F-based probe, and their research demonstrated the synthesis of a novel chemotype of radiofluorinated compounds.[163]

5.2 – Modification of Synthetic Scheme to Attain ^{18}F-Labelled Compounds

Based on the work of Rotstein et al., spirocyclic iodonium ylide-mediated radiofluorination appears to be an attractive method to use for the ^{18}F-radiolabeling of the compounds proposed in this thesis. ^{18}F radiolabeling of these compounds will likely be performed on the same aromatic ring as the other proposed substitutions due to reasons previously discussed in Chapter 2. This will require nucleophilic substitution by iodine-substituted building blocks. However, the use of this method with the reaction scheme shown in **Scheme 1** would prove to be ineffective. Suzuki-Miyaura cross-coupling is known to have an order of reactivity of I >> Br > OTf >> Cl for the electrophilic coupling partner, meaning that for the Suzuki-Miyaura coupling reaction used for the synthesis of these compounds, iodine-substituted building blocks would likely and undesirably act as the major coupling partner, giving undesired products.[164] Therefore, for the production of radiolabeled compounds, an alternate synthetic scheme is proposed (**Scheme 2**).

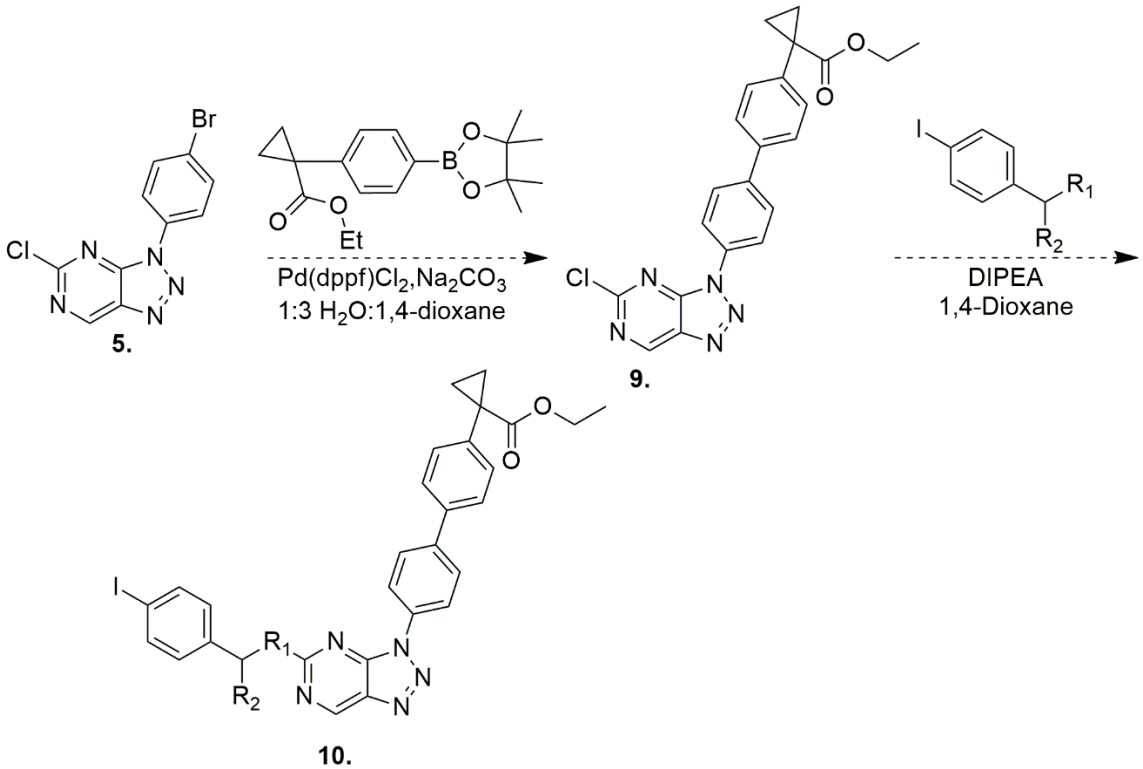

Scheme 2 – Alternate synthetic scheme for the synthesis of iodine-containing final compounds

The proposed alternate synthetic scheme shown in **Scheme 2** allows for the synthesis of iodine-containing final compounds while avoiding undesired Suzuki-Miyaura side products. Since chlorine is generally unreactive in Suzuki-Miyaura coupling reactions, only the aryl bromide should function as a coupling partner, thus giving the corresponding ester product **9** in high yield. Subsequent nucleophilic substitution by the iodine-containing building blocks should then give Compound **10** and its analogues.

With this synthetic challenge resolved, the next stage of the synthesis will be detailed. According to the work done by Rotstein et al., the synthesis of SPIAd will be required in order for this radiolabeling method to be performed.[161] This is shown at the top of **Scheme 3**. After the synthesis and purification of both Compound **10** and SPIAd, the two compounds can be reacted together to produce the iodonium ylide **11**. At this stage, it is desirable for the carboxylic acid to remain protected as an ester due to the possibility of undesirable interaction between the carboxylic acid and the reagents used for iodonium ylide synthesis. Compound **11** may then be further reacted in a two-reaction, one-pot synthesis with the fluorine-18 anion, a phase transfer catalyst such as the cryptand Kryptofix 222 (K222), and potassium cations reacting to yield the radiolabeled ester, upon which LiOH hydrolysis will give the final radiolabeled acid compound, Compound **[^{18}F]8.** For this reaction, K222 will bind the potassium cations, allowing them to interact with the negatively charged ^{18}F anions but preventing the true formation of potassium fluoride, thereby enhancing the nucleophilicity of the ^{18}F.[165] Additionally, since ^{18}F will be added at the end of the synthesis according to this method, this should maximize the activity of the ^{18}F and limit the number of half-lives that will have occurred to allow for more accurate PET imaging.

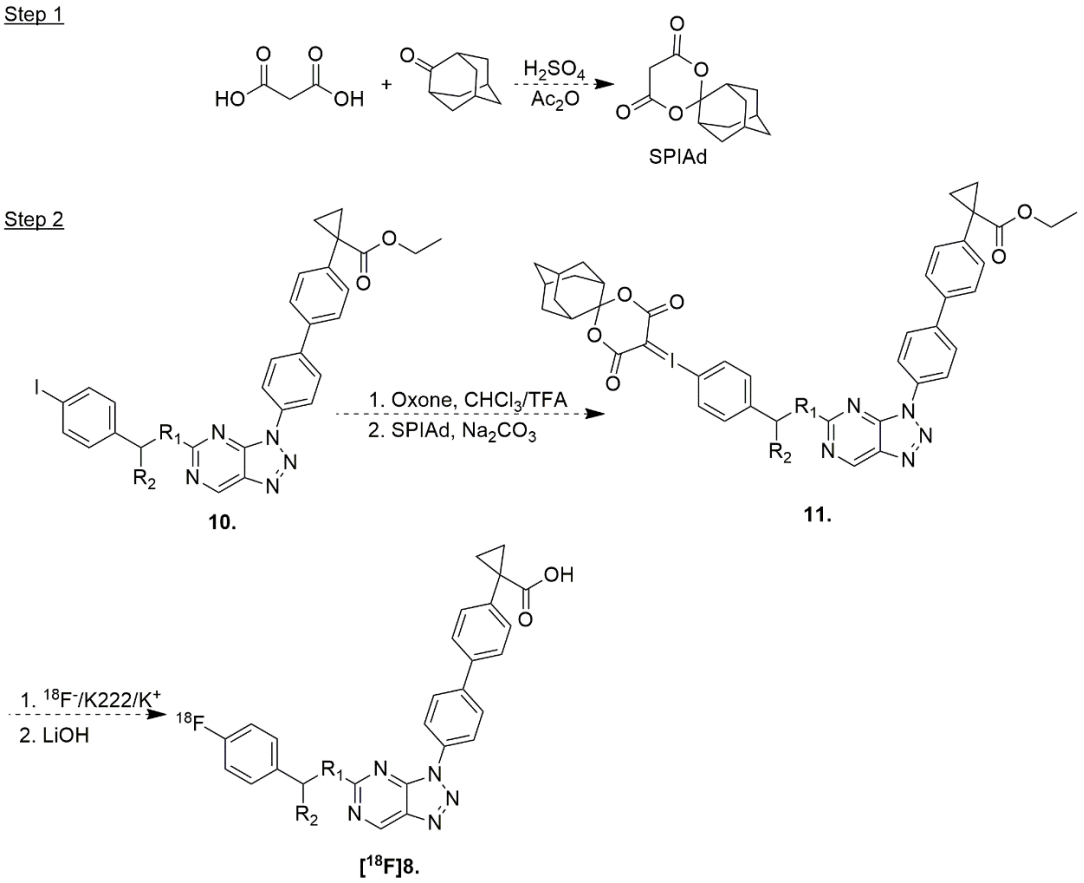

Scheme 3 – Proposed radiolabeling scheme to produce ^{18}F-labeled compounds (Step 1, top: synthesis of SPIAd; Step 2, bottom: production of the iodonium ylide species and subsequent one-pot reaction with ^{18}F and LiOH to yield the final hot compound).

Chapter 6: Conclusion

In 2023, the detection of breast cancer and subsequent therapy remain a challenge in Canada. To address this need, this study focused on the design, synthesis, and biological evaluation of novel small molecules that have the potential to act as breast cancer diagnostic and therapeutic agents. The LPA_1 receptor represented an attractive target due to its elevated expression levels in breast cancer cell lines and implication in the development and progression of breast cancer. In recent literature, several compounds targeting LPA_1 have been reported, but none have made it to the market thus far. One of these compounds, RO6842262, demonstrated high selectivity and potency for the LPA_1 receptor.

To aid in the discovery of novel compounds, scaffold hopping was employed to identify new bioisosteric molecular structures that could have similar or enhanced pharmacological properties based on this reference compound. A novel 3*H*-1,2,3-triazolo[4,5-*d*]pyrimidine scaffold was identified using this method, and a comparative molecular docking study was conducted using AutoDock Vina and the crystal structure of LPA_1. In this docking study, it was predicted that many of the key interactions between LPA_1 and RO6842262 are conserved between LPA_1 and this novel scaffold, and the best binding poses of the reference and new scaffold superimposed quite well. Additionally, the novel scaffold (-11.1 kcal/mol) was predicted to have a lower binding free energy than RO6842262 (-10.1 kcal/mol), indicating that this novel scaffold may have comparable or enhanced biological activity.

A rational six-step synthetic scheme was proposed for the synthesis of 3*H*-1,2,3-triazolo[4,5-*d*]pyrimidine analogues. These compounds differentiate at the fourth reaction step by the addition of building blocks with three possibly distinct 'R' groups. Three different intermediate compounds, **6a-c**, have been synthesized. Compound **6a**, bearing a fluorine-substituted phenyl ring, was progressed to the Suzuki-Miyaura coupling reaction and then hydrolyzed to yield the final compound **8a**. **8a** has been characterized and confirmed by ^{1}H NMR, ^{13}C NMR, and mass spectrometry, and its purity has been determined to be above 95% by HPLC.

After purification, Compound **8a** was evaluated using the cAMP assay. This compound was found to inhibit the LPA-induced antagonistic effects of LPA_1 on forskolin-mediated cAMP production in a dose-dependent manner. The IC_{50} of this compound was found to be 172.1 nM. Although not as potent as the reference compound, this is only the first compound to be synthesized and tested. Compound **8a** was also evaluated using a wound healing assay in the MDA-MB-231 breast cancer cell line. The results of this assay concluded that this synthesized compound can effectively inhibit LPA-induced cell migration in a time and-dose dependent manner, indicating that it has therapeutic potential for the treatment of metastatic breast cancer. In the future, a library containing many compounds with different substituents will be synthesized and evaluated. It is anticipated that some of these compounds will have comparable or enhanced biological activities compared to RO6842262. These analogues will be structurally optimized by analyzing the structure-activity relationship between each of the previously tested analogues to guide the synthesis of subsequent analogues. After the synthesis of several more compounds, a calcium mobilization assay will also be performed in order to more comprehensively evaluate their biological activities.

PET has been identified as an underutilized imaging modality for breast cancer detection and diagnosis. To enable the usage of the synthesized compounds as PET radiopharmaceuticals, an alternate synthetic scheme has been proposed that will allow for the radiofluorination of these compounds while minimizing undesirable side products. Chosen compounds will go through an iodonium ylide intermediate, be treated with fluorine-18 ions, and finally hydrolyzed to give radiolabeled final compounds.

Overall, the work presented in this thesis holds great significance as a novel scaffold of LPA_1 antagonists has successfully been identified, synthesized, and biologically evaluated. In the future, this research will be further built upon to give even more potent LPA_1 antagonists, and additional biological studies will be used to evaluate these compounds.

References

1. Canadian Cancer Statistics Advisory Committee in collaboration with the Canadian Cancer Society, Statistics Canada and the Public Health Agency of Canada. *Canadian Cancer Statistics 2021*. (2021).
2. Canadian Cancer Society. Types of cancer. https://cancer.ca/en/cancer-information/what-is-cancer/types-of-cancer (2023).
3. Mancini, M., Righetto, M. & Baggio, G. Spotlight on gender-specific disparities in bladder cancer. *Urologia* **87**, 103–114 (2020).
4. Poirier, A. E., Ruan, Y., Grevers, X., Walter, S. D., Villeneuve, P. J., Friedenreich, C. M. & Brenner, D. R. Estimates of the current and future burden of cancer attributable to active and passive tobacco smoking in Canada. *Preventive Medicine* **122**, 9–19 (2019).
5. United States Surgeon General. The Health Consequences of Smoking -- 50 Years of progress: A Report of the Surgeon General: (510072014-001). (2014).
6. Statistics Canada. Health characteristics, annual estimates. Table 13-10-0096-10 Smokers, by age group.
7. Government of Canada. *Seizing the opportunity: the future of tobacco control in Canada.* (2017).
8. American Institute for Cancer Research / World Cancer Research Fund. *Continuous Update Project Report: Diet, Nutrition, Physical Activity and Breast Cancer*. (2018).
9. Sun, Y.-S., Zhao, Z., Yang, Z.-N., Xu, F., Lu, H.-J., Zhu, Z.-Y., Shi, W., Jiang, J., Yao, P.-P. & Zhu, H.-P. Risk Factors and Preventions of Breast Cancer. *Int. J. Biol. Sci.* **13**, 1387–1397 (2017).

10. Van Middendorp, J. J., Sanchez, G. M. & Burridge, A. L. The Edwin Smith papyrus: a clinical reappraisal of the oldest known document on spinal injuries. *Eur Spine J* **19**, 1815–1823 (2010).

11. Lakhtakia, R. A Brief History of Breast Cancer: Part I: Surgical domination reinvented. *Sultan Qaboos Univ Med J* **14**, e166-169 (2014).

12. Retief, F. P. & Cilliers, L. Breast cancer in antiquity. *S Afr Med J* **101**, 513–515 (2011).

13. Skuse, A. *Constructions of Cancer in Early Modern England: Ravenous Natures*. (Palgrave Macmillan UK, 2015). doi:10.1057/9781137487537.

14. Ghosh, S. K. Giovanni Battista Morgagni (1682–1771): father of pathologic anatomy and pioneer of modern medicine. *Anat Sci Int* **92**, 305–312 (2017).

15. Kalaf, J. M. Mamografia: uma história de sucesso e de entusiasmo científico. *Radiol Bras* **47**, VII–VIII (2014).

16. Reeves, R. A. & Kaufman, T. Mammography. in *StatPearls* (StatPearls Publishing, 2023).

17. Canadian Cancer Society. Mammography. https://cancer.ca/en/treatments/tests-and-procedures/mammography (2023).

18. Steyerova, P. & Burgetova, A. Current imaging techniques and impact on diagnosis and survival —a narrative review. *Ann Breast Surg* **6**, 25–25 (2022).

19. Canadian Cancer Society. Screening for breast cancer. https://cancer.ca/en/cancer-information/cancer-types/breast/screening (2023).

20. Pisano, E. D., Hendrick, R. E., Yaffe, M. J., Baum, J. K., Acharyya, S., Cormack, J. B., Hanna, L. A., Conant, E. F., Fajardo, L. L., Bassett, L. W., D'Orsi, C. J., Jong, R. A., Rebner, M., Tosteson, A. N. A., Gatsonis, C. A., & DMIST Investigators Group. Diagnostic accuracy of digital versus

film mammography: exploratory analysis of selected population subgroups in DMIST. *Radiology* **246**, 376–383 (2008).

21. Weigel, S., Heindel, W., Heidrich, J., Hense, H.-W. & Heidinger, O. Digital mammography screening: sensitivity of the programme dependent on breast density. *Eur Radiol* **27**, 2744–2751 (2017).

22. Pai, V. R. & Rebner, M. How to Minimize Patient Anxiety From Screening Mammography. *Journal of Breast Imaging* **3**, 603–606 (2021).

23. de Groot, J. E., Broeders, M. J. M., Grimbergen, C. A. & den Heeten, G. J. Pain-preventing strategies in mammography: an observational study of simultaneously recorded pain and breast mechanics throughout the entire breast compression cycle. *BMC Womens Health* **15**, 26 (2015).

24. Evans, A., Trimboli, R. M., Athanasiou, A., Balleyguier, C., Baltzer, P. A., Bick, U., Camps Herrero, J., Clauser, P., Colin, C., Cornford, E., Fallenberg, E. M., Fuchsjaeger, M. H., Gilbert, F. J., Helbich, T. H., Kinkel, K., Heywang-Köbrunner, S. H., Kuhl, C. K., Mann, R. M., Martincich, L., Panizza, P., Pediconi, F., Pijnappel, R. M., Pinker, K., Zackrisson, S., Forrai, G., Sardanelli, F., & European Society of Breast Imaging (EUSOBI) , with language review by Europa Donna–The European Breast Cancer Coalition. Breast ultrasound: recommendations for information to women and referring physicians by the European Society of Breast Imaging. *Insights Imaging* **9**, 449–461 (2018).

25. Chen, H.-L., Zhou, J.-Q., Chen, Q. & Deng, Y.-C. Comparison of the sensitivity of mammography, ultrasound, magnetic resonance imaging and combinations of these imaging

modalities for the detection of small (≤2 cm) breast cancer. *Medicine (Baltimore)* **100**, e26531 (2021).

26. Kieturakis, A. J., Wahab, R. A., Vijapura, C. & Mahoney, M. C. Current Recommendations for Breast Imaging of the Pregnant and Lactating Patient. *AJR Am J Roentgenol* **216**, 1462–1475 (2021).
27. Appleton, D. C., Hackney, L. & Narayanan, S. Ultrasonography alone for diagnosis of breast cancer in women under 40. *Ann R Coll Surg Engl* **96**, 202–206 (2014).
28. Wang, Y., Li, Y., Song, Y., Chen, C., Wang, Z., Li, L., Liu, M., Liu, G., Xu, Y., Zhou, Y., Sun, Q. & Shen, S. Comparison of ultrasound and mammography for early diagnosis of breast cancer among Chinese women with suspected breast lesions: A prospective trial. *Thorac Cancer* **13**, 3145–3151 (2022).
29. Canadian Cancer Society. Diagnosis of breast cancer. https://cancer.ca/en/cancer-information/cancer-types/breast/diagnosis (2023).
30. Berger, A. Magnetic resonance imaging. *BMJ* **324**, 35 (2002).
31. Nofiele, J. T., Haedicke, I. E., Zhu, Y. L. K., Zhang, X. & Cheng, H.-L. M. Gadolinium-free extracellular MR contrast agent for tumor imaging. *J Magn Reson Imaging* **41**, 397–403 (2015).
32. He, Z., Chen, Z., Tan, M., Elingarami, S., Liu, Y., Li, T., Deng, Y., He, N., Li, S., Fu, J. & Li, W. A review on methods for diagnosis of breast cancer cells and tissues. *Cell Prolif* **53**, e12822 (2020).
33. Riedl, C. C., Luft, N., Bernhart, C., Weber, M., Bernathova, M., Tea, M.-K. M., Rudas, M., Singer, C. F. & Helbich, T. H. Triple-Modality Screening Trial for Familial Breast Cancer

Underlines the Importance of Magnetic Resonance Imaging and Questions the Role of Mammography and Ultrasound Regardless of Patient Mutation Status, Age, and Breast Density. *JCO* **33**, 1128–1135 (2015).

34. Kuhl, C. K., Schrading, S., Leutner, C. C., Morakkabati-Spitz, N., Wardelmann, E., Fimmers, R., Kuhn, W. & Schild, H. H. Mammography, breast ultrasound, and magnetic resonance imaging for surveillance of women at high familial risk for breast cancer. *J Clin Oncol* **23**, 8469–8476 (2005).
35. Winter, L., Seifert, F., Zilberti, L., Murbach, M. & Ittermann, B. MRI-Related Heating of Implants and Devices: A Review. *J Magn Reson Imaging* **53**, 1646–1665 (2021).
36. Hargreaves, B. A., Worters, P. W., Pauly, K. B., Pauly, J. M., Koch, K. M. & Gold, G. E. Metal-induced artifacts in MRI. *AJR Am J Roentgenol* **197**, 547–555 (2011).
37. O'Flynn, E. a. M., Wilson, A. R. M. & Michell, M. J. Image-guided breast biopsy: state-of-the-art. *Clin Radiol* **65**, 259–270 (2010).
38. Versaggi, S. L. & De Leucio, A. Breast Biopsy. in *StatPearls* (StatPearls Publishing, 2023).
39. Schinzinger, A. Üeber carcinoma mammae. *Verh Dtsch Ges Chir.* **18**, 28–29 (1889).
40. Clarke, M. J. Ovarian ablation in breast cancer, 1896 to 1998: milestones along hierarchy of evidence from case report to Cochrane review. *BMJ* **317**, 1246–1248 (1998).
41. Grubbé, E. H. Priority in the Therapeutic Use of X-rays. *Radiology* **21**, 156–162 (1933).
42. Jolliffe, D. M. A history of the use of arsenicals in man. *J R Soc Med* **86**, 287–289 (1993).
43. DeVita, V. T. & Chu, E. A History of Cancer Chemotherapy. *Cancer Research* **68**, 8643–8653 (2008).

44. Plesca, M., Bordea, C., El Houcheimi, B., Ichim, E. & Blidaru, A. Evolution of radical mastectomy for breast cancer. *J Med Life* **9**, 183–186 (2016).

45. Dobosz, P. & Dzieciątkowski, T. The Intriguing History of Cancer Immunotherapy. *Front Immunol* **10**, 2965 (2019).

46. Ben-Dror, J., Shalamov, M. & Sonnenblick, A. The History of Early Breast Cancer Treatment. *Genes (Basel)* **13**, 960 (2022).

47. Waks, A. G. & Winer, E. P. Breast Cancer Treatment: A Review. *JAMA* **321**, 288 (2019).

48. Crozier, J. A. Adjuvant chemotherapy in breast cancer: To use or not to use, the anthracyclines. *WJCO* **5**, 529 (2014).

49. Willson, M. L., Burke, L., Ferguson, T., Ghersi, D., Nowak, A. K. & Wilcken, N. Taxanes for adjuvant treatment of early breast cancer. *Cochrane Database Syst Rev* **9**, CD004421 (2019).

50. Iacobuzio-Donahue, C. A. Epigenetic Changes in Cancer. *Annu. Rev. Pathol. Mech. Dis.* **4**, 229–249 (2009).

51. Finlay, D. B., Duffull, S. B. & Glass, M. 100 years of modelling ligand–receptor binding and response: A focus on GPCRs. *British J Pharmacology* **177**, 1472–1484 (2020).

52. Hauser, A. S., Attwood, M. M., Rask-Andersen, M., Schiöth, H. B. & Gloriam, D. E. Trends in GPCR drug discovery: new agents, targets and indications. *Nat Rev Drug Discov* **16**, 829–842 (2017).

53. Wacker, D., Stevens, R. C. & Roth, B. L. How Ligands Illuminate GPCR Molecular Pharmacology. *Cell* **170**, 414–427 (2017).

54. Rosenbaum, D. M., Rasmussen, S. G. F. & Kobilka, B. K. The structure and function of G-protein-coupled receptors. *Nature* **459**, 356–363 (2009).

55. Coleman, J. L. J., Ngo, T. & Smith, N. J. The G protein-coupled receptor N-terminus and receptor signalling: N-tering a new era. *Cell Signal* **33**, 1–9 (2017).

56. Liu, W., Hopkins, A. M. & Hou, J. The development of modulators for lysophosphatidic acid receptors: A comprehensive review. *Bioorganic Chemistry* **117**, 105386 (2021).

57. Julius, D. & Nathans, J. Signaling by sensory receptors. *Cold Spring Harb Perspect Biol* **4**, a005991 (2012).

58. Barmania, F. & Pepper, M. S. C-C chemokine receptor type five (CCR5): An emerging target for the control of HIV infection. *Appl Transl Genom* **2**, 3–16 (2013).

59. Betke, K. M., Wells, C. A. & Hamm, H. E. GPCR mediated regulation of synaptic transmission. *Prog Neurobiol* **96**, 304–321 (2012).

60. Rivera, G., Bocanegra-García, V., Galiano, S., Cirauqui, N., Ceras, J., Pérez, S., Aldana, I. & Monge, A. Melanin-concentrating hormone receptor 1 antagonists: a new perspective for the pharmacologic treatment of obesity. *Curr Med Chem* **15**, 1025–1043 (2008).

61. Yang, D., Zhou, Q., Labroska, V., Qin, S., Darbalaei, S., Wu, Y., Yuliantie, E., Xie, L., Tao, H., Cheng, J., Liu, Q., Zhao, S., Shui, W., Jiang, Y. & Wang, M.-W. G protein-coupled receptors: structure- and function-based drug discovery. *Sig Transduct Target Ther* **6**, 7 (2021).

62. Chaudhary, P. K. & Kim, S. An Insight into GPCR and G-Proteins as Cancer Drivers. *Cells* **10**, 3288 (2021).

63. Kapolka, N. J., Taghon, G. J., Rowe, J. B., Morgan, W. M., Enten, J. F., Lambert, N. A. & Isom, D. G. DCyFIR: a high-throughput CRISPR platform for multiplexed G protein-coupled receptor profiling and ligand discovery. *Proc. Natl. Acad. Sci. U.S.A.* **117**, 13117–13126 (2020).

64. Atanes, P., Ashik, T. & Persaud, S. J. Obesity-induced changes in human islet G protein-coupled receptor expression: Implications for metabolic regulation. *Pharmacology & Therapeutics* **228**, 107928 (2021).

65. Choi, J. W., Herr, D. R., Noguchi, K., Yung, Y. C., Lee, C.-W., Mutoh, T., Lin, M.-E., Teo, S. T., Park, K. E., Mosley, A. N. & Chun, J. LPA receptors: subtypes and biological actions. *Annu Rev Pharmacol Toxicol* **50**, 157–186 (2010).

66. Yung, Y. C., Stoddard, N. C. & Chun, J. LPA receptor signaling: pharmacology, physiology, and pathophysiology. *J Lipid Res* **55**, 1192–1214 (2014).

67. Hecht, J. H., Weiner, J. A., Post, S. R. & Chun, J. Ventricular zone gene-1 (vzg-1) encodes a lysophosphatidic acid receptor expressed in neurogenic regions of the developing cerebral cortex. *J Cell Biol* **135**, 1071–1083 (1996).

68. Funke, M., Zhao, Z., Xu, Y., Chun, J. & Tager, A. M. The lysophosphatidic acid receptor LPA1 promotes epithelial cell apoptosis after lung injury. *Am J Respir Cell Mol Biol* **46**, 355–364 (2012).

69. Lin, Y.-H., Lin, Y.-C. & Chen, C.-C. Lysophosphatidic Acid Receptor Antagonists and Cancer: The Current Trends, Clinical Implications, and Trials. *Cells* **10**, 1629 (2021).

70. Cui, R., Cao, G., Bai, H. & Zhang, Z. LPAR1 regulates the development of intratumoral heterogeneity in ovarian serous cystadenocarcinoma by activating the PI3K/AKT signaling pathway. *Cancer Cell Int* **19**, 201 (2019).

71. Li, T. T., Alemayehu, M., Aziziyeh, A. I., Pape, C., Pampillo, M., Postovit, L.-M., Mills, G. B., Babwah, A. V. & Bhattacharya, M. Beta-arrestin/Ral signaling regulates lysophosphatidic

acid-mediated migration and invasion of human breast tumor cells. *Mol Cancer Res* **7**, 1064–1077 (2009).

72. Hopkins, M. M., Zhang, Z., Liu, Z. & Meier, K. E. Eicosopentaneoic Acid and Other Free Fatty Acid Receptor Agonists Inhibit Lysophosphatidic Acid- and Epidermal Growth Factor-Induced Proliferation of Human Breast Cancer Cells. *J Clin Med* **5**, 16 (2016).

73. Boucharaba, A., Serre, C.-M., Guglielmi, J., Bordet, J.-C., Clézardin, P. & Peyruchaud, O. The type 1 lysophosphatidic acid receptor is a target for therapy in bone metastases. *Proc Natl Acad Sci U S A* **103**, 9643–9648 (2006).

74. Li, T. T., Alemayehu, M., Aziziyeh, A. I., Pape, C., Pampillo, M., Postovit, L.-M., Mills, G. B., Babwah, A. V. & Bhattacharya, M. β-Arrestin/Ral Signaling Regulates Lysophosphatidic Acid–Mediated Migration and Invasion of Human Breast Tumor Cells. *Molecular Cancer Research* **7**, 1064–1077 (2009).

75. Qu, Y., Han, B., Yu, Y., Yao, W., Bose, S., Karlan, B. Y., Giuliano, A. E. & Cui, X. Evaluation of MCF10A as a Reliable Model for Normal Human Mammary Epithelial Cells. *PLoS One* **10**, e0131285 (2015).

76. Boucharaba, A., Serre, C.-M., Grès, S., Saulnier-Blache, J. S., Bordet, J.-C., Guglielmi, J., Clézardin, P. & Peyruchaud, O. Platelet-derived lysophosphatidic acid supports the progression of osteolytic bone metastases in breast cancer. *J Clin Invest* **114**, 1714–1725 (2004).

77. Marshall, J.-C. A., Collins, J. W., Nakayama, J., Horak, C. E., Liewehr, D. J., Steinberg, S. M., Albaugh, M., Vidal-Vanaclocha, F., Palmieri, D., Barbier, M., Murone, M. & Steeg, P. S. Effect

of inhibition of the lysophosphatidic acid receptor 1 on metastasis and metastatic dormancy in breast cancer. *J Natl Cancer Inst* **104**, 1306–1319 (2012).

78. Sahay, D., Leblanc, R., Grunewald, T. G. P., Ambatipudi, S., Ribeiro, J., Clézardin, P. & Peyruchaud, O. The LPA1/ZEB1/miR-21-activation pathway regulates metastasis in basal breast cancer. *Oncotarget* **6**, 20604–20620 (2015).

79. David, M., Ribeiro, J., Descotes, F., Serre, C.-M., Barbier, M., Murone, M., Clézardin, P. & Peyruchaud, O. Targeting lysophosphatidic acid receptor type 1 with Debio 0719 inhibits spontaneous metastasis dissemination of breast cancer cells independently of cell proliferation and angiogenesis. *International Journal of Oncology* **40**, 1133–1141 (2012).

80. An, S., Bleu, T., Hallmark, O. G. & Goetzl, E. J. Characterization of a novel subtype of human G protein-coupled receptor for lysophosphatidic acid. *J Biol Chem* **273**, 7906–7910 (1998).

81. Yamada, T., Yano, S., Ogino, H., Ikuta, K., Kakiuchi, S., Hanibuchi, M., Kanematsu, T., Taniguchi, T., Sekido, Y. & Sone, S. Lysophosphatidic acid stimulates the proliferation and motility of malignant pleural mesothelioma cells through lysophosphatidic acid receptors, LPA1 and LPA2. *Cancer Sci* **99**, 1603–1610 (2008).

82. Lee, S.-J., No, Y. R., Dang, D. T., Dang, L. H., Yang, V. W., Shim, H. & Yun, C. C. Regulation of Hypoxia-inducible Factor 1α (HIF-1α) by Lysophosphatidic Acid Is Dependent on Interplay between p53 and Krüppel-like Factor 5. *Journal of Biological Chemistry* **288**, 25244–25253 (2013).

83. Rusovici, R., Ghaleb, A., Shim, H., Yang, V. W. & Yun, C. C. Lysophosphatidic acid prevents apoptosis of Caco-2 colon cancer cells via activation of mitogen-activated protein kinase and phosphorylation of Bad. *Biochim Biophys Acta* **1770**, 1194–1203 (2007).

84. Lin, S., Wang, D., Iyer, S., Ghaleb, A. M., Shim, H., Yang, V. W., Chun, J. & Yun, C. C. The absence of LPA2 attenuates tumor formation in an experimental model of colitis-associated cancer. *Gastroenterology* **136**, 1711–1720 (2009).

85. Kitayama, J., Shida, D., Sako, A., Ishikawa, M., Hama, K., Aoki, J., Arai, H. & Nagawa, H. Over-expression of lysophosphatidic acid receptor-2 in human invasive ductal carcinoma. *Breast Cancer Res* **6**, R640-646 (2004).

86. Chen, M., Towers, L. N. & O'Connor, K. L. LPA2 (EDG4) mediates Rho-dependent chemotaxis with lower efficacy than LPA1 (EDG2) in breast carcinoma cells. *American Journal of Physiology-Cell Physiology* **292**, C1927–C1933 (2007).

87. Bandoh, K., Aoki, J., Hosono, H., Kobayashi, S., Kobayashi, T., Murakami-Murofushi, K., Tsujimoto, M., Arai, H. & Inoue, K. Molecular Cloning and Characterization of a Novel Human G-protein-coupled Receptor, EDG7, for Lysophosphatidic Acid. *Journal of Biological Chemistry* **274**, 27776–27785 (1999).

88. Im, D.-S., Heise, C. E., Harding, M. A., George, S. R., O'Dowd, B. F., Theodorescu, D. & Lynch, K. R. Molecular Cloning and Characterization of a Lysophosphatidic Acid Receptor, Edg-7, Expressed in Prostate. *Mol Pharmacol* **57**, 753–759 (2000).

89. Okabe, K., Hayashi, M., Kato, K., Okumura, M., Fukui, R., Honoki, K., Fukushima, N. & Tsujiuchi, T. Lysophosphatidic acid receptor-3 increases tumorigenicity and aggressiveness of rat hepatoma RH7777 cells. *Mol Carcinog* **52**, 247–254 (2013).

90. Zuckerman, V., Sokolov, E., Swet, J. H., Ahrens, W. A., Showlater, V., Iannitti, D. A. & Mckillop, I. H. Expression and function of lysophosphatidic acid receptors (LPARs) 1 and 3 in human hepatic cancer progenitor cells. *Oncotarget* **7**, 2951–2967 (2016).

91. Altman, M. K., Gopal, V., Jia, W., Yu, S., Hall, H., Mills, G. B., McGinnis, A. C., Bartlett, M. G., Jiang, G., Madan, D., Prestwich, G. D., Xu, Y., Davies, M. A. & Murph, M. M. Targeting melanoma growth and viability reveals dualistic functionality of the phosphonothionate analogue of carba cyclic phosphatidic acid. *Mol Cancer* **9**, 140 (2010).

92. Sun, K., Cai, H., Duan, X., Yang, Y., Li, M., Qu, J., Zhang, X. & Wang, J. Aberrant expression and potential therapeutic target of lysophosphatidic acid receptor 3 in triple-negative breast cancers. *Clin Exp Med* **15**, 371–380 (2015).

93. Kishi, Y., Okudaira, S., Tanaka, M., Hama, K., Shida, D., Kitayama, J., Yamori, T., Aoki, J., Fujimaki, T. & Arai, H. Autotaxin Is Overexpressed in Glioblastoma Multiforme and Contributes to Cell Motility of Glioblastoma by Converting Lysophosphatidylcholine TO Lysophosphatidic Acid. *Journal of Biological Chemistry* **281**, 17492–17500 (2006).

94. Kitayoshi, M., Fukui, R., Tanabe, E., Kato, K., Yoshikawa, K., Fukushima, N. & Tsujiuchi, T. Different effects on cell proliferation and migration abilities of endothelial cells by LPA_1 and LPA_3 in mammary tumor FM3A cells. *Journal of Receptors and Signal Transduction* **32**, 209–213 (2012).

95. O'Dowd, B. F., Nguyen, T., Jung, B. P., Marchese, A., Cheng, R., Heng, H. H., Kolakowski, L. F., Lynch, K. R. & George, S. R. Cloning and chromosomal mapping of four putative novel human G-protein-coupled receptor genes. *Gene* **187**, 75–81 (1997).

96. Janssens, R., Boeynaems, J. M., Godart, M. & Communi, D. Cloning of a human heptahelical receptor closely related to the P2Y5 receptor. *Biochem Biophys Res Commun* **236**, 106–112 (1997).

97. Noguchi, K., Ishii, S. & Shimizu, T. Identification of p2y9/GPR23 as a novel G protein-coupled receptor for lysophosphatidic acid, structurally distant from the Edg family. *J Biol Chem* **278**, 25600–25606 (2003).

98. Lee, D. K., Nguyen, T., Lynch, K. R., Cheng, R., Vanti, W. B., Arkhitko, O., Lewis, T., Evans, J. F., George, S. R. & O'Dowd, B. F. Discovery and mapping of ten novel G protein-coupled receptor genes. *Gene* **275**, 83–91 (2001).

99. Lee, C.-W., Rivera, R., Gardell, S., Dubin, A. E. & Chun, J. GPR92 as a New G12/13- and Gq-coupled Lysophosphatidic Acid Receptor That Increases cAMP, LPA5. *Journal of Biological Chemistry* **281**, 23589–23597 (2006).

100. Kaplan, M. H., Smith, D. I. & Sundick, R. S. Identification of a G protein coupled receptor induced in activated T cells. *J Immunol* **151**, 628–636 (1993).

101. Webb, T. E., Kaplan, M. G. & Barnard, E. A. Identification of 6H1 as a P2Y purinoceptor: P2Y5. *Biochem Biophys Res Commun* **219**, 105–110 (1996).

102. Yanagida, K., Masago, K., Nakanishi, H., Kihara, Y., Hamano, F., Tajima, Y., Taguchi, R., Shimizu, T. & Ishii, S. Identification and characterization of a novel lysophosphatidic acid receptor, p2y5/LPA6. *J Biol Chem* **284**, 17731–17741 (2009).

103. Lee, Z., Cheng, C.-T., Zhang, H., Subler, M. A., Wu, J., Mukherjee, A., Windle, J. J., Chen, C.-K. & Fang, X. Role of LPA4/p2y9/GPR23 in negative regulation of cell motility. *Mol Biol Cell* **19**, 5435–5445 (2008).

104. Dong, Y., Hirane, M., Araki, M., Fukushima, N., Honoki, K. & Tsujiuchi, T. Lysophosphatidic acid receptor-5 negatively regulates cell motile and invasive activities of human sarcoma cell lines. *Mol Cell Biochem* **393**, 17–22 (2014).

105. Pasternack, S. M., von Kügelgen, I., Al Aboud, K., Lee, Y.-A., Rüschendorf, F., Voss, K., Hillmer, A. M., Molderings, G. J., Franz, T., Ramirez, A., Nürnberg, P., Nöthen, M. M. & Betz, R. C. G protein-coupled receptor P2Y5 and its ligand LPA are involved in maintenance of human hair growth. *Nat Genet* **40**, 329–334 (2008).

106. Tao, K., Guo, S., Chen, R., Yang, C., Jian, L., Yu, H. & Liu, S. Lysophosphatidic Acid Receptor 6 (LPAR6) Expression and Prospective Signaling Pathway Analysis in Breast Cancer. *Mol Diagn Ther* **23**, 127–138 (2019).

107. Ming, Y., Wu, N., Qian, T., Li, X., Wan, D. Q., Li, C., Li, Y., Wu, Z., Wang, X., Liu, J. & Wu, N. Progress and Future Trends in PET/CT and PET/MRI Molecular Imaging Approaches for Breast Cancer. *Front Oncol* **10**, 1301 (2020).

108. Du, Y., Lai, P. T., Leung, C. H. & Pong, P. W. T. Design of superparamagnetic nanoparticles for magnetic particle imaging (MPI). *Int J Mol Sci* **14**, 18682–18710 (2013).

109. Gillings, N. Radiotracers for positron emission tomography imaging. *Magn Reson Mater Phy* **26**, 149–158 (2013).

110. Bartnicka, J. J. & Blower, P. J. Insights into Trace Metal Metabolism in Health and Disease from PET: 'PET Metallomics'. *J Nucl Med* **59**, 1355–1359 (2018).

111. Müller, K., Faeh, C. & Diederich, F. Fluorine in pharmaceuticals: looking beyond intuition. *Science* **317**, 1881–1886 (2007).

112. Shah, P. & Westwell, A. D. The role of fluorine in medicinal chemistry. *J Enzyme Inhib Med Chem* **22**, 527–540 (2007).

113. Banister, S., Roeda, D., Dolle, F. & Kassiou, M. Fluorine-18 Chemistry for PET: A Concise Introduction. *CRP* **3**, 68–80 (2010).

114. Langer, A. A systematic review of PET and PET/CT in oncology: A way to personalize cancer treatment in a cost-effective manner? *BMC Health Serv Res* **10**, 283 (2010).

115. Petersen, H., Holdgaard, P. C., Madsen, P. H., Knudsen, L. M., Gad, D., Gravergaard, A. E., Rohde, M., Godballe, C., Engelmann, B. E., Bech, K., Teilmann-Jørgensen, D., Mogensen, O., Karstoft, J., Johansen, J., Christensen, J. B., Johansen, A., Høilund-Carlsen, P. F., & PET/CT Task Force of the Region of Southern Denmark. FDG PET/CT in cancer: comparison of actual use with literature-based recommendations. *Eur J Nucl Med Mol Imaging* **43**, 695–706 (2016).

116. Liberti, M. V. & Locasale, J. W. The Warburg Effect: How Does it Benefit Cancer Cells? *Trends Biochem Sci* **41**, 211–218 (2016).

117. Lim, H. S., Yoon, W., Chung, T. W., Kim, J. K., Park, J. G., Kang, H. K., Bom, H. S. & Yoon, J. H. FDG PET/CT for the Detection and Evaluation of Breast Diseases: Usefulness and Limitations. *RadioGraphics* **27**, S197–S213 (2007).

118. Heise, C. E., Santos, W. L., Schreihofer, A. M., Heasley, B. H., Mukhin, Y. V., Macdonald, T. L. & Lynch, K. R. Activity of 2-Substituted Lysophosphatidic Acid (LPA) Analogs at LPA Receptors: Discovery of a LPA_1/LPA_3 Receptor Antagonist. *Mol Pharmacol* **60**, 1173–1180 (2001).

119. Xu, Y., Jiang, G., Tsukahara, R., Fujiwara, Y., Tigyi, G. & Prestwich, G. D. Phosphonothioate and Fluoromethylene Phosphonate Analogues of Cyclic Phosphatidic Acid: Novel Antagonists of Lysophosphatidic Acid Receptors. *J. Med. Chem.* **49**, 5309–5315 (2006).

120. Ohta, H., Sato, K., Murata, N., Damirin, A., Malchinkhuu, E., Kon, J., Kimura, T., Tobo, M., Yamazaki, Y., Watanabe, T., Yagi, M., Sato, M., Suzuki, R., Murooka, H., Sakai, T., Nishitoba,

T., Im, D.-S., Nochi, H., Tamoto, K., Tomura, H. & Okajima, F. Ki16425, a subtype-selective antagonist for EDG-family lysophosphatidic acid receptors. *Mol Pharmacol* **64**, 994–1005 (2003).

121. Swaney, J., Chapman, C., Correa, L., Stebbins, K., Bundey, R., Prodanovich, P., Fagan, P., Baccei, C., Santini, A., Hutchinson, J., Seiders, T., Parr, T., Prasit, P., Evans, J. & Lorrain, D. A novel, orally active LPA $_1$ receptor antagonist inhibits lung fibrosis in the mouse bleomycin model. *British J Pharmacology* **160**, 1699–1713 (2010).

122. Castelino, F. V., Seiders, J., Bain, G., Brooks, S. F., King, C. D., Swaney, J. S., Lorrain, D. S., Chun, J., Luster, A. D. & Tager, A. M. Amelioration of dermal fibrosis by genetic deletion or pharmacologic antagonism of lysophosphatidic acid receptor 1 in a mouse model of scleroderma. *Arthritis & Rheumatism* **63**, 1405–1415 (2011).

123. Gabriel, S. D., Hamilton, M. M., Qian, Y. & Sidduri, A. N-aryltriazole compounds as lpar antagonists. WO2013189865A1. (2013).

124. Qian, Y., Hamilton, M., Sidduri, A., Gabriel, S., Ren, Y., Peng, R., Kondru, R., Narayanan, A., Truitt, T., Hamid, R., Chen, Y., Zhang, L., Fretland, A. J., Sanchez, R. A., Chang, K.-C., Lucas, M., Schoenfeld, R. C., Laine, D., Fuentes, M. E., Stevenson, C. S. & Budd, D. C. Discovery of Highly Selective and Orally Active Lysophosphatidic Acid Receptor-1 Antagonists with Potent Activity on Human Lung Fibroblasts. *J. Med. Chem.* **55**, 7920–7939 (2012).

125. Sidduri, A., Budd, D. C., Fuentes, M. E., Lambros, T., Ren, Y., Roongta, V., Schoenfeld, R. C., Gillespie, P., Stevenson, C. S., Truitt, T. & Qian, Y. Discovery of novel non-carboxylic acid 5-amino-4-cyanopyrazole derivatives as potent and highly selective LPA1R antagonists. *Bioorganic & Medicinal Chemistry Letters* **24**, 4450–4454 (2014).

126. Terakado, M., Suzuki, H., Hashimura, K., Tanaka, M., Ueda, H., Kohno, H., Fujimoto, T., Saga, H., Nakade, S., Habashita, H., Takaoka, Y. & Seko, T. Discovery of ONO-7300243 from a Novel Class of Lysophosphatidic Acid Receptor 1 Antagonists: From Hit to Lead. *ACS Med. Chem. Lett.* **7**, 913–918 (2016).

127. Zhao, P., Wu, S., Li, Y., Bao, G., Pei, J., Wang, Y., Ma, Q., Sun, H. & Damirin, A. LPA receptor1 antagonists as anticancer agents suppress human lung tumours. *European Journal of Pharmacology* **868**, 172886 (2020).

128. Terakado, M., Suzuki, H., Hashimura, K., Tanaka, M., Ueda, H., Hirai, K., Asada, M., Ikura, M., Matsunaga, N., Saga, H., Shinozaki, K., Karakawa, N., Takada, Y., Minami, M., Egashira, H., Sugiura, Y., Yamada, M., Nakade, S. & Takaoka, Y. Discovery of a Slow Tight Binding LPA1 Antagonist (ONO-0300302) for the Treatment of Benign Prostatic Hyperplasia. *ACS Med. Chem. Lett.* **8**, 1281–1286 (2017).

129. Sakamoto, K., Noguchi, Y., Ueshima, K., Yamakuni, H., Ohtake, A., Sato, S., Ishizu, K., Hosogai, N., Kawaminami, E., Takeda, M. & Masuda, N. Effect of ASP6432, a Novel Type 1 Lysophosphatidic Acid Receptor Antagonist, on Urethral Function and Prostate Cell Proliferation. *J Pharmacol Exp Ther* **366**, 390–396 (2018).

130. ClinicalTrials.gov:NCT02068053. https://Clinicaltrials.Gov/Ct2/Show/NC T02068053.

131. ClinicalTrials.gov:NCT01766817. https://Clinicaltrials.Gov/Ct2/Show/NC T01766817.

132. ClinicalTrials.gov:NCT02017730. https://Clinicaltrials.Gov/Ct2/Show/NC T02017730.

133. ClinicalTrials.gov:NCT01651143. https://Clinicaltrials.Gov/Ct2/Show/NC T01651143.

134. Schaefer, M., Pernerstorfer, J., Kadereit, D., Strobel, H., Czechtizky, W., Chen, L. C., Safarova, A., Weichsel, A. & Patek, M. Acylamino-substituted fused cyclopentanecarboxylic acid derivatives and their use as pharmaceuticals. WO2009135590A1. (2009).

135. Ellery, J., Dickson, L., Cheung, T., Ciuclan, L., Bunyard, P., Mack, S., Buffham, W. J., Farnaby, W., Mitchell, P., Brown, D., Isaacs, R. & Barnes, M. Identification of compounds acting as negative allosteric modulators of the LPA1 receptor. *European Journal of Pharmacology* **833**, 8–15 (2018).

136. Allanore, Y., Distler, O., Jagerschmidt, A., Illiano, S., Ledein, L., Boitier, E., Agueusop, I., Denton, C. P. & Khanna, D. Lysophosphatidic Acid Receptor 1 Antagonist SAR100842 for Patients With Diffuse Cutaneous Systemic Sclerosis: A Double-Blind, Randomized, Eight-Week Placebo-Controlled Study Followed by a Sixteen-Week Open-Label Extension Study. *Arthritis Rheumatol* **70**, 1634–1643 (2018).

137. Smith, M. J., Lawler, M. J., Kopp, N., Mcleod, D. D., Davulcu, A. H., Lin, D., Katipally, K. & Sfouggatakis, C. Development of a Concise Multikilogram Synthesis of LPA-1 Antagonist BMS-986020 via a Tandem Borylation–Suzuki Procedure. *Org. Process Res. Dev.* **21**, 1859–1863 (2017).

138. Palmer, S. M., Snyder, L., Todd, J. L., Soule, B., Christian, R., Anstrom, K., Luo, Y., Gagnon, R. & Rosen, G. Randomized, Double-Blind, Placebo-Controlled, Phase 2 Trial of BMS-986020, a Lysophosphatidic Acid Receptor Antagonist for the Treatment of Idiopathic Pulmonary Fibrosis. *Chest* **154**, 1061–1069 (2018).

139. Gaire, B. P., Sapkota, A. & Choi, J. W. BMS-986020, a Specific LPA1 Antagonist, Provides Neuroprotection against Ischemic Stroke in Mice. *Antioxidants* **9**, 1097 (2020).

140. Tirucherai, G. S., Yu, D., Revankar, R., Klinger, G., Van Lier, J. J., Taubel, J. & Charles, E. D. BMS-986278, A Lysophosphatidic Acid 1 (LPA $_1$) Receptor Antagonist, in Healthy Participants: A Single/Multiple Ascending Dose (SAD/MAD) and Japanese MAD (JMAD) Phase 1 Study. in *A37. ILD THERAPY I* A1492–A1492 (American Thoracic Society, 2020). doi:10.1164/ajrccm-conference.2020.201.1_MeetingAbstracts.A1492.

141. Gill, M. W., Lakshmi, S., Cheng, P. T. W., Murphy, B. J., Chadwick, K., Lehman-McKeeman, L. & Graziano, M. BMS-986278, an LPA $_1$ Receptor Antagonist for Idiopathic Pulmonary Fibrosis: Preclinical Assessments of Potential Hepatobiliary Toxicity. in *D17. TOWARDS THE NEXT IPF THERAPIES* A5882–A5882 (American Thoracic Society, 2019). doi:10.1164/ajrccm-conference.2019.199.1_MeetingAbstracts.A5882.

142. ClinicalTrials.gov:NCT04308681. https://Clinicaltrials.Gov/Ct2/Show/NC T04308681.

143. Donnelly, D. J., Bonacorsi, S. J., Cao, J., Tran, T., Pena, A., Kim, J., Carson, R. E., Nabulsi, N., Gallezot, J.-D., Huang, Y., Creiders, T. J. & Roppe, J. R. Radioligands for imaging the lpa-1 receptor. WO2015066456A1. (2015).

144. Gallezot, J.-D., Nabulsi, N. B., Holden, D., Lin, S.-F., Labaree, D., Ropchan, J., Najafzadeh, S., Donnelly, D. J., Cao, K., Bonacorsi, S., Seiders, J., Roppe, J., Hayes, W., Huang, Y., Du, S. & Carson, R. E. Evaluation of the Lysophosphatidic Acid Receptor Type 1 Radioligand ^{11} C-BMT-136088 for Lung Imaging in Rhesus Monkeys. *J Nucl Med* **59**, 327–333 (2018).

145. Hadebe, B., Harry, L., Ebrahim, T., Pillay, V. & Vorster, M. The Role of PET/CT in Breast Cancer. *Diagnostics* **13**, 597 (2023).

146. Callis, T. B., Garrett, T. R., Montgomery, A. P., Danon, J. J. & Kassiou, M. Recent Scaffold Hopping Applications in Central Nervous System Drug Discovery. *J Med Chem* **65**, 13483–13504 (2022).

147. Sun, H., Tawa, G. & Wallqvist, A. Classification of scaffold-hopping approaches. *Drug Discov Today* **17**, 310–324 (2012).

148. Furet, P., Bold, G., Hofmann, F., Manley, P., Meyer, T. & Altmann, K.-H. Identification of a new chemical class of potent angiogenesis inhibitors based on conformational considerations and database searching. *Bioorg Med Chem Lett* **13**, 2967–2971 (2003).

149. Fujisaka, Y., Yamada, Y., Yamamoto, N., Shimizu, T., Fujiwara, Y., Yamada, K., Tamura, T., Watanabe, H., Sun, Y.-N., Bass, M. B. & Seki, M. Phase 1 study of the investigational, oral angiogenesis inhibitor motesanib in Japanese patients with advanced solid tumors. *Cancer Chemother Pharmacol* **66**, 935–943 (2010).

150. Trott, O. & Olson, A. J. AutoDock Vina: improving the speed and accuracy of docking with a new scoring function, efficient optimization, and multithreading. *J Comput Chem* **31**, 455–461 (2010).

151. Chrencik, J. E., Roth, C. B., Terakado, M., Kurata, H., Omi, R., Kihara, Y., Warshaviak, D., Nakade, S., Asmar-Rovira, G., Mileni, M., Mizuno, H., Griffith, M. T., Rodgers, C., Han, G. W., Velasquez, J., Chun, J., Stevens, R. C. & Hanson, M. A. Crystal Structure of Antagonist Bound Human Lysophosphatidic Acid Receptor 1. *Cell* **161**, 1633–1643 (2015).

152. BIOVIA, Dassault Systèmes. DS Viewer. Version 3.5. (2022).

153. Forli, S., Huey, R., Pique, M. E., Sanner, M. F., Goodsell, D. S. & Olson, A. J. Computational protein–ligand docking and virtual drug screening with the AutoDock suite. *Nat Protoc* **11**, 905–919 (2016).

154. Padilla, A. G. & Pearlman, B. A. Highly Selective Hydrolysis of Chloropyrimidines to Pyrimidones in 12 N Hydrochloric Acid. *Org. Process Res. Dev.* **10**, 921–926 (2006).

155. Bellamy, F. D. & Ou, K. Selective reduction of aromatic nitro compounds with stannous chloride in non acidic and non aqueous medium. *Tetrahedron Letters* **25**, 839–842 (1984).

156. Hoffman, G. R. & Schoffstall, A. M. Syntheses and Applications of 1,2,3-Triazole-Fused Pyrazines and Pyridazines. *Molecules* **27**, 4681 (2022).

157. Frank, K. E., Burchat, A., Cox, P., Ihle, D. C., Mullen, K. D., Somal, G., Vasudevan, A., Wang, L. & Wilson, N. S. WO2012149280 - NOVEL TRICYCLIC COMPOUNDS. (2012).

158. Hayashi, K., Ichimaru, Y., Sugiura, K., Maeda, A., Harada, Y., Kojima, Y., Nakayama, K. & Imai, M. Efficiency of Lithium Cations in Hydrolysis Reactions of Esters in Aqueous Tetrahydrofuran. *Chem Pharm Bull (Tokyo)* **69**, 581–584 (2021).

159. Jacobson, O., Kiesewetter, D. O. & Chen, X. Fluorine-18 radiochemistry, labeling strategies and synthetic routes. *Bioconjug Chem* **26**, 1–18 (2015).

160. Bratteby, K., Shalgunov, V. & Herth, M. M. Aliphatic 18 F-Radiofluorination: Recent Advances in the Labeling of Base-Sensitive Substrates**. *ChemMedChem* **16**, 2612–2622 (2021).

161. Rotstein, B. H., Wang, L., Liu, R. Y., Patteson, J., Kwan, E. E., Vasdev, N. & Liang, S. H. Mechanistic studies and radiofluorination of structurally diverse pharmaceuticals with spirocyclic iodonium(III) ylides. *Chem. Sci.* **7**, 4407–4417 (2016).

162. Chen, W., Wang, H., Tay, N. E. S., Pistritto, V. A., Li, K.-P., Zhang, T., Wu, Z., Nicewicz, D. A. & Li, Z. Arene radiofluorination enabled by photoredox-mediated halide interconversion. *Nat Chem* **14**, 216–223 (2022).

163. Zheng, Q., Xu, H., Wang, H., Du, W.-G. H., Wang, N., Xiong, H., Gu, Y., Noodleman, L., Sharpless, K. B., Yang, G. & Wu, P. Sulfur [^{18} F]Fluoride Exchange Click Chemistry Enabled Ultrafast Late-Stage Radiosynthesis. *J. Am. Chem. Soc.* **143**, 3753–3763 (2021).

164. Chemler, S. R., Trauner, D. & Danishefsky, S. J. The B-Alkyl Suzuki-Miyaura Cross-Coupling Reaction: Development, Mechanistic Study, and Applications in Natural Product Synthesis. *Angew. Chem. Int. Ed.* **40**, 4544–4568 (2001).

165. Yu, S. Review of 18F-FDG synthesis and quality control. *Biomed. Imaging Interv. J.* **2**, (2006).